Development of microcellular conductive foams based on polyetherimide with graphene nanoplatelets

By

Hooman Abbasi

In partial fulfillment of the requirements for the degree of Doctor of Philosophy

In

Materials Science and Engineering

Director:

Prof. José Ignacio Velasco Perero

Co-Director:

Prof. Marcelo de Sousa Pais Antunes

Department of Materials Science and Metallurgy

July 2019

Centre Català del Plàstic

UNIVERSITAT POLITÈCNICA DE CATALUNYA BARCELONATECH

UNIVERSITAT POLITÈCNICA DE CATALUNYA
BARCELONATECH
Escola de Doctorat

Acta de calificación de tesis doctoral

Curso académico:

Nombre y apellidos

Programa de doctorado

Unidad estructural responsable del programa

Resolución del Tribunal

Reunido el Tribunal designado a tal efecto, el doctorando / la doctoranda expone el tema de la su tesis doctoral titulada _____

_____.

Acabada la lectura y después de dar respuesta a las cuestiones formuladas por los miembros titulares del tribunal, éste otorga la calificación:

NO APTO ☐ APROBADO ☐ NOTABLE ☐ SOBRESALIENTE ☐

(Nombre, apellidos y firma) Presidente/a		(Nombre, apellidos y firma) Secretario/a
(Nombre, apellidos y firma) Vocal	(Nombre, apellidos y firma) Vocal	(Nombre, apellidos y firma) Vocal

_____, _____ de _____ de _____

El resultado del escrutinio de los votos emitidos por los miembros titulares del tribunal, efectuado por la Escuela de Doctorado, a instancia de la Comisión de Doctorado de la UPC, otorga la MENCIÓN CUM LAUDE:

SÍ ☐ NO ☐

(Nombre, apellidos y firma) Presidente de la Comisión Permanente de la Escuela de Doctorado	(Nombre, apellidos y firma) Secretario de la Comisión Permanente de la Escuela de Doctorado

Barcelona a _____ de _____ de _____

Acknowledgments

I am greatly in debt of many people that have assisted me during this entire process. Firstly, I want to express my gratitude to Professor José Ignacio Velasco for enabling this opportunity and also for his guidance which helped me overcome obstacles alongside the path and for his generous support during my research. This work would not have been possible without his indispensable advices and helpful aid.

I also want to thank my co-director Professor Marcelo Antunes for sharing his knowledge, guidance and his undeniable assistance on preparation and finalization of this study throughout the whole process. His determination and discipline will always be a paragon in my mind. I could not have wished for a better group of people to work with and my gratitude could not be simply put into few words.

I am greatly thankful to all professors and employees at Centre Català del Plàstic (CCP), Including but not limited to Prof. Maria Lluisa Maspoch, Prof. Antonio Martinez Benasat, Prof. Vera Realinho, Prof. David Arencón, Prof. Miguel Sánchez, Prof. Orlando Santana, Anna Carreras, Susana Ortiz and Alba Giménez. My special gratitude to all the PhD students at the center and the ones who have already finished their study during my time of stay at this facilities including Dr. Hakim, Dr. Noel, Pilar, Dr. Tobias, Dr. Liang, Dr. Jonathan, Nil, David and finally Dr. Gabriel who helped me a lot at the initiation of this research.

I am greatly thankful for the financial support from Centre Català del Plàstic joint with the Spanish Ministry of Economy and Competitiveness through MAT2014-56213-P and MAT2017-89787-P projects which provided the budget and facilities essential to carry out this work.

I would like to thank those who assisted me during the experimental procedures. Josep and Francisco in Material department of ESEIAAT (CMEM-UPC) and Dr. Xavier Alcobé in CCiTUB (UB).

It is needless to say that my parents and my brothers supported me vastly throw this journey and I am forever in their debt. I wish I can return all the favors and help they provided me one day.

I would also like to thank two friends, Krishna, Behshad, Jesus and Vegard who I shared lots of thoughts and conversations during the past 4 years and I will cherish their friendship far into the future.

Last but not least, I would like to thank my girlfriend, Shadi, who has been there for me and never gave up motivating me through thick and thin. I am looking forward to continue this journey with you.

Abstract

The aim of this dissertation was to develop and investigate novel foams based on polyetherimide (PEI) and carbon-based nanoparticles, particularly graphene nanoplatelets (GnP) and carbon nanotubes (CNT), using two main foaming methods: water vapor induced phase separation (WVIPS) and one-step supercritical CO_2 ($scCO_2$) dissolution. WVIPS foaming method consists in initially preparing a polymer-solvent solution and promoting the nucleation of cells through phase separation due to water vapor absorption and exchange with the solvent. The second foaming method consists in the dissolution of $scCO_2$ in a high-pressure vessel followed by the expansion of the nanocomposite precursor by applying a sudden pressure drop.

The foams were characterized in terms of their cellular structure and morphology, mechanical and thermal properties and their electrical conductivity in order to address the effects of foaming methods and its variables (solution concentration, ultrasonication) alongside with the composition of the foams on the mentioned properties.

In the WVIPS method the concentration of polymer in the solvent during mixture showed to have a great impact on the morphology of the foams. The foams prepared with a lower concentration of polymer in solvent resulted in lighter foams with larger cells. Additionally, the composition seems to have various effects on the cellular structure. When a blend of PEI with polyamide-imide (PAI) was prepared using this method, the cellular formation evolved drastically depending on the amounts of PAI added to the mixture. Moreover, the incorporation of GnP and CNT affected the cellular structure and morphology with various levels of impact depending on whether nanoparticle ultrasonication was applied. The ultrasonication also proved to reduce the GnP and CNT agglomeration and promote a better distribution of the particles. These factors provided the feasibility for preparing multifunctional foams with various densities and cellular structures using the WVIPS foaming method.

Using the one-step $scCO_2$ dissolution foaming method, foams were obtained with homogenous closed-cell structure. The incorporation of GnP did not seem to affect the cellular structure of PEI foams. However, the application of ultrasonication, melt mixing and one-step foaming seem to have induced a proper level of particle dispersion, which was confirmed by X-ray diffraction analysis.

The studies of mechanical properties of foams prepared via WVIPS method suggested that the densities of the foams alter their viscoelastic behaviour in a direct manner. Additionally, the mechanical behaviour followed a similar increasing trend by incrementing the amount of graphene content. Surprisingly, this behaviour changed when using CNT as reinforcement. A clear decreasing trend was observed in the specific storage modulus of the foams by increasing the amount of CNT, which seemed to be a side effect of structural differences arose from the influence of CNT on the phase separation process.

Moreover, considering the case of polymeric blends, the mechanical behaviour seem to have been affected vastly by the structural changes. The PEI/PAI polymer composition played a key role in determining the cellular structure and, therefore, the eventual mechanical behaviour of these foams.

Regarding the viscous part, the addition of carbon-based nanoparticles did not have a notable impact on the peaks that appeared in the loss modulus and *tan δ* curves of the foams, showing that the glass transition temperatures (T_g) of the foams did not have any major changes. The slight variation of the T_g seemed to be a result of few contradictive effects, such as possible lubricating effect of carbon-based nanofillers and the restriction of polymer chain mobility due to their interaction with the nanoparticles.

The foams prepared by $scCO_2$ dissolution showed an increasing trend of the normalized modulus (E_{norm}) with increasing the density and a rise in the specific modulus (E_{spec}) with increasing the GnP volume fraction. Regarding their viscous part, the existence of GnP seemed capable of inducing minor restrictions on molecular mobility due to possible interfacial interaction with the polymer.

In terms of thermal stability, all foams have shown a faster degradation when compared to that of the unfilled unfoamed polymer, which could be related to the availability of oxygen during various stages of the decomposition. The influence of nanofillers on the thermal stability seemed to have arose from two contradictory factors: on the one hand, the fillers acting as a barrier to the escape of volatile gases and therefore delaying the decomposition; and the other effect being the facilitation of heat transfer due to the high thermal conductivity of carbon-based nanofillers. In an overall view, the nanoparticles provided a general delay in degradation temperatures of the nanocomposite foams, extending their use temperature.

Significant enhancements were achieved regarding the electrical conductivity of the foams. The ultrasonication of the nanoparticles have provided the possibility to increase the value of electrical conductivity by six orders of magnitude from 1.8×10^{-7} S/m to 1.7×10^{-1} S/m for foams containing 10 wt% of GnP. Additionally, the study of foams with different porosities indicated that the electrical conductivity could be further improved by increasing the porosity due to a reduction in inter-particle distance due to a decrease in the characteristic dimension of the continuous phase. Furthermore, the preparation and characterization of foams containing Hybrid nanoparticles (CNT/GnP) showed a possibility of producing an optimized system (50% GnP - 50% CNT) with the capability of maximizing the electrical conductivity of the foams while maintaining their mechanical properties. The foams with 1/1 ratio of GnP and CNT reached an electrical conductivity value of 8.8×10^{-3} S/m containing only a total amount of nanoparticles of 2 wt%.

Resumen

El objetivo de esta tesis doctoral fue desarrollar e investigar nuevas espumas celulares basadas en polieterimida (PEI) y nanopartículas basadas en carbono, como son las nanopartículas de grafeno (GnP) y los nanotubos de carbono (CNT). Para ello se utilizó dos métodos principales de formación de espumas, uno de ellos fue el método de separación de fases inducida por vapor de agua (WVIPS) y el otro fue la disolución de dióxido de carbono en estado supercrítico ($scCO_2$) en su estado supercrítico en una-etapa. El método WVIPS consiste en la preparación inicial de la solución de polímero-disolvente y la nucleación de las células a través de la separación de fases debido a la absorción del vapor de agua. La disolución de $scCO_2$ se aplicó en un reactor de alta presión seguido por la expansión del precursor nanocompuesto por aplicar una caída brusca de presión.

Las espumas se caracterizaron posteriormente en términos de su estructura celular y morfología, propiedades mecánicas y térmicas y su conductividad eléctrica para abordar los efectos de los métodos de formación de espuma y sus variables (concentración de solución, ultrasonidos) junto con los efectos de la composición de las espumas en las propiedades mencionadas.

En el método WVIPS, la concentración del polímero en el disolvente durante la mezcla mostró un gran impacto sobre la morfología de las espumas. Las espumas preparadas con una menor concentración de polímero en el disolvente dieron como resultado, espumas más ligeras con tamaños medios de células mayores. Además, la composición parece tener diversos efectos sobre la estructura celular. Cuando se preparó una mezcla de PEI con poliamida-imida (PAI) usando este método, la formación celular evolucionó drásticamente dependiendo de la fracción de PAI añadida a la mezcla. Por otra parte, la incorporación de GnP y CNT parece haber afectado la estructura celular y la morfología en diferentes niveles de impacto dependiendo de si se aplicó la ultrasonicación de las nanopartículas o no. La ultrasonicación también demostró reducir la aglomeración de GnP y CNT y facilitar una mejor distribución de las partículas. Estos factores proporcionaron la viabilidad de preparar espumas multifuncionales con diversas densidades y estructuras celulares mediante el proceso WVIPS.

Usando el método de espumación por disolución de $scCO_2$ en un paso, espumas con homogeneidad estructural y con celdas cerradas fueron obtenidas. La incorporación de GnP no pareció afectar la estructura celular de las espumas de PEI. Sin embargo, la aplicación de ultrasonidos, mezcla en fusión y espumación en un solo paso parece haber inducido un nivel adecuado de dispersión de partículas que se confirmó mediante análisis de difracción de rayos-X.

Los estudios de las propiedades mecánicas de las espumas preparadas mediante el método WVIPS sugirieron que las densidades de las espumas alteran su comportamiento viscoelástico de manera directa. Además, el comportamiento mecánico sigue una tendencia similar al aumentar la fracción de grafeno. Sorprendentemente, este comportamiento cambia cuando se usa CNT como refuerzo. Se observó una clara tendencia decreciente en el módulo de almacenamiento específico con el aumento de la cantidad de CNT

que parecía ser un efecto secundario de las diferencias estructurales que surgió por el efecto de CNT en el proceso de separación de fases.

Además, considerando el caso de las mezclas poliméricas, el comportamiento mecánico parece haber sido afectado enormemente por los cambios estructurales. La composición del polímero PEI / PAI desempeñó un parte clave en la determinación de la estructura celular y, por lo tanto, el comportamiento mecánico final de estas espumas.

Con respecto a la parte viscosa, la adición de nanopartículas basadas en carbono no tuvo un gran impacto sobre los picos que aparecían en las curvas de módulo de perdida y *tan δ* de las espumas, mostrando que la temperatura de transición vítrea (T_g) de las espumas no ha tenido cambios graves. Los ligeros variaciones en los T_g parecen resultados de algunos efectos contradictorios, tales como el posible efecto lubricante de los nanocargas basadas en carbono y la restricción de la movilidad de las cadenas de polímero debido a posibles interacciones con las nanopartículas.

Las espumas preparadas a través de la disolución de $scCO_2$ mostraron una tendencia creciente de módulo normalizado ($E´_{norm}$) con el aumento de la densidad y un aumento en el módulo específico ($E´_{spec}$) con el aumento de la fracción volumétrica de GnP. Con respecto a su parte viscosa, la existencia de GnP parecía ser capaz de inducir restricciones menores en la movilidad molecular debido a la posible interacción interfacial con el polímero.

En términos de estabilidad térmica, todas las espumas han demostrado una degradación más rápida en comparación con la del polímero sólido puro que podría estar relacionado con la disponibilidad de oxígeno durante varias etapas de la descomposición. La influencia de las partículas en la estabilidad térmica parece surgir a partir de dos factores contradictorios: Por una parte, dichas partículas actúan como una barrera en forma de capas contra los gases volátiles y, por lo tanto, retrasan la descomposición y, por otra parte, facilitan la disipación de calor debido a su alta conductividad térmica. De forma general, las nanopartículas proporcionaron un retraso general en las temperaturas de degradación de las espumas nanocompuestas que podrían proporcionar la posibilidad de su aplicación en entornos de alta temperatura.

Se lograron mejoras significativas con respecto a la conductividad eléctrica de las espumas. La ultrasonicación de las nanopartículas proporcionó la posibilidad de aumentar el valor de la conductividad eléctrica en seis órdenes de magnitud desde $1{,}8 \times 10^{-7}$ S/m hasta $1{,}7 \times 10^{-1}$ S/m en espumas que contienen 10% en peso de GnP. Además, el estudio de las espumas con diferentes porosidades indicó que la conductividad eléctrica podría mejorarse aún más al aumentar la porosidad. Esto dio como resultado una reducción en la distancia entre partículas debido a una disminución en la dimensión característica de la fase continua. Además, la preparación y caracterización de espumas que contienen nanopartículas híbridas (GnP/CNT) mostró la posibilidad de generar un sistema optimizado (50% GnP - 50% CNT) con la capacidad de maximizar la conductividad eléctrica de las espumas mientras se mantenían sus propiedades

mecánicas. Las espumas con proporción 1/1 de GnP y CNT alcanzaron un valor de conductividad eléctrica de $8{,}8 \times 10^{-3}$ S/m que contenía solo un 2% en peso de nanopartículas.

Table of Contents

Acknowledgments v

Abstract and resumen vi

Abbreviations, symbols and units xv

List of Tables xvii

List of Figures xviii

Chapter 1. Introduction, context and general objective 1

1.1 Investigation antecedents 3
1.2 Strategy and objectives of the research 4
1.3 Research structure and scientific production 6
1.4 References 10

Chapter 2: State of the art 13

2.1 Basic concepts of polymeric foams 15
2.1.1 Foam structure, foaming methods and applications 15
2.1.2 References 24
2.2 *Polyimides* 26
2.2.1 Abstract 26
2.2.2 Published book chapter (*Chapter 16 in 2nd edition of Handbook of Thermoplastics, 2016*) 26
2.3 Polyetherimides (PEI) and PEI-based foams 68
2.4 Carbon nanofillers and PEI-based nanocomposites 76
2.5 Polyetherimide nanocomposite foams 79
2.6 References 84
2.7 *Recent advances in carbon-based polymer nanocomposites* 91
2.7.1 Abstract 91
2.7.2 Published article (Journal of *Progress in Materials Science, Vol. 103, Page 319-373, 2019*) 91

Chapter 3. Materials and experimental procedure 147

3.1 Materials 149
3.1.1 Polyetherimide 149

3.1.2 Polyamide-imide 151
3.1.3 Graphene nanoplatelets 152
3.1.4 Carbon nanotubes 153
3.1.5 Solvents 153
3.1.6 Carbon dioxide 155
3.2 Preparation of foams 155
3.2.1 Polymer dissolution 155
3.2.2 Ultrasonication 155
3.2.3 Melt compounding 156
3.2.4 Compression molding 157
3.2.5 Foaming methods 157
3.2.5.1 Water vapor induced phase separation (WVIPS) process ... 157
3.2.5.2 One-step supercritical CO_2 dissolution process 158
3.3 Characterization procedure 159
3.3.1 Density measurement 159
3.3.2 Scanning electron microscopy (SEM) 160
3.3.3 Wide angle X-ray scattering (WAXS) 162
3.3.4 Differential scanning calorimetry (DSC) 163
3.3.5 Thermogravimetric analysis (TGA) 165
3.3.6 Dynamic mechanical thermal analysis (DMTA) 165
3.3.7 Electrical conductivity measurements 167
3.4 References 168

Chapter 4. The WVIPS foaming method: PEI, PEI-GnP and PEI/PAI microcellular foams 171

4.1 *Graphene nanoplatelets-reinforced polyetherimide foams prepared by water vapor-induced phase separation* 173
4.1.1 Abstract and conclusions 173
4.1.2 References 174
4.1.3 Published article (*Journal of eXPRESS Polymer Letters, Vol. 9, Page 412-423, 2015*) 175
4.2 *Influence of polyamide–imide concentration on the cellular structure and thermo-mechanical properties of PEI/PAI blend foams*..... 188
4.2.1 Abstract and conclusions 188
4.2.2 References 189

4.2.3 Published article (*Journal of European Polymer Journal, Vol. 69, Page 273-283, 2015*) 191

Chapter 5. Improving the microstructure through `solution concentration and GnP ultrasonication..... 203

5.1 *Enhancing the electrical conductivity of polyetherimide-based foams by simultaneously increasing the porosity and graphene nanoplatelets dispersion* 205

5.1.1 Abstract and conclusions 205

5.1.2 References..... 206

5.1.3 Published article (*Journal of Polymer Composites, Vol. 40, Page E1416-E1425, 2019*) 208

Chapter 6. PEI foams with enhanced electrical conductivity through an optimized hybrid nanofiller system 219

6.1 *Effects of carbon nanotubes/graphene nanoplatelets hybrid systems on the structure and properties of polyetherimide-based foams* 221

6.1.1 Abstract and conclusions 221

6.1.2 References..... 223

6.1.3 Published article (*Journal of Polymers, Vol. 10, Page 348, 2018*) . 224

Chapter 7. Enhancing the electrical conductivity through high pressure $scCO_2$ dissolution process 247

7.1 *Polyetherimide foams filled with low content of graphene nanoplatelets prepared by $scCO_2$ dissolution* 249

7.1.1 Abstract and conclusions 249

7.1.2 References..... 250

7.1.3 Published article (*Journal of Polymers, Vol. 11, Page 328, 2019*) . 251

Chapter 8. General discussion, conclusions and future studies 271

8.1 General discussion 273

8.1.1 The effects of carbon-based nanofillers 273

8.1.2 The effects of polymer blending 274

8.1.3 The effects of foaming process 278

8.2 Conclusions 280

8.3 Future studies 281
8.4 References 282

Abbreviations

AR	Aspect ratio
CB	Carbon black
CBA	Chemical blowing agent
CFC	Chlorofluorocarbon
CMEM	Department of Materials Science and Metallurgy
CNF	Carbon nanofibers
CNT	Carbon nanotubes
CO_2	Carbon dioxide
CVD	Chemical vapor deposition
DMF	*N*,*N*-Dimethylformamide
DTUL	Deflection temperature under load
EMI	Electromagnetic interference
ER	Expansion ratio
ESD	Electrostatic discharge
ESEIAAT	School of Industrial, Aerospace and Audiovisual Engineering of Terrassa
GnP	Graphene nanoplatelets
HCFC	Hydrochlorofluorocarbon
HT	Hydrotalcite
IF	Impact factor
LCP	Liquid crystalline polymer
$Mg(OH)_2$	Magnesium hydroxide
MMT	Montmorillonite
MWCNT	Multi-wall carbon nanotube
NMP	*N*-methyl pyrrolidone
PAI	Polyamide-imide
PANI	Polyaniline
PBA	Physical blowing agent
PC	Polycarbonate
PE	Polyethylene
PEEK	Polyether ether ketone
PEI	Polyetherimide
PMMA	Poly (methyl methacrylate)
PP	Polypropylene
PPSU	Polyphenylsulfone
PS	Polystyrene
PSU	Polysulfone
PTFE	Polytetrafluoroethylene
PU	Polyurethane
PVA	Poly (vinyl alcohol)
RH	Relative humidity
SAN	Styrene-acrylonitrile resin
$scCO_2$	Supercritical carbon dioxide
SWCNT	Single-wall carbon nanotube
THF	Tetrahydrofuran
WAXS	Wide angle X-ray scattering
WVIPS	Water vapor induced phase separation
XRD	X-ray diffraction

Symbols

Φ	Average cell size
N_f	Cell density
N_0	Cell nucleation density
C	Concentration
ρ	Density
σ	Electrical conductivity
T_g	Glass transition temperature
m	Mass
E	Elasticity modulus
E_{norm}	Normalized modulus
P	Pressure
ρ_{rev}	Relative density
ρ_s	Solid density
E_{spec}	Specific modulus
E'	Storage modulus
E''	Loss modulus
T	Temperature
t	Time
V	Volume
ϕ	Volume fraction
λ	Wavelength

Units

A	Ampere
a.u.	Arbitrary units
bar	Bar
cm	Centimetre
°C	Degree centigrade (degree Celsius)
g	Gram
h	Hour
kJ	Kilojoule
kW	Kilowatt
L	Litre
MPa	Megapascal
m	Metre
µm	Micrometre
mm	Millimetre
mPa.s	Millipascal second
nm	Nanometre
Ω	Ohm
%	Percentage
psi	Pound per square inch
s	Second
S/m	Siemens per metre
V	Volt
vol%	Volume percentage
W	Watt
wt%	Weight percentage

List of Tables

Table 2.1 Chemical blowing agents and their characteristics 19
Table 2.2 List of commercial PEIs and their characteristic temperatures. Gathered from datasheets of SABIC, Mitsui and DuPont Chemicals 69
Table 3.1 Properties of PEI (Ultem 1000) 150
Table 3.2 Properties of PAI (Torlon 4203) 152
Table 3.3 Characteristics of graphene powder (xGnP M-15) 153
Table 3.4 Characteristics of *N*-methyl pyrrolidone (NMP) 155

List of Figures

Figure 1.1 Considered strategies to reach the principal goal of the thesis..... 5
Figure 2.1 Cellular structure of open-cell and closed-cell foams 16
Figure 2.2 Schematic of one-step foaming using $scCO_2$ dissolution in a high pressure vessel .. 20
Figure 2.3 Schematic of the phase inversion processes occurring during the humid air exposure 21
Figure 2.4 (a) Schematic of electromagnetic wave transfer through PEI/graphene@Fe_3O_4 foams; (b) Schematic diagram demonstrating the multireflection path of electromagnetic wave between the graphene@Fe_3O_4 laminates; (c) TEM image showing the possible reflection path of an electromagnetic wave between two parallel graphene@Fe_3O_4 sheets 23
Figure 2.5 Last step in synthesis of polyetherimide 68
Figure 2.6 Chemical structure of (a) BPADA-PPD polyetherimide (Ultem® 5000 series) (b) bisphenol diamine PMDA polyetherimide (Aurum®, Vespel® TP-8000 series) (c) BPADA-DDS polyetherimide sulfone (Ultem® XH6050) (d) BPADA-MPD polyetherimide (Ultem® 1000 series) (e) BPADA-PMDA-MPD copolyetherimide (Ultem® 6000 series)..... 70
Figure 2.7 Medical equipment made from PEI 71
Figure 2.8 Computer and lightening components made from PEI 72
Figure 2.9 Dissipation factor vs. frequency of PEI at 50% RH 73
Figure 2.10 PEI-based components in automotive industry 74
Figure 2.11 Fluid handling components made from PEI 74
Figure 2.12 Interior cladding parts in aircrafts made from PEI 75
Figure 2.13 Schematics of allotropes of carbon-based nano-particles: carbon black (CB), single-wall carbon nanotubes (SWNT), multi-wall carbon nanotubes (MWCNT) and graphene 77
Figure 2.14 Electrical conductivity and EMI shielding efficiency of PEI-GnP foams 80
Figure 2.15 Tensile properties of PEI/graphene nanocomposite foams 81
Figure 2.16 (a) EMI shielding performance as a function of frequency in the 8–12 GHz range of the PEI/GnP@Fe_3O_4; (b) total EMI shielding effectiveness (SE_{total}), microwave reflection (S_{ER}) and microwave absorption (S_{EA}) of microcellular foams at 9.6 GHz 83
Figure 3.1 PEI Ultem 1000 repetitive unit 149
Figure 3.2 PEI Ultem 1000 bar 149
Figure 3.3 PAI Torlon 4203 repetitive unit 151
Figure 3.4 PAI Torlon 4203 bar 151
Figure 3.5 Visual comparison of GnP dispersion in organic solvents 154

Figure 3.6 Photograph of the melt mixing equipment (Brabender Plastic-Corder W50 EHT) (a) General view, (b) Temperature and rotation speed/direction control and (c) chamber 156
Figure 3.7 Schematic of WVIPS foaming process 158
Figure 3.8 Schematic of one-step foaming using $scCO_2$ dissolution 159
Figure 3.9 Photograph of sputter coater used for sample preparation prior to SEM 160
Figure 3.10 Photograph of scanning electron microscope used for morphological analysis 161
Figure 3.11 Photograph of X-ray diffraction equipment 162
Figure 3.12 Double-furnace differential scanning calorimetry equipment 164
Figure 3.13 Single-furnace differential scanning calorimetry equipment 164
Figure 3.14 Photograph of thermogravimetric equipment used for thermal degradation analysis 164
Figure 3.15 Dynamic mechanical thermal analysis equipment with single cantilever configuration 166
Figure 3.16 Voltage source and sample configuration used for electrical conductivity measurements 168

Chapter 1

Introduction, context and general objective

1.1 Investigation antecedents

This dissertation is written in partial fulfilment of requirements for the degree of Doctor of Philosophy in Department of Materials Science and Metallurgy (CMEM) at Universitat Politècnica de Catalunya (UPC. BarcelonaTech). Major portions of both experimental and theoretical aspects of this thesis were carried out in the Centre Català del Plàstic (CCP) in Terrassa, Barcelona, Spain. Additionally, some parts of the experimental procedures were performed at the Department of Materials Science and Metallurgy of the School of Industrial, Aerospace and Audiovisual Engineering of Terrassa (ESEIAAT).

This project is a continuation of the research developed at the CCP in the Polyfunctional Polymeric Materials (POLY2) research group led by Prof. José Ignacio Velasco in order to advance on the study of multifunctional lightweight polymer nanocomposite foams. Deep insight into polymeric composites based on thermoplastics such as polypropylene (PP), polyethylene (PE), polystyrene (PS), styrene-acrylonitrile copolymer (SAN), poly (methyl methacrylate) (PMMA) and polycarbonate (PC) have already been provided by this group. Early works of POLY2 group were dedicated to the preparation and characterization of thermoplastic composites, resulting in doctoral thesis studying these polymers combined with various fillers, such as talc [1,2], glass micro-spheres [3,4], magnesium and aluminum hydroxides [5,6], hydrotalcite (HT) and montmorillonite (MMT) [5,7–9], alongside with numerous derivative publications.

During the last decade, the focus of this group was shifted towards multifunctional foams. The reason behind the focus on foaming was to provide weight reduction, improvement of thermal and/or acoustic insulation, impact energy absorption and enhancement of some specific properties. The combination of lightness and improved properties allows the redesign of components for multiple applications. Additionally, the addition of nanoparticles could counteract the drawbacks of foaming such as losses in mechanical properties and/or add functional characteristics depending on the properties of the pristine filler. In particular, carbon-based nanoparticles have raised a lot of attention due to their outstanding properties. Therefore, this group has developed various studies based on the addition of nano-size carbon-based fillers to foams of polyolefins (PP and PE in particular) and polycarbonate, which resulted in 2 dissertations investigating the effects of carbon nanofibers (CNF) [5] and graphene [10], as well as additional reviewed articles [11-22].

To go one step further, as the interest in lightweight materials arise in cutting edge sections of industry, the development and characterization of novel foams using **high performance polymers**, such as polyetherimide (PEI), polysulfone (PSU) and polyphenylsulfone (PPSU) could provide valuable knowledge for applications in automotive and aeronautic industries. Taking into account that PEI has proven itself as a viable candidate among high performance thermoplastics, it was considered as the main matrix in all foams prepared in this thesis.

Carbon-based nanofillers such as GnP and CNT have received great amounts of scientific attention in the past decade due to their outstanding properties. Furthermore, the incorporation of carbon-based

fillers, such as carbon nanotubes (CNT) and graphene nanoplatelets (GnP), could provide specific functionalities to these foams to serve advanced applications such as electromagnetic interference (EMI) shielding and electrostatic discharge (ESD).

As the first step towards developing this project, compatibility of various commercial forms of PEI (Ultem 1000 by Sabic and Vespel by DuPont) with multiple solvents, the foaming process and the addition of GnP to these foams were investigated in a Master thesis project entitled "Preparation and characterization of electrically conductive foams made of polyetherimide (PEI) filled with graphene nanoparticles". The obtained knowledge during this master thesis, with approximate duration of 9 months, formed the basic foundation for the study of high performance foams, which was further developed into a doctoral thesis, exploring the possibilities of these microcellular foams.

Since very few studies have been done regarding high performance and conductive polymeric foams, this thesis was planned and dedicated to investigate the preparation and characterization of foams based on PEI. Simultaneously, the effects of carbon-based nanoparticles additions such as GnP and CNT and blending with other polymers were investigated.

While developing the plan of this investigation, it was discovered that numerous possibilities could arise from variations in compositions and foaming techniques. To name a few, the effect of polymer concentration in the solvent on the cellular structure and electrical conductivity of the foams, the influence of applying ultrasonication on the dispersion level of nanoparticles and its eventual effects on the properties of the foams, foaming behavior of PEI-polyamide-imide (PAI) blends, and foaming process using supercritical carbon dioxide ($scCO_2$).

Ultimately, by investigating these factors and how they affect the final properties of the foams, it was considered that by optimizing them, various properties such as electrical conductivity and specific mechanical properties could be significantly improved for particular applications of these foams. As an example, previous studies showed that the combination of GnP and CNT nanofillers in foams resulted in a synergic effect improving the electrical conductivity of the foams using considerably lower concentration of these nanofillers [23–25].

1.2 Strategy and objectives of the research

In this dissertation, three main strategies were considered in order to achieve the principal objectives of the project. The global objective of this study was to develop and characterize a novel cellular nanocomposite based on polyetherimide reinforced with carbon nanoparticles, namely GnP and/or CNT. To do so, three main strategies were considered. Firstly, by blending PEI with other high performance polymers such as PAI, various aspects of the foams such as their mechanical properties could be improved.

Secondly, by using reinforcements such as GnP and CNT, functionalities like electrical conductivity could be introduced to these foams, as well as improving other aspects of the foams such as their mechanical and thermal properties.

Finally, the optimization of foaming methods could provide valuable knowledge on how to modify the foam's eventual cellular structure with regards to their application's requirements.

A schematic of these main strategies are presented in Figure 1.1.

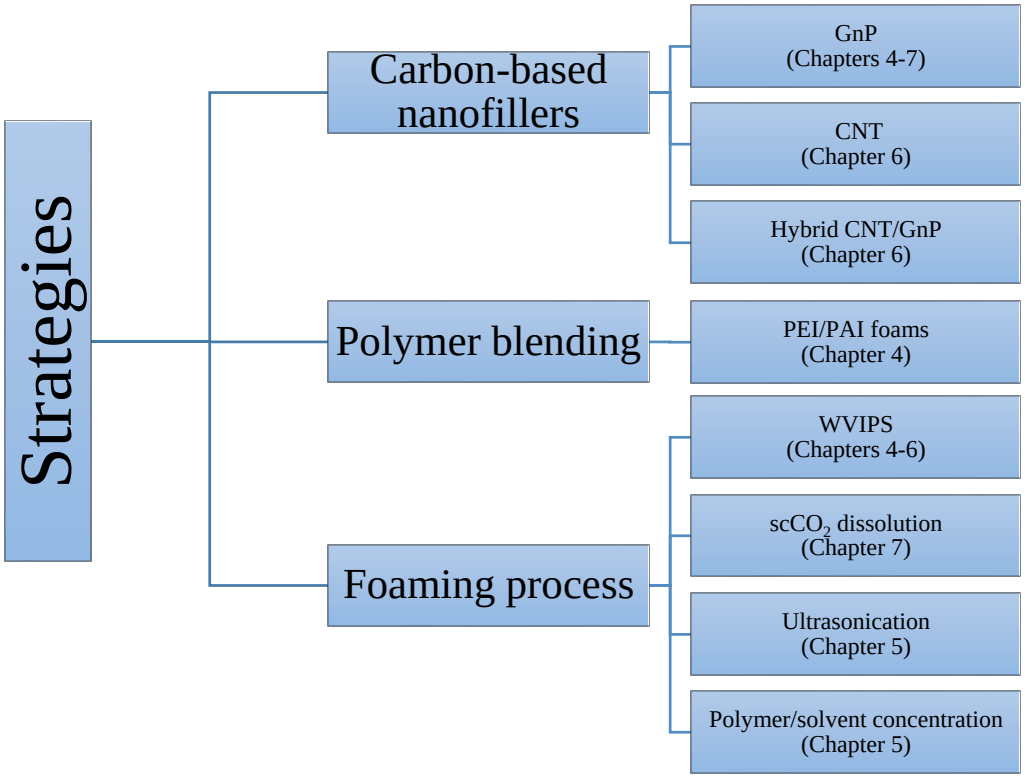

Figure 1.1 Considered strategies to reach the principal goal of the thesis.

These strategies were designed in this manner to fulfill the principal objectives of this study through the tasks presented below:

- **Investigation of carbon-based nanoparticles influence on the properties of PEI foams through:**
  - Preparation of PEI foams reinforced with graphene nanoparticles using WVIPS method and characterization of their cellular structure and morphology, mechanical and thermal properties and electrical conductivity.

- Investigating the effects of changes in the composition of the foams on the final characteristics of the foams.

- **Preparation and characterization of polymer blends based on high performance thermoplastics such as PEI and PAI through:**

  - Investigation of high performance thermoplastic blends and their compatibility with PEI and its effect on the foaming behavior of PEI.
  - Characterization of blend foams in terms of their cellular structure, mechanical and thermal properties.

- **The effect of various foaming methods and the variables involved on the cellular structure, mechanical and thermal properties and electrical conductivity of the foams through:**

  - Analysis of the results from both WVIPS and high pressure supercritical CO_2 ($scCO_2$) dissolution foaming methods and their effects on the final properties of the foams.
  - Investigating the effects of nanoparticles incorporation on both WVIPS and $scCO_2$ dissolution foaming processes.
  - Investigate the effects of variables such as polymer/solvent concentration and the application of ultrasonication on the properties of the foams.

1.3 Research structure and scientific production

The structure of this dissertation is based on compendium of articles published during the 5-year research and includes eight chapters dedicated to the development of PEI-based foams with various compositions and foaming methods.

- **Chapter 1. Introduction, context and general objective.**

  The present chapter includes a brief introduction to the history of the previous works of this research group, the objectives of the thesis and the main strategies in order to meet the principal goals of this project.

- **Chapter 2. State of the art.**

  This chapter considers of the main concepts and previous works related to this work including two publications:

1- Book chapter titled "Polyimides" authored by Hooman Abbasi, Marcelo Antunes, and José Ignacio Velasco. Chapter 16, 491-531 of Handbook of Thermoplastics (2nd Edition) edited by Olagoke Olabisi, Kolapo Adewale and published by CRC Press, Taylor & Francis Group in 2015.

2- Review article titled "Recent advances in carbon-based polymer nanocomposites for electromagnetic interference shielding" authored by Hooman Abbasi, Marcelo Antunes, and José Ignacio Velasco. Published in Progress in Materials Science, 103, 319-373 in 2019 with an impact factor of 23.750.

- **Chapter 3. Materials and experimental procedure.**

This chapter presents a resume of the experimental characterization procedures and equipment used in this study as well as the processes used for foam preparation. Additionally, it provides the basic information about the virgin materials used during the development of this work.

- **Chapter 4. The WVIPS foaming method:**
  PEI, PEI-GnP and PEI/PAI microcellular foams.

This chapter presents the results of initially developed PEI, PEI-GnP and PEI/PAI nanocomposite foams and the characterization of their mechanical, thermal, morphological and electrical properties. Two peer-reviewed articles are included in this chapter:

1- Article titled "Graphene nanoplatelets-reinforced polyetherimide foams prepared by water vapor-induced phase separation" authored by Hooman Abbasi, Marcelo Antunes, and José Ignacio Velasco. Published in eXPRESS Polymer Letters, 9(5), 412-423, 2015 with an impact factor of 3.064.

2- Article titled "Influence of polyamide–imide concentration on the cellular structure and thermo-mechanical properties of polyetherimide/polyamide–imide blend foams" authored by Hooman Abbasi, Marcelo Antunes, and José Ignacio Velasco. Published in European Polymer Journal 69(0), 273-283, 2015 with an impact factor of 3.741.

- **Chapter 5. Improving the microstructure through the solution concentration and GnP ultrasonication.**

Chapter 5 is dedicated to similar foams prepared by WVIPS method presented in the previous chapter with an improved microstructure and enhanced electrical conductivity, which was achieved through the variation of polymer/solvent ratios and the application of ultrasonication. This chapter includes the following peer-reviewed article:

1- Article titled “Enhancing the electrical conductivity of polyetherimide-based foams by simultaneously increasing the porosity and graphene nanoplatelets dispersion’ authored by Hooman Abbasi, Marcelo Antunes, and José Ignacio Velasco. Published in Polymer Composites, 40(S2), E1416-E1425, 2018 with an impact factor of 1.943.

- **Chapter 6. PEI foams with enhanced electrical conductivity through an optimized hybrid nanofiller system.**

In this chapter, the influence of different nanofiller contents is taken into account. The GnP and CNT reinforcements have obvious effects on the structure, mechanical properties, thermal properties and electrical conductivity of the foams. One peer-reviewed article is included in this chapter:

1- Article titled “Effects of carbon nanotubes/graphene nanoplatelets hybrid systems on the structure and properties of polyetherimide-based foams” authored by Hooman Abbasi, Marcelo Antunes, and José Ignacio Velasco. Published in Polymers, 10(4), 1-22, 2018 with an impact factor of 2.935.

- **Chapter 7. Enhancing the electrical conductivity through high pressure scCO_2 dissolution process.**

This chapter is dedicated to the preparation and characterization of foams by dissolution of supercritical CO_2 using a high pressure vessel. The effects of foaming technique on the properties of the foams are discussed in this section. This chapter includes the following peer-reviewed article:

1- Article titled “Polyetherimide foams Filled with low content of graphene nanoplatelets prepared by scCO_2 dissolution” authored by Hooman Abbasi, Marcelo Antunes, and José Ignacio Velasco. Published in Polymers 11(2), 328, 2019 with an impact factor of 2.935.

- **Chapter 8. General discussion, conclusions and future studies.**

In this final chapter, a general discussion of the results, main conclusions of this work and possible paths for continuation of this research is presented.

Besides the published articles mentioned previously in each chapter, various **international conference** presentations were derived from this study, which are presented below:

1- The 3rd Edition of the European Graphene Forum, Paris, France, 2017. Presentation titled “Conductive lightweight composites of polyetherimide with graphene Nanoplatelets-Carbon Nanotube Hybrids” authored by Marcelo Antunes, Hooman Abbasi and José Ignacio Velasco.

2- 5th International Conference on Multifunctional, Hybrid and nano materials, Lisbon, Portugal, 2017. Presentation titled "Structure-properties relationships of electrically conductive nanocomposite foams" authored by Marcelo Antunes, Gabriel Gedler, Hooman Abbasi and José Ignacio Velasco.

3- 21st International Conference on Composite structures, Bologna, Italy, 2018. Presentation titled "Structure and physical properties of PEI foams containing low amounts of graphene nanoplatelets prepared by supercritical CO_2 dissolution" authored by Hooman Abbasi, Marcelo Antunes, and José Ignacio Velasco.

Moreover, this work was a part of financed projects awarded by the Spanish Ministry of Economy and Competitiveness in form of the following projects:

1- Project **MAT2014-56213-P** titled "Polymeric Foams and Multifunctional Cellular Composite Materials" for a duration of two years starting from 2014.

2- Project **MAT2017-89787-P** titled "Multifunctional Polymeric Foams based on high temperature thermoplastics" for a duration of 4 years starting from 2017.

There were two more publications which were not included in this thesis but were derived as the results of this work paved a path for further research in this field.

1- Article titled "Graphene Nanoplatelets as a Multifunctional Filler for Polymer Foams" authored by Marcelo Antunes, Gabriel Gedler, Hooman Abbasi and José Ignacio Velasco. Published in the journal of Materials Today: Proceedings, 3(2), 233-239, 2016.

2- 19th International Metallurgy and Materials Congress, Istanbul, Turkey, 2018. Presentation titled "Preparation of Nanocomposite Foams Based on Polysulfone and Carbon-based Nanoparticles Using WVIPS" authored by Mustafa Kerem Yücetürk, Hooman Abbasi, Marcelo Antunes, S. Aydin, José Ignacio Velasco.

1.4 References

1. Velasco Perero, J. I. Fractura de compuestos polipropileno-talco, Universitat Politècnica de Catalunya, Doctoral thesis, 1996.
2. Gordillo, A. Influencia de la inyección sobre el comportamiento mecánico de compuestos de polipropileno, Universitat Politècnica de Catalunya, Doctoral thesis, 2000.
3. Sánchez Soto, M. Comportamiento mecánico y fractura de mezclas de poliestireno y microesferas de vidrio, Universitat Politècnica de Catalunya, Doctoral thesis, 2000.
4. Arencón Osuna, D. Efectos de la incorporación de polietilentereftalato sobre la estructura y propiedades mecánicas de materiales compuesto polipropileno-vidrio, Universitat Politècnica de Catalunya, Doctoral thesis, 2003.
5. Sousa Pais Antunes, M. de Preparación y caracterización de espumas multifuncionales a base de nanocompuestos de poliolefinas, Universitat Politècnica de Catalunya, Doctoral thesis, 2010.
6. Morhain, C. Microestructura y propiedades mecánicas de compuestos de polipropileno con hidróxido de magnesio y aluminio moldeados por inyección, Universitat Politècnica de Catalunya, Doctoral thesis, 2001.
7. Ardanuy, R. M. Síntesis y Caracterización de Nanocompuestos de Poliolefinas e Hidróxidos dobles Laminares, Universitat Politècnica de Catalunya, Doctoral thesis, 2007.
8. Franco-Urquiza, E. Preparación y caracterización de nanocompuestos EVOH/Montmorillonita, Universitat Politècnica de Catalunya, Doctoral thesis, 2009.
9. De Redondo Realinho, V. C. Caracterización estructural, térmica y mecánica de nanocompuestos termoplásticos de matriz amorfa (PS, SAN y PMMA), preparados por mezcla en fundido, con partículas laminares de hidrotalcita y montmorillonita modificadas, Universitat Politècnica de Catalunya, Doctoral thesis, 2009.
10. Gedler Chacón, G. E. Development of polycarbonate multifunctional foams with graphene nanoplatelets, Universitat Politècnica de Catalunya, Doctoral thesis, 2016.
11. Antunes, M.; Velasco, J. I.; Realinho, V.; Arencón, D. Characterization of carbon nanofibre-reinforced polypropylene foams. *J. Nanosci. Nanotechnol.* 2010, *10*, 1241–1250.
12. Antunes, M.; Realinho, V.; Velasco, J. I. Foaming behaviour, structure, and properties of polypropylene nanocomposites foams. *J. Nanomater.* 2010, 4.
13. Gedler, G.; Antunes, M.; Velasco, J. I. Enhanced electrical conductivity in graphene-filled polycarbonate nanocomposites by microcellular foaming with sc-CO_2. *J. Adhes. Sci. Technol.* 2016, *30*, 1017–1029.
14. Gedler, G.; Antunes, M.; Velasco, J. I.; Ozisik, R. Enhanced electromagnetic interference shielding effectiveness of polycarbonate/graphene nanocomposites foamed via 1-step supercritical carbon dioxide process. *Mater. Des.* 2016, *90*, 906–914.
15. Antunes, M.; Realinho, V.; Solórzano, E.; Rodríguez-Pérez, M. A.; de Saja, J. A.; Velasco, J. I.

Thermal conductivity of carbon nanofibre-polypropylene composite foams. In *Defect and Diffusion Forum*; Trans Tech Publ, 2010; 297, 996–1001.

16. Antunes, M.; Mudarra, M.; Velasco, J. I. Broad-band electrical conductivity of carbon nanofibre-reinforced polypropylene foams. *Carbon N. Y.* 2011, *49*, 708–717.
17. Gedler, G.; Antunes, M.; Realinho, V.; Velasco, J. I. Thermal stability of polycarbonate-graphene nanocomposite foams. *Polym. Degrad. Stab.* 2012, *97*, 1297–1304.
18. Gedler, G.; Antunes, M.; Realinho, V.; Velasco, J. I. Novel polycarbonate-graphene nanocomposite foams prepared by CO2 dissolution. In *IOP Conference Series: Materials Science and Engineering*; IOP Publishing, 2012; 31, 2008.
19. Antunes, M.; Gedler, G.; Velasco, J. I. Multifunctional nanocomposite foams based on polypropylene with carbon nanofillers. *J. Cell. Plast.* 2013, *49*, 259–279.
20. Gedler, G.; Antunes, M.; Velasco, J. I. Graphene-induced crystallinity of bisphenol A polycarbonate in the presence of supercritical carbon dioxide. *Polymer.* 2013, *54*, 6389–6398.
21. Antunes, M.; Realinho, V.; Gedler, G.; Arencón, D.; Velasco, J. I. Diffusion of CO_2 in Polymer Nanocomposites Containing Different Types of Carbon Nanoparticles for Solid-State Microcellular Foaming Applications. *J. Nano Res.* 2014, *26*.
22. Gedler, G.; Antunes, M.; Velasco, J. I. Effects of graphene nanoplatelets on the morphology of polycarbonate–graphene composite foams prepared by supercritical carbon dioxide two-step foaming. *J. Supercrit. Fluids* 2015, *100*, 167–174.
23. Li, P. S. and L. L. and S. F. and Y. Y. and C. J. and Q. W. and Y. Z. and Q. Striking multiple synergies created by combining reduced graphene oxides and carbon nanotubes for polymer nanocomposites. *Nanotechnology* 2013, *24*, 125704.
24. Al-Haik, M. S. and M. Electrical conductivity of synergistically hybridized nanocomposites based on graphite nanoplatelets and carbon nanotubes. *Nanotechnology* 2012, *23*, 405202.
25. Yue, L.; Pircheraghi, G.; Monemian, S. A.; Manas-Zloczower, I. Epoxy composites with carbon nanotubes and graphene nanoplatelets – Dispersion and synergy effects. *Carbon N. Y.* 2014, *78*, 268–278.

Chapter 2

State of the art

2.1 Basic concepts of foams

New applications of cellular materials alongside with the development of foaming methods have provided a variety of possibilities regarding thermoplastic foams. A foam consists of at least two phases, a solid continuous phase and a gaseous phase. Among all cellular materials, polymeric foams in particular could provide weight reduction, thermal barrier effect, energy absorption, high specific strength, etc. For this reason, foam's applications have reached many sectors of industries such as, transportation, building, thermal and acoustic insulators among many others. These applications mainly seek for specific foams with tailored properties based on their composition, cellular structure and consequently their physical properties.

Regarding the polymers used for preparation of cellular materials, they could be categorized in three main groups.

- Thermoset foams such as polyurethane (PU) or phenolics.
- Thermoplastic foams such as PS, PE, PP, PC.
- Elastomeric foams such as rubber blends.

Each group is capable of delivering some specific properties such as low thermal conductivity, flexibility or rigidity and fire resistance. Additionally, facile installation of some of these foams allows them to be considered by the providers who need to go through an extensive selection process in order to optimize both cost effectiveness and performance of their product.

2.1.1 Foam structure, foaming methods and applications

With respect to the foam's cellular structure, the first criteria referred to when classifying foams is whether they have open or close-cell structure. Existing foams could consist of closed-cell where cells are individually isolated from their neighbors by the continuous phase or of open-cells where the cell struts provide a connected path among cells (see Figure 2.1); The cellular structure could be a combination of these two resulting in a partially open or closed-cell structure which could be altered by composition, foaming method and possible post-processing steps.

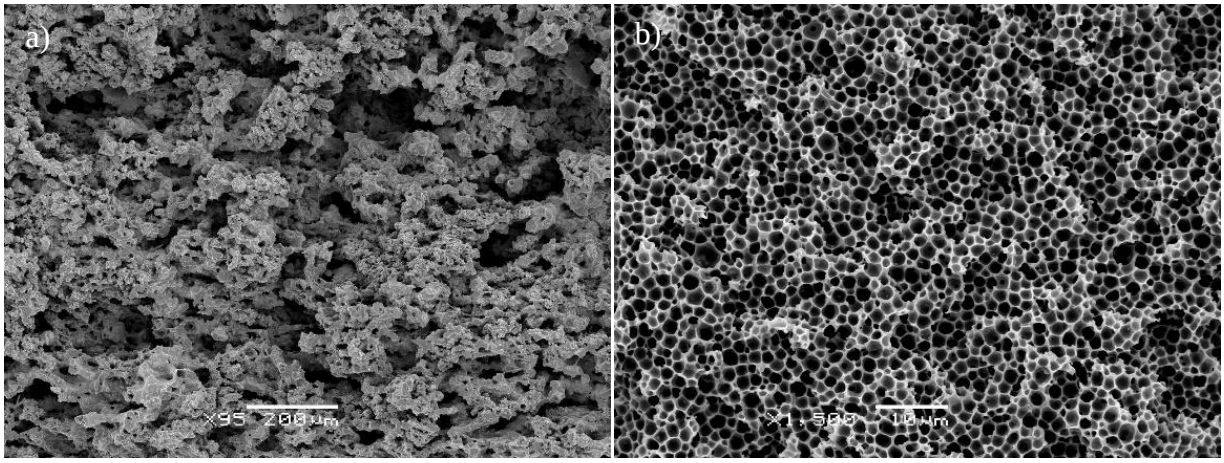

Figure 2.1 Cellular structure of a) open-cell and b) closed-cell foams

Other important parameters when studying the cellular structure of the foams include solid and foam density, relative density, expansion ratio (ER), porosity, average cell size (Φ) and its distribution, cell orientation (isotropy/anisotropy), cell nucleation density and cell density (N_0 and N_f, respectively). Solid density is equal to the density of virgin material when the foam consists of only one component. In case of composite foams, the solid density could be measured directly from the prepared unfoamed composites or it could be calculated theoretically using:

$$\rho_s = V_1\rho_1 + V_2\rho_2 + \cdots \tag{2.1}$$

Where ρ_s is the density of unfoamed composite (g/cm^3), V_n is the concentration of a component in volume percentage and ρ_n represents its respective density (g/cm^3). The density of the foamed material could be measured and calculated according to the ISO-845 standard procedure where the dimension and mass of a representative part of foam is measured and later placed in:

$$\rho = \frac{m}{V} \tag{2.2}$$

Where ρ is the density of the foam (g/cm^3), m is the respective mass of the sample (g) and V is its volume (cm^3). The density value plays a key role on classification of the foams. Particularly, considering the typical values of polymeric foams, they could be categorized in:

- Low density foams (ρ <0.05 g/cm^3 or 50 kg/m^3)
- Intermediate density foams (0.05 < ρ < 0.18 g/cm^3 or 50 < ρ < 180 kg/m^3)
- High density foams (ρ > 0.18 g/cm^3 or ρ > 180 kg/m^3)

Consequently, the relative density (ρ_{rel}), ER and porosity could be calculated respectively as follows:

$$\rho_{rel} = \frac{\rho}{\rho_s} \tag{2.3}$$

$$ER = \frac{\rho_s}{\rho} \tag{2.4}$$

$$Porosity(\%) = \left(1 - \frac{\rho}{\rho_s}\right) \times 100 \tag{2.5}$$

Relative density is unquestionably the most important feature of the foam since various properties could be related and predicted knowing the original properties of the unfoamed material. Although foams usually present inferior mechanical and transport properties (electrical conductivity and thermal conductivity), they can provide a significant improvement when considering their specific properties which is related to their density. Therefore, as the model presented by Gibson and Ashby [1] an estimation of foam's properties could be achieved with regards to respective properties of the solid material using:

$$\frac{P}{P_s} = C\left(\frac{\rho}{\rho_s}\right)^n \tag{2.6}$$

In this model, *C* represents the geometry constant of proportionality and is commonly assumed to be equal to 1. The value of *n* is commonly in between 1 and 2, where 1 represents the linear behaviour of foam's property as a function of its density, and 2 showing a more abrupt reduction of the respective property by reducing the density. Therefore, the preparation of microcellular closed-cell foams with *n* value equal to 1 has gained considerable importance during the past decade [2].

Regarding the cell size of foams, they could be classified into different groups:

- Macrocellular foams (ϕ >100 μm),
- Microcellular foams (1 < ϕ < 100 μm),
- Sub-microcellular foams (0.1 < ϕ < 1 μm),
- Nanocellular foams (0.1 < ϕ < 100 nm).

The average cell size value is one of the factors in determining the final properties of the foams. As an example, Miller *et al.* [3,4] have prepared and characterized PEI-based foams with microcellular and nanocellular structure. They claimed that although the nanocellular structure did not affect the foam's tensile modulus and its yield stress in the same density range, but the decrease in cell size led to significant increment of toughness and enhanced impact resistance due to their increased ductility.

Regarding the cell orientation, since most of physical foaming techniques result in a directional expansion of the polymer, it is safe to assume that the properties of such foams are not unidirectional. On the other hand, in case of homogeneous isotropic cellular structures, most of the properties of these foams would have unidirectional criteria.

One of the main industrial foaming methods is using a blowing agent to obtain the gaseous phase in a polymer. The blowing agent could define the final properties of the foam by controlling the density. It can also alter the cellular structure of the foam which could affect the eventual properties of the foams as mentioned before. Particularly, the blowing agent's characteristics play an important role in closed-cell foams as it could be encapsulated within cellular structure.

Blowing agents can be mainly categorized into two groups: Physical blowing agents (PBAs) such as hydrocarbons and inert gases and chemical blowing agents (CBAs) which are usually derive from a chemical reaction or a thermal decomposition. In the case of physical blowing agents, halogenated hydrocarbons such as chlorofluorocarbons (CFCs) and hydrochlorofluorocarbons (HCFCs) were vastly used in the past, however, their environmental impact was criticized heavily and therefore phased out in most regions. Although hydrofluorocarbons (HFC) were suggested as a proper replacement of CFC and HCFC, thanks to lack of chlorine in their structure, their usage was limited due to their high cost, global warming potential, and relatively less effective in insulation performance when compared to its predecessors (CFC and HCFC) or chemically inert gases such as CO_2 and N_2 [5]. Additionally, water has also showed promising results as a blowing agent (both chemical and physical) for polymers such as PU [6–8], PS [9,10] and PC [11].

Physical blowing agents can be introduced in various stages of foam preparation with various pressure and temperature conditions. Foaming occurs by volatilisation of a liquid or the release of gas during depressurization. For foams prepared by extrusion or injection, the blowing agent is usually introduced during the melting stage at high pressure and afterwards, a rapid depressurization results in the expansion of the material while solidifying. In the injection process the nucleation of cells occurs in the mold while in extrusion process, the depressurization takes place while the polymer/gas mixture leaves the die.

Chemical blowing agents provide gas(es) during the foaming process either by a thermal decomposition or a chemical reaction. Although CBA's gas liberation generally costs 10 times more than the gases themselves, their usage is justified in smaller processing lines since they require minimum modification to the production line of thermoplastic foams, and they do not require any special storage or handling equipment. Additionally, they could be simply introduced by blending with the plastic or simply fed directly to the hopper [5]. On the other hand, their cost over time and the residual byproducts that continues to remain in the material are their main disadvantages [12]. Their reaction could be exothermic or endothermic depending on their characteristic and formula. Various CBAs are presented in the table below accompanied by their characteristics required for their processing.

Table 2.1 Chemical blowing agents and their characteristics. modified from [5]

Description	Type	Decomposition temperature (°C)	Gases
Azodicarbonamide	Exo	200-230	N_2, CO, NH_3, O_2
4,4-Oxybis(benzenesulfonyl- hydrazide)	Exo	150-160	N_2, H_2O
P-Toluenesulfonylhydrazide	Exo	110-120	N_2, H_2O
P-Toluenesulfonylsemicarbazide	Exo	215-235	N_2, CO_2
Dinitrosopentamethlenetetramine	Exo	195	N_2, NH_3, HCHO
Polyphenylene sulfoxide	Exo	300-340	SO_2, CO, CO_2
Sodium bicarbonate	Endo	120-150	CO_2, H_2O
Zinc carbonate	Endo		CO_2
Citric acid derivatives	Endo	200-220	CO_2, H_2O
5-Phenyltetrazole	Endo	240-250	N_2

The process of foaming using a blowing agent could follow a continuous or discontinuous path. Either way, cell nucleation occurs by liberation of a gas triggered due to an increase in temperature or sudden drop of pressure. Continuous and semi-continuous processes provide a better time efficiency using extrusion or injection molding where the nucleation of cells take place while the polymer/gas mixture leaves the die or enters the mold. Due to sudden depressurization, the material expands following a stabilization step by cooling.

A discontinuous process to obtain microcellular foams was introduced by Martini *et al.* [13] as a result of a master project at Massachusetts Institute of Technology which was patented afterwards. In this process, the dissolution of gas takes place while the polymer is at its solid or semi-solid state by introducing the gas into a high pressure vessel containing the polymer at a temperature below its T_g. When the diffusion of gas in precursor reaches its equilibrium state, the sample is removed and heated, usually using an oil based hot bath or hot plate to a temperature above its T_g, resulting in nucleation of cells. Additionally, foams could be obtained by increasing the temperature of high pressure vessel to the T_g of the base polymer or above during the saturation period and induce the expansion by sudden depressurization after saturation of the precursor with the dissolved gas. This method is commonly referred to as one-step or batch foaming (see Figure 2.2).

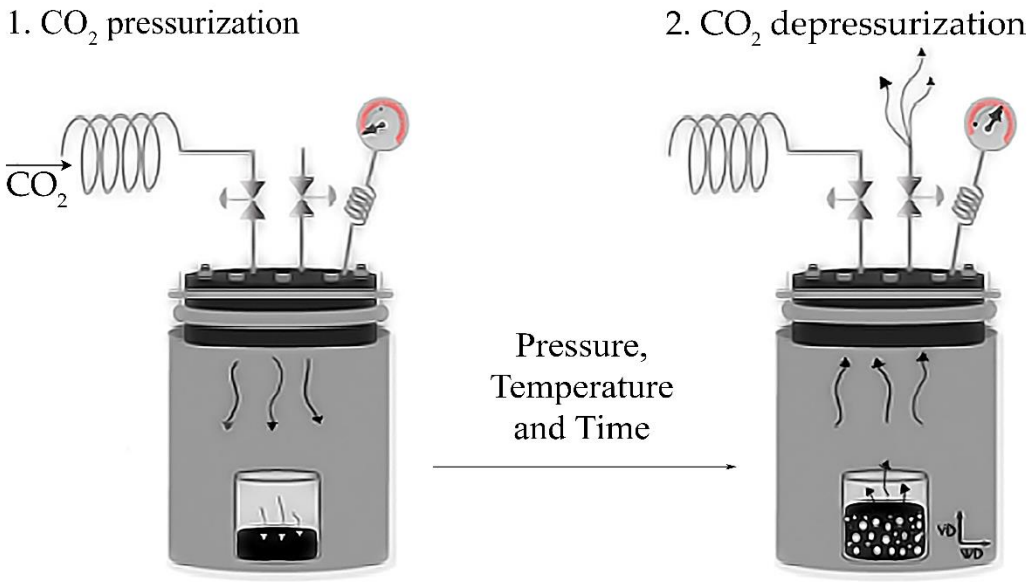

Figure 2.2 Schematic of one-step foaming using $scCO_2$ dissolution in a high pressure vessel. Adapted from [14].

Supercritical carbon dioxide ($scCO_2$) is commonly used in this foaming method due to its low cost, non-toxicity, non-flammability, chemical inertness and mild supercritical conditions (T = 31°C, P = 7.4 MPa) [15]. Moreover, this method has shown promising results in the formation of homogeneous microcellular foams with closed-cell structure, which enhances the mechanical properties of the foam in comparison with unevenly distributed cells or foams with an open-cell structure [16,17].

Another foaming method used mainly to prepare foams is phase separation. The principal of this foaming technique was initially introduced during the late 1950s as a method to prepare membranes for sea water demineralization by Loeb and Sourirajan [18]. Particularly, water vapor induced phase separation (WVIPS) is commonly used for producing polymeric membranes. This method simply consists in a polymer/solvent solution being poured into a recipient and then exposed to a non-solvent to provoke the phase exchange.

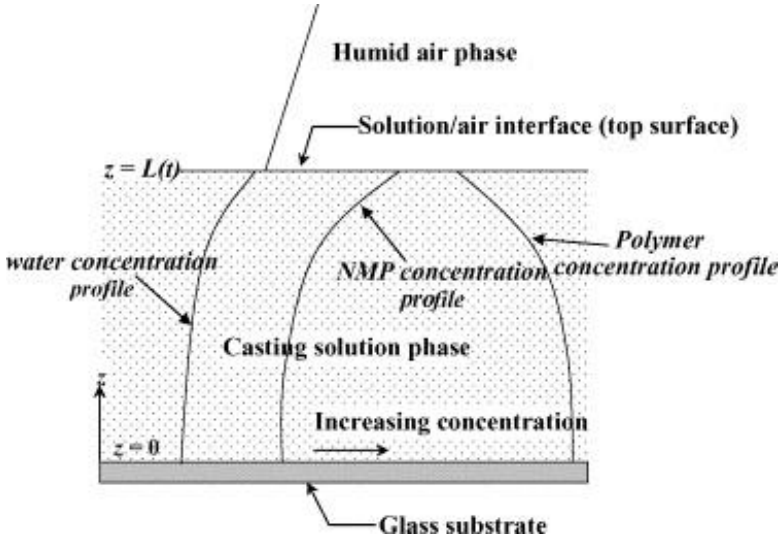

Figure 2.3 Schematic of the phase inversion processes occurring during the humid air exposure. Adapted from [19].

Water is a usual non-solvent used in this method which could be provided by humid air or immersion into a water bath. The schematic presented in Figure 2.3 shows a solvent/polymer casted film with an initial thickness of L_0 at time t=0. As can be seen in this process the transfer of water occurs as a function of time and thickness, meaning that the inversion takes longer by increasing the thickness of the sample. Simultaneously, the solvent would be expelled from the structure or evaporate at the surface leaving a cellular structure filled with water.

In order to gasp the importance of foams and more specifically, the high performance polymeric foams such as ones based on polyetherimide, this section presents a brief insight into their principal applications.

Traditional foams are commonly known for their weight reduction and providing specific properties such as sound and thermal insulation, energy absorption and buoyancy. Taking advantage of their low thermal conductivity, they could provide applications such as insulation for booster rockets, modern buildings, transport vehicles in order to promote significant reduction in energy consumption. Another application of traditional foams is their usage in packaging, exploiting their energy absorption properties in order to protect the content from any possible external stress. Additionally, being light weight is an essential characteristic for packing since it results in major savings in handling and shipping costs. The usage of foams in structural applications by mankind is historically inspired by natural structural cellular such as wood and bones leading to modern designs of sandwich panels and honeycomb structures. The usage of cellulose acetate foams in deHavilland Mosquito bomber and sandwich panels made of glass and carbon fibers and aluminum honeycombs in modern airplanes are some examples of their structural applications providing significant enhancement in strength and weight reduction. Closed-cell foams can

also be used in floating structures due to their buoyancy retaining ability even when damaged. Furthermore, their chemical resistance prevents any corrosion in extreme environments [1].

Some other specific applications of the foams include membrane production. An open-cell or porous structure can be used in separation. For instance, polytetrafluoroethylene (PTFE) microporous membrane is used as a breathing fabric in high-end sportswear, which thanks to its hydrophilic properties, allows the passage of air while preventing water to pass [20]. These properties are also useful in artificial skin provided for protection of damaged skin by allowing the passage of air during the recovery of burned tissue. Another application of cellular materials is damping panels in ceiling and walls of theaters [1].

In terms of more advanced applications, the addition of conductive fillers such as carbon-based nanofillers to foams could introduce variety of applications such as electrostatic discharge (ESD) (in fuel system components, packaging materials for ESD sensitive items, etc.) and electromagnetic interference (EMI) shielding (in fuel cells, gaskets for electronic devices, among others).

Among high performance polymers, PEI-based foams have been investigated for electrical conductivity and electromagnetic shielding. Ling et al. [21] reported a facile approach to produce lightweight microcellular PEI/graphene nanocomposite foams with a density of about 0.3 g/cm^3 by WVIPS in which the in-situ generated extensional flow induced the re-dispersion and re-orientation of graphene nanoplatelets located on the cell walls, decreasing the electrical percolation concentration and increasing the specific EMI shielding efficiency.

Additionally, Shen et al. [22] have suggested a theory of multiple reflection as the absorbing mechanism, which mainly consist of reflection at multiple interfaces or surfaces of conducting nanofillers in foams. As illustrated in Figure 2.4, the microcells in the PEI/graphene@Fe_3O_4 foams provided a large cell-matrix interface area. The emitted electromagnetic waves entering the composite foam could be continuously reflected and scattered between these interfaces, and limiting their escape from the composite foam until being dissipated as heat. In addition, the layered structure and high aspect ratio of the filler can cause the multiple reflection as demonstrated in Figure 2.4 (b) and (c).

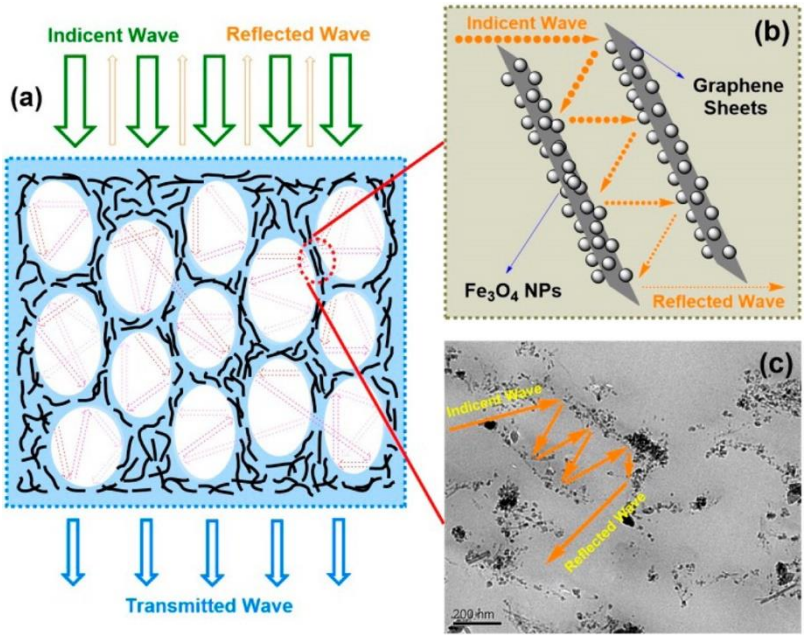

Figure 2.4 (a) Schematic of electromagnetic wave transfer through PEI/graphene@Fe_3O_4 foams; (b) Schematic diagram demonstrating the multireflection path of electromagnetic wave between the graphene@Fe_3O_4 laminates; (c) TEM image showing the possible reflection path of an electromagnetic wave between two parallel graphene@Fe_3O_4 sheets. Adapted from [22].

Gedler et al. [23,24] have suggested that the EMI shielding properties of PC/graphene nanocomposite foams could be enhanced with augmenting cell size, which promoted a random orientation of graphene nanoparticles, while reflection remained the main EMI shielding mechanism. They also revealed that the EMI shielding efficiency values were slightly higher in PC/graphene foams prepared by one-step batch foaming using $scCO_2$ dissolution than that of foams with considerably lower relative densities prepared by two-step foaming method due to formation of larger cells. Other researches represented that increasing the filler content will result in an increase of both reflection and absorption-based EMI shielding at relatively low filler contents, whereas at higher conductive filler levels the reflection characteristics would be weakened while preserving a high absorption behavior [25].

2.1.2 References

1. Gibson, L.J.; Ashby, M.F. *Cellular solids: structure and properties*; Cambridge university press, 1999.
2. Kumar, V.; Nadella, K. V. Microcellular Foams. In *Handbook of polymer foams*; Eaves, D., Ed.; Rapa Technology Limited: Shawbury, Shopshire, United Kingdom, 2004; *25*, 243–268.
3. Miller, D.; Chatchaisucha, P.; Kumar, V. Microcellular and nanocellular solid-state polyetherimide (PEI) foams using sub-critical carbon dioxide I. Processing and structure. *Polymer.* 2009, *50*, 5576–5584.
4. Miller, D.; Kumar, V. Microcellular and nanocellular solid-state polyetherimide (PEI) foams using sub-critical carbon dioxide II. Tensile and impact properties. *Polymer.* 2011, *52*, 2910–2919.
5. Singh, S.N. Blowing Agents. In *Handbook of polymer foams*; Eaves, D., Ed.; Rapa Technology Limited: Shawbury, Shopshire, United Kingdom, 2004; *25*, 9–36.
6. Thirumal, M.; Khastgir, D.; Singha, N.K.; Manjunath, B.S.; Naik, Y.P. Effect of foam density on the properties of water blown rigid polyurethane foam. *J. Appl. Polym. Sci.* 2008, *108*, 1810–1817.
7. Gao, L.; Liu, Y.; Lei, H.; Peng, H.; Ruan, R. Preparation of semirigid polyurethane foam with liquefied bamboo residues. *J. Appl. Polym. Sci.* 2010, *116*, 1694–1699.
8. Xu, Z.; Tang, X.; Gu, A.; Fang, Z. Novel preparation and mechanical properties of rigid polyurethane foam/organoclay nanocomposites. *J. Appl. Polym. Sci. 106*, 439–447.
9. Crevecoeur, J.J.; Nelissen, L.; Lemstra, P.J. Water expandable polystyrene (WEPS): Part 1. Strategy and procedures. *Polymer.* 1999, *40*, 3685–3689.
10. Crevecoeur, J.J.; Nelissen, L.; Lemstra, P.J. Water expandable polystyrene (WEPS): Part 2. In-situ synthesis of (block) copolymer surfactants. *Polymer.* 1999, *40*, 3691–3696.
11. Peng, J.; Turng, L.-S.; Peng, X.-F. A new microcellular injection molding process for polycarbonate using water as the physical blowing agent. *Polym. Eng. Sci.* 2012, *52*, 1464–1473.
12. Berry, M. Microcellular Injection Molding. In *Applied plastics engineering handbook: processing and materials*; Kutz, M., Ed.; William Andrew: 225 Wyman Street, Waltham, 02451, USA, 2011; pp. 215–226
13. Martini-Vvedensky, J.E.; Suh, N.P.; Waldman, F.A. Microcellular closed cell foams and their method of manufacture 1984.
14. Gedler, G.; Antunes, M.; Realinho, V.; Velasco, J.I. Novel polycarbonate-graphene nanocomposite foams prepared by CO2 dissolution. In Proceedings of the IOP Conference Series: Materials Science and Engineering; IOP Publishing, 2012; *31*, 2008.
15. Cooper, A.I. Polymer synthesis and processing using supercritical carbon dioxide. *J. Mater. Chem.* 2000, *10*, 207–234.
16. Goren, K.; Chen, L.; Schadler, L.S.; Ozisik, R. Influence of nanoparticle surface chemistry and size on supercritical carbon dioxide processed nanocomposite foam morphology. *J. Supercrit. Fluids*

2010, *51*, 420–427.

17. Lee, L.J.; Zeng, C.; Cao, X.; Han, X.; Shen, J.; Xu, G. Polymer nanocomposite foams. *Compos. Sci. Technol.* 2005, *65*, 2344–2363.
18. Loeb, S.; Sourirajan, S. Sea Water Demineralization by Means of an Osmotic Membrane. In *Saline Water Conversion—II*; Advances in Chemistry; American Chemical Society: Washington, D.C., 1963; *38*, 117–132.
19. Khare, V.P.; Greenberg, A.R.; Krantz, W.B. Vapor-induced phase separation—effect of the humid air exposure step on membrane morphology: Part I. Insights from mathematical modeling. *J. Memb. Sci.* 2005, *258*, 140–156.
20. Venkatraman, P. Fibers for sportswear. In *Materials and technology for sportswear and performance apparel*; Hayes, S.G., Venkatraman, P., Eds.; CRC Press Boca Raton, FL, 2016.
21. Ling, J.; Zhai, W.; Feng, W.; Shen, B.; Zhang, J.; Zheng, W. ge Facile Preparation of Lightweight Microcellular Polyetherimide/Graphene Composite Foams for Electromagnetic Interference Shielding. *ACS Appl. Mater. Interfaces* 2013, *5*, 2677–2684.
22. Shen, B.; Zhai, W.; Tao, M.; Ling, J.; Zheng, W. Lightweight, Multifunctional Polyetherimide/Graphene@Fe_3O_4 Composite Foams for Shielding of Electromagnetic Pollution. *ACS Appl. Mater. Interfaces* 2013, *5*, 11383–11391.
23. Gedler, G.; Antunes, M.; Velasco, J.I.; Ozisik, R. Enhanced electromagnetic interference shielding effectiveness of polycarbonate/graphene nanocomposites foamed via 1-step supercritical carbon dioxide process. *Mater. Des.* 2016, *90*, 906–914.
24. Gedler, G.; Antunes, M.; Velasco, J.I.; Ozisik, R. Electromagnetic shielding effectiveness of polycarbonate/graphene nanocomposite foams processed in 2-steps with supercritical carbon dioxide. *Mater. Lett.* 2015, *160*, 41–44.
25. Liu, Z.; Bai, G.; Huang, Y.; Ma, Y.; Du, F.; Li, F.; Guo, T.; Chen, Y. Reflection and absorption contributions to the electromagnetic interference shielding of single-walled carbon nanotube/polyurethane composites. *Carbon N. Y.* 2007, *45*, 821–827.

2.2 Polyimides

2.2.1 Abstract

In this section, a detailed review of polyimides, their synthesis process, characteristics, blends and some of their applications are given.

One of the most popular synthesis processes for obtaining conventional polyimide through condensation is derived by thermal or chemical cyclodehydration using dianhydrides and diamines. Moreover, *N*-Silylated diamines reaction with dianhydrides at room temperature results in intermediate poly (amide trimethylsilyl ester)s, which could be converted to polyimides by subsequent imidization with the elimination of trimethylsilanol during heating. Polyimides with high thermal stability are commercially produced by the acylation of diamines utilizing semiesters of tetracarboxylic acid. High-molecular-weight aliphatic–aromatic polyimides on the other hand, are obtained by polycondensation of the salts derived from tetracarboxylic acids and aliphatic diamines at high temperatures and pressures. Additionally, the chemical dehydration of polyamic acids to polyimides through acetic anhydride and pyridine forms isoimide structure alongside with imide structures in the polymer backbone.

Furthermore, the synthesis of polyimides could be achieved through addition using the Diels–Alder reaction of a bisdiene and a bisdienophile resulting in linear high-molecular-weight polyimides. Linear poly(bismaleimidediamine)s could be synthesized from bismaleimides by means of Michael addition.

During the synthesis of polyimides via thermal or chemical dehydration, numerous chemical reactions, participate in polyimide formation, and/or dehydration take place. FT-IR, Raman and UV spectroscopies, as well as NMR spectroscopies are available methods for determining the molecular entities in the reaction systems and for a better understanding of the reaction processes. Additionally, crystal structure, morphology, and phase transition of organic-soluble and thermoplastic polyimides and oligomers have been studied by FT-IR, X-ray diffraction, electron diffraction, and transmission electron microscopy (TEM).

Polyimides can provide various functionalities including but not limited to gas permeability and permselectivity, photosensitivity, nonlinear optical properties, electrical insulation.

2.2.2 Published book chapter (Chapter 16 in 2nd edition of Handbook of Thermoplastics, 2016)

This section gives insight into the synthesis process, characterizations and some functionalities of polyimides. The book chapter included in this section is titled **Polyimides** which was published in **Handbook of thermoplastics** by **CRC press** in **2016**.

ATTENTION¡¡
Pages 27 to 67 of the thesis, containing this book chapter, are available at the editor's web
https://www.crcpress.com/Handbook-of-Thermoplastics/Olabisi-Adewale/p/book/9781466577220

2.3 Polyetherimides (PEI) and PEI-based foams

In this section, a brief introduction of high performance thermoplastic polyetherimide alongside with previous works on this polymer and its nanocomposites will be given. The following sections will be dedicated to a preview on the foams prepared using PEI and its composites, mainly focusing on carbon-based nanofillers used in these foams and their characteristics and applications.

Polyetherimide is one of the most advanced high performance thermoplastics in high-end applications thanks to its exceptional combination of high mechanical properties, chemical and flame resistance without the use of additives, thermal and dimensional stability, low smoke generation, smooth as-mold surface, and transparency [1]. It has proven itself as a suitable candidate in high-end industries such as aerospace, medical equipment and automotive.

General Electric Plastics (acquired by SABIC in 2007) introduced Ultem® polyetherimide thermoplastic in 1982 as an amorphous, high performance polymer. Early works of J.G. Wirth on development of this polymer in early 1970s resulted in a cost-effective synthesis process of PEI. The final step of the production consists of the imidization of diacid anhydride with *m*-phenylene diamine as shown in Figure 2.5 [2].

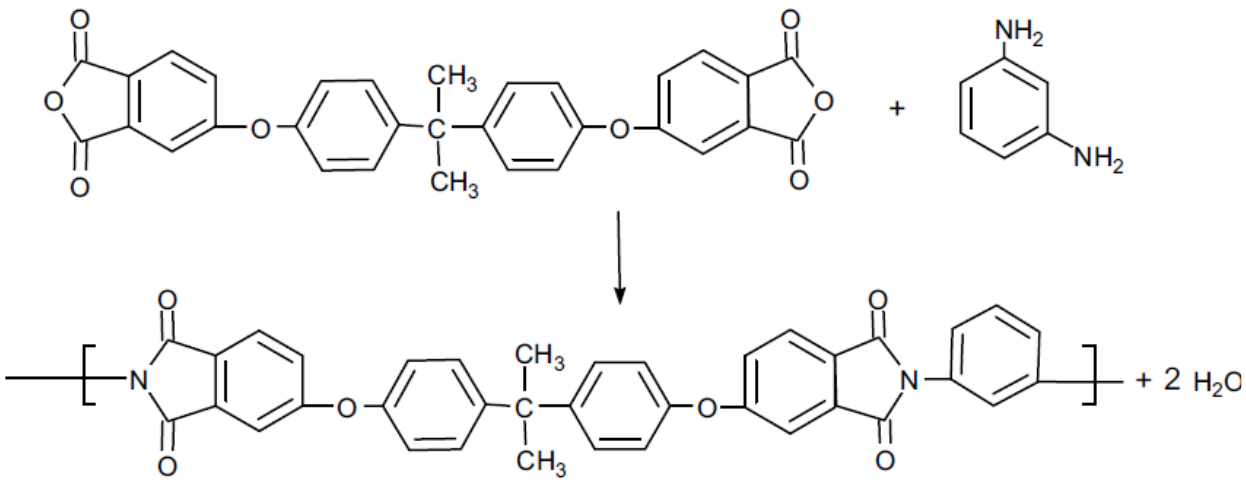

Figure 2.5 Last step in synthesis of polyetherimide. Adapted from [2].

The ether link in the PEI structure provides flexibility while retaining the aromatic imide characteristics of exceptional mechanical and thermal properties [3]. Beside its outstanding combination of properties, PEI has the processability of traditional engineering thermoplastics such as ABS and PC, however a higher melt temperature is required, its thermal stability provides a stable melt viscosity after several regrinds and remolding and it could be processed using most existing equipment [4].

A more recent development in PEI production by SABIC has resulted in a new amorphous thermoplastic containing sulfone group by commercial name of Extem XH® with a T_g of 249°C and outstanding dimensional stability, stiffness and creep resistance at high temperatures [5]. This grade of PEI has potential for preparation of composites, fibers, high temperature powder coating and other application in sectors such as optoelectronics. They also make copolymers based on PEI with polysiloxane with a commercial name of Siltem® with more flexibility when compared to its PEI cousins [6]. Some of the commercial thermoplastic PEI and PEI based polymers are listed in the table below:

Table 2.2 Commercial PEI thermoplastics. Gathered from datasheets of SABIC, Mitsui and DuPont Chemicals

Manufacturer	**Trade name**	**Product code**	**T_g (°C)**	**T_M (°C)**	**Melt flow rate (g/10 min @ 337°C/6.6kgf)**
GE (SABIC)	Ultem®	1000/1010/1100	217	350-400	9
GE (SABIC)	Ultem®	5001/5011	227	360-410	17.8
GE (SABIC)	Ultem®	6202	235	370-410	N/A
GE (SABIC)	Ultem®	ATX200	N/A	340-380	24
GE (SABIC)	Ultem®	9075	N/A	295-330	N/A
GE (SABIC)	Siltem®	STM1500	N/A	285-320	N/A
GE (SABIC)	Extem XH®	XH1015	249	380-410	10*
GE (SABIC)	Extem XH®	VH1003/F/M/P	247	380-405	N/A
Mitsui	Aurum®	PL150C	250	388	N/A
DuPont	Vespel	TP-8000	250	388	N/A

* @367°C

Some of the variations in structure of different commercial grades of PEI with references to the production company and their commercial names are presented below:

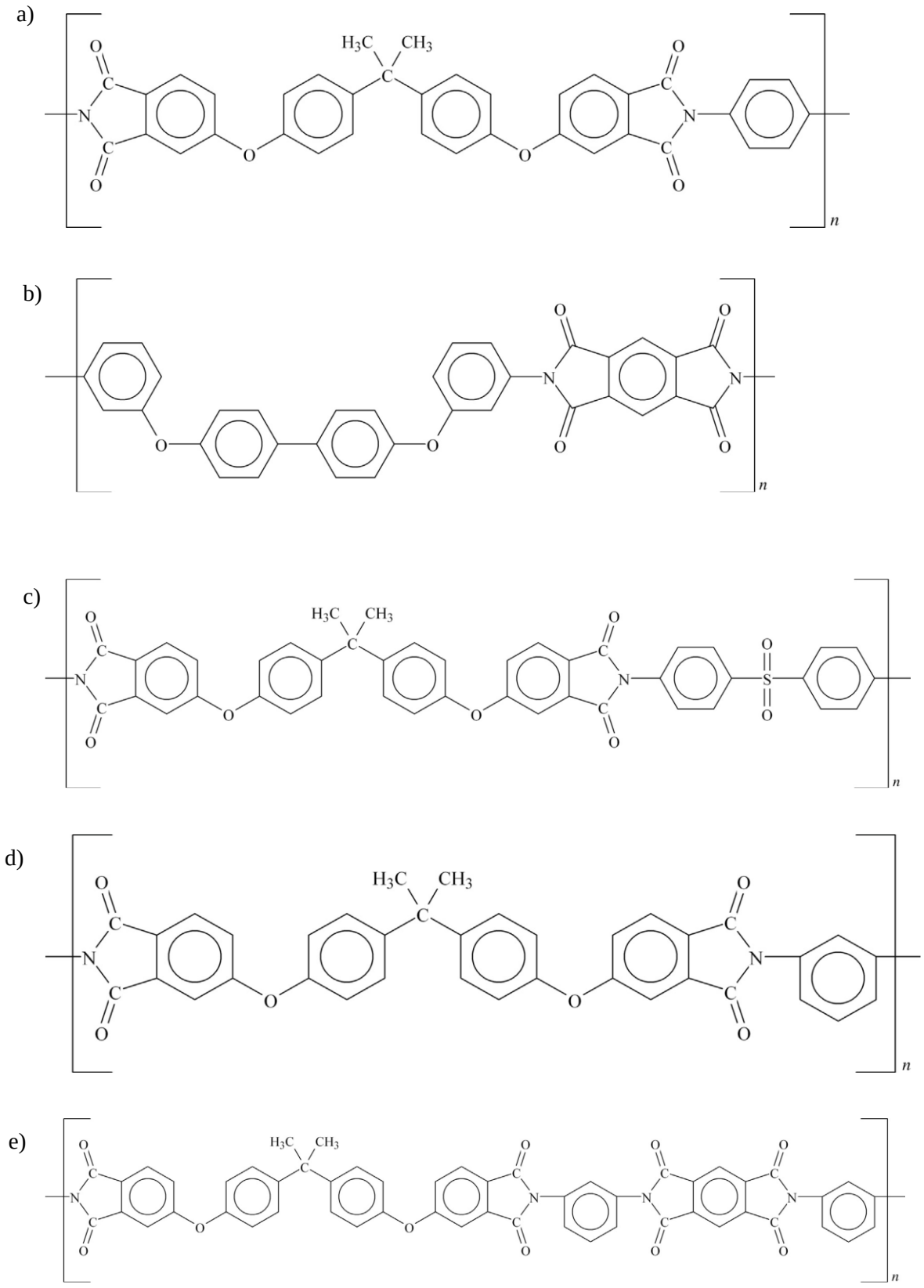

Figure 2.6 Chemical structure of (a) BPADA-PPD polyetherimide (Ultem® 5000 series) (b) bisphenol diamine PMDA polyetherimide (Aurum®, Vespel® TP-8000 series) (c) BPADA-DDS polyetherimide sulfone (Ultem® XH6050) d) BPADA-MPD polyetherimide (Ultem® 1000 series) (e) BPADA-PMDA-MPD copolyetherimide (Ultem® 6000 series). Modified from [7].

Polyetherimide has been already used in many sectors of industry for applications such as surgical probes, pharmaceutical manifolds for process equipment, insulators used for high-frequency communications, clamps for printed circuit board´s connection to video display units used in airplanes, tanks and ships [1].

PEI has also been utilized in medical applications such as sterile equipment e.g., trays, intravenous (IV) sets, pumps, stapler, tubing, drug delivery equipment among other medical, surgical and dental instruments due to its gamma radiation, ethylene oxide (EtO), steam and dry heat resistance and compliance with ISO 10993, EU, FDA and USP class VI [8].

Smaoui *et al.* [9] study on aerospace applications of PEI have shown that irradiation could lead to a few structural changes in PEI resulting in β relaxation and minor differences in the infrared spectra. Additionally the mechanical properties of PEI under radiation have been reported by NASA [10] showing that for high doses of radiation (6×10^9 rad) PEI films responded with 22% decrease in tensile strength, 96% decrease in strain to failure and 8-10% increase in modulus as a result of dehydrogenation of the pendent methyl groups, rupture of the main-chain bonds at ether linkages, and opening of imide rings. These conditions are extreme when compared to that of sterilization with irradiation of only 2.5×10^6 rad (according to Pharmacopoeia [11]) which proves the eligibility of PEI for these medical applications. Additionally, the mechanical properties of PEI Ultem® 1000 is only slightly affected after exposure to 100 Eto sterilization cycles showing 100% of its initial tensile strength and 75% of its tensile elongation [8,12].

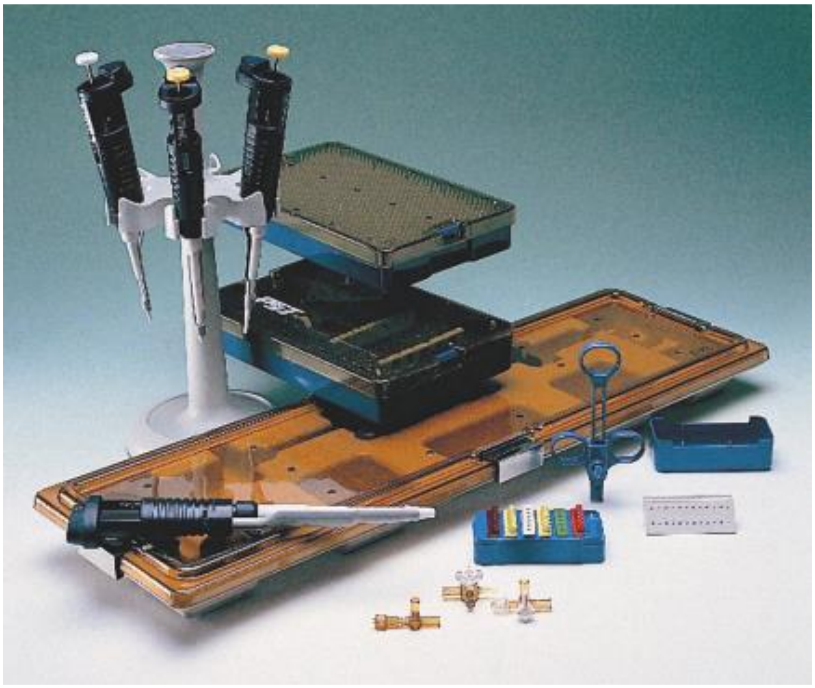

Figure 2.7 Medical equipments made from PEI. Adapted from [12].

PEI also demonstrates a good balance of electrical properties with stability over wide range of environmental conditions, maintaining stable dielectric constant and low dissipation factor at frequencies as high as 10^9 Hz even at elevated temperatures [13] as shown in Figure 2.9. The combination of this ability with other thermal, mechanical and chemical properties of PEI could be used in applications such as printed wiring boards suitable for high frequencies. Thanks to its high service temperature, it can also withstand wave soldering which is an important factor for circuit board designers. It can also be injection-molded into complicated 3D dimensions for easy integration assembly through methods such as snap fit. It is also compatible with UL file E75735 for use as insulation materials in transformers and motors of up to 600 volts. These properties are used in components such as electrical control units, internal antenna in cellphones, connectors for fiber optics, rf-duplexers and microfilters.

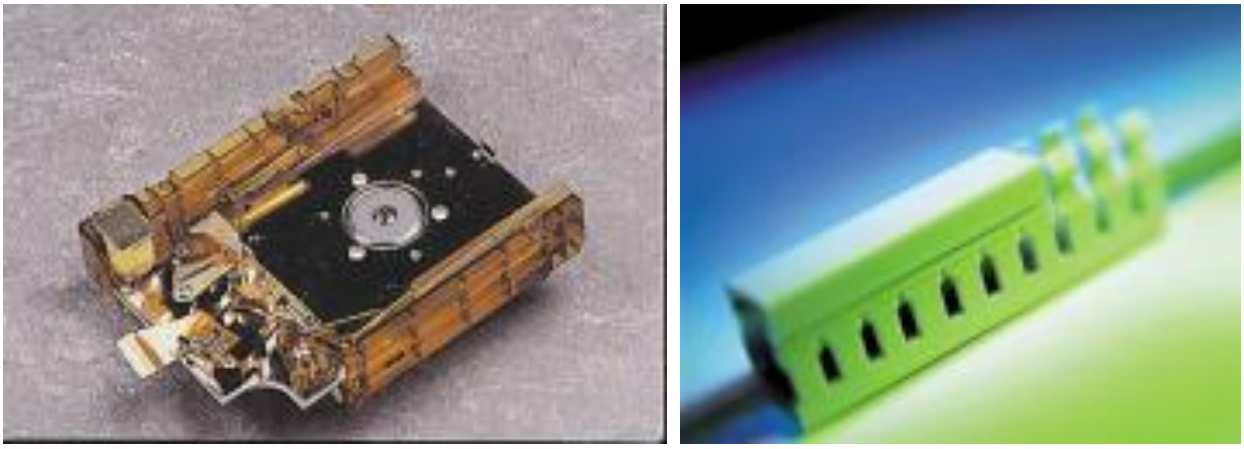

Figure 2.8 Computer and lightening components made from PEI. Adapted from [12].

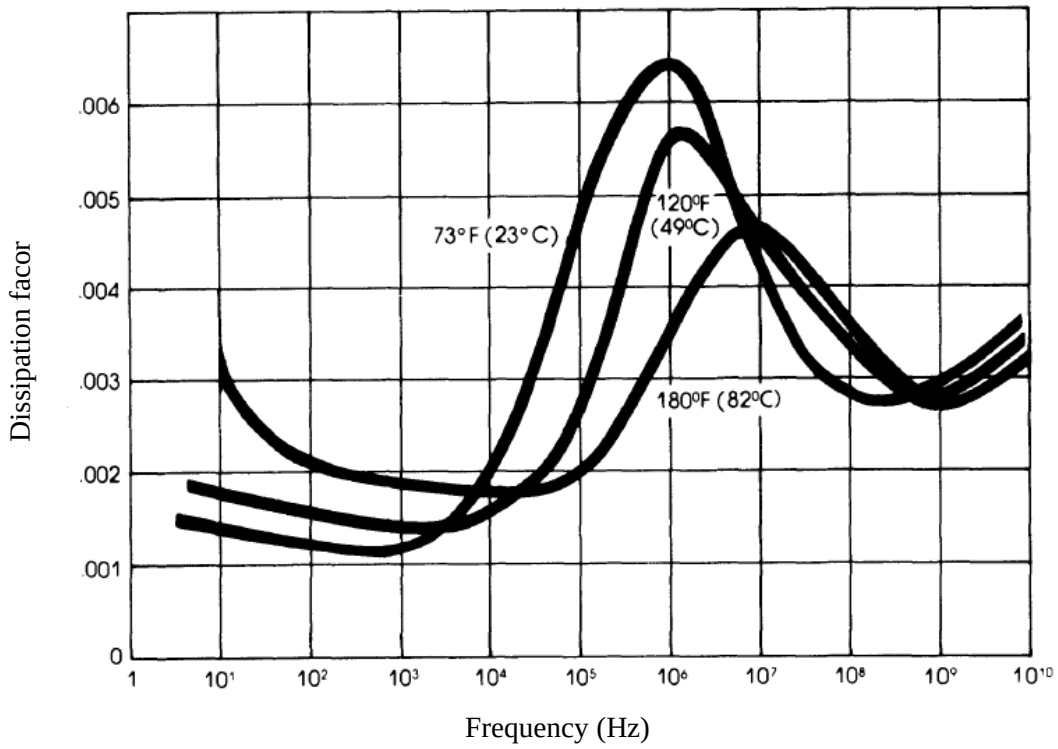

Figure 2.9 Dissipation factor vs. frequency of PEI at 50% relative humidity. Adapted from [13].

As mentioned before, one of the notable properties of PEI is its service temperature. PEI has a heat deflection temperature under load (DTUL) of 200°C allowing significant retention of its mechanical properties at high temperatures. Therefore, PEI allows a continuous service temperature of 170 °C as reported by Underwriters Laboratories Inc. [13]. Taking advantage of its heat resistance, PEI is used in automotive industry in components including under-the-hood, heat exchange system and electrical. The usage of PEI in automotive industry also benefits from its resistance to lubricants and other automotive fluids, ductility and low creep sensitivity. A study by Lisa *et al.* [14] assessed the thermal and thermo-oxidative stability of PEI and the effect of its structure and working atmosphere on the thermal degradation of the polymer. The obtained result showed that the introduction of an oxadiazole derivative in the side chain leads to a decrease in thermal stability in both air and helium atmosphere.

Figure 2.10 PEI-based components in automotive industry as throttle body and headlight reflectors. Adapted from [12].

Furthermore, PEI has good mechanical stability while exposed to water at various temperatures. PEI offers a good hydrolytic stability, retaining its tensile strength in long term exposure to 100 °C water, which makes PEI suitable for applications such as water pump impellers, expansion valves in hot water reservoirs and heat exchange equipment.*[13]*.

Figure 2.11 Fluid handling components made from PEI. Adapted from [12].

Additionally, PEI is inherently resistance to ignition which makes it a listed V-0 according to Bulletin 94 at 0.75 mm dimension or a V-2 at 0.4 mm and a limiting oxygen index is only 47% according

to ISO 4589. PEI is also extremely low in smoke generation when compared to conventional engineering thermoplastics which makes it easy to pass FAA approvals for aircraft parts such as non-panel lining and non-metallic air ducts [15]. Additionally, it will provide weight reduction, chemical and stain resistance for uses in seat frames, electrical hardware, lighting and wiring.

Figure 2.12 Interior cladding parts in aircrafts made from PEI. Adapted from [12].

Foaming of high performance thermoplastic polymers could provide desirable features such as weight reduction, energy absorption properties, high thermal and noise insulation and electromagnetic absorption by promoting the dissipation of waves [16–18]. Miller and Kumar [19,20] have investigated the processing, structure and mechanical properties of microcellular PEI foams prepared using sub-critical CO_2 with 40% and higher relative densities. They have suggested that above 3 MPa pressure of CO_2 a sufficient gas concentration in PEI sheets can be achieved in order to allow the creation of either microcellular or nanocellular foams. In term of their mechanical properties, they have reported that a significantly higher strain to failure, and as a consequence, a 350% increase in modulus of toughness was achieved by nanocellular foams in comparison with microcellular PEI foams. Additionally, the results of falling weight impact test suggested a 600% increase in impact energy for nanocellular foams when compared to that of microcellular foams. Their results could lead into promising nanofoams as a new class of materials.

Zhou et al. [21] have also pointed out that unique nanoscale cellular structure could provide outstanding properties. They have carried out preparation PEI-based nanofoams using supercritical CO_2 dissolution. They have reported a higher specific modulus than that of unfoamed PEI and a general increase in the thermal resistivity of the nanocellular foams when compared with the foams having microcellular structure.

Li *et al.* [22] have suggested another method for preparing microcellular PEI foams. They have successfully prepared PEI foams and PEI/filler nanocomposites using MuCell® injection molding using supercritical nitrogen gas (scN_2) as the blowing agent and demonstrated how the processing parameters could affect the cellular morphology of these foams. They have also revealed that these parameters could greatly affect the final mechanical properties of the foams. They have reported that the mechanical properties of the foams could be improved by increasing the shot size and injection speed while a decrease in their tensile strength was observed by increasing the scN_2 content. They have also mentioned that the temperature of the mold could be optimized in order to achieve a cellular structure with enhanced tensile strength. Their results are in agreement with another study of PEI and PEI-based blend foams prepared using the MuCell® injection molding process by Liu *et al.* [23].

2.4 Carbon nanofillers and PEI-based nanocomposites

The high structure-dependent electrical conductivity of the carbon-based nanofillers could play a key role in modification of the electronic properties of polymers, and partially crack down some of the issues regarding the use of conductive polymers [24]. Carbon-based nanofillers may be categorize regarding their geometry into 3-dimentional spherical-shape nano-size carbon black (CB) and carbon nanofibers (CNF), 2-dimensional platelet-shape graphene,1-dimensional cylindrical-shape carbon nanotubes (CNT), and 0-dimensional fullerene, all allotropes of carbon. A schematic of these allotropes is presented in figure below:

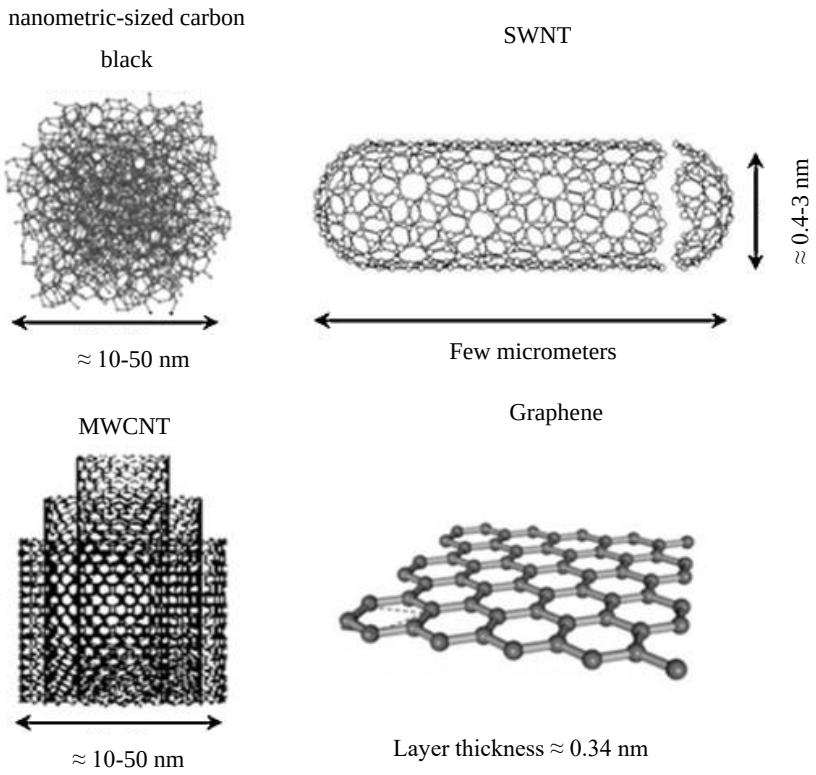

Figure 2.13 Schematics of allotropes of carbon-based nano-particles: carbon black (CB), single-wall carbon nanotubes (SWNT), multi-wall carbon nanotubes (MWCNT) and graphene. Adapted from [25].

Carbon black was conventionally used excessively in automotive industry, however, it has been recently considered as an electrical conductivity enhancer in polymers for static dissipative use [26,27].

Carbon nanofibers are in dimensions between carbon fibers and carbon nanotubes with diameters of about 200 nm. Due to more irregularity and orientations in graphitic layers forming CNFs, their surface lacks the uniformity of nanotubes since the variation in orientation of graphene layers may result in edge terminals on the surface of CNFs.

Graphene has been introduced as a single layer of carbon sheet that when piled together forms graphite. Theses layers are also kept together with Van der Waals forces which makes it easy to separate them using simple methods like micromechanical cleavage which was first used by Novoselov *et al.* [28,29] to isolate a single layer of graphene. Since then, this 2-dimensional form of carbon has shown most promising results with their incorporation in wide range of polymers such as PVA [30,31], PMMA [32], PS [33], polyaniline (PANI) [34], PP [35], PC [17,18,36,37] among many others.

Wu *et al.* [38] have presented a fabrication of PEI-GnP nanocomposite using melt-extrusion, pre-coating, and solid ball milling. The results indicate that by using a pre-coating approach, the electrical conductivity value was significantly improved resulting in a percolation threshold of 2 wt% as compared to 10 wt% for melt-extruding method. However, the mechanical properties of nanocomposites prepared by

this method showed lower values. Furthermore, the solid state ball milling preparation technique showed a better dispersion resulting in higher electrical conductivity values and enhanced modulus. A combination of solid state ball milling and extrusion was also examined which illustrated that by doing so, further improvement of mechanical properties could be achieved.

Carbon nanotubes are simply carbon atoms assembled in a cylindrical shape which can be considered as a graphitic layer-like structure rolled into a cylindrical shape with diameters in nanoscale order. Depending on the number of tubes forming the CNTs, they can be classified into single-wall and multi-wall carbon nanotubes. The MWCNTs are maintained together with weak secondary Van der Waals forces [39]. Although the dimension of MWCNTs depends on the number of layers stacked together, the typical diameter of these fillers are typically about ten times higher than that of SWNTs.

Thermoset polymers such as polyurethane (PU), epoxy and phenolic are examples of suitable medium for nanotube dispersions [25]; since they are liquid at ambient temperature, the fillers can be dispersed easily to form an electrically conductive network with relatively low nanotube content using techniques such as ultrasonication [40]. Sandler *et al.* [41] have reported an ultra-low electrical percolation threshold (0.0025 wt% of CNT) in an epoxy-based nanocomposite which also reported an electrical conductivity value of 2 S/m for only 1 wt% of CNT content. Regarding thermoplastic nanocomposites reinforced with CNT, various polymers such as poly (vinyl alcohol) (PVA) [42], PE [43], ABS [44],PP [24,45], PC [46,47] were investigated among many others.

PEI-MWCNT nanocomposite films have been prepared by Liu *et al.* [48] using casting and imidization. They achieved a fine dispersion and strong adhesion between the nanotubes and the matrix which resulted in an increase of glass transition temperature by 10 °C and a 250% improvement of elastic moduli for the addition of only 1 wt% MWCNTs.

Using a hybrid system of carbon-based fillers can bring important advantages over the conventional non-carbon-based fillers. For instance, the addition of CNTs to epoxy/unidirectional CF has shown promising results in terms of improving mechanical performance as well as their electronic properties [49] which provided a novel method for monitoring the damage accumulation for these nanocomposites under load. Various studies were carried out to prepare and analyze CNT/GnP hybrid materials for applications such as transparent conductors [50–53], electrodes [53,54], electron field emitters [55], field effect transistors [53], supercapacitors [56], and Li-ion batteries [57,58]. Another study by Kumar *et al.* [59] has revealed that by hybridizing GnP with functionalized MWCNTs in PEI nanocomposite, significant improvement in dynamic mechanical properties, electrical and thermal conductivity could be achieved when compared to that of GnP or MWCNT alone at the same loading amounts. Their result showed a synergic effect of hybrid nanofillers resulting in protection of CNTs by GnP during high power sonication process while maintaining a fine dispersion of both nanofillers.

The geometrical characteristics (aspect ratio, diameter, number of stacks, entanglement, etc.) of carbon-based nanoparticles are strongly depend on the specifities of their synthesis method. This can also affect other aspects of these nanofillers such as crystalline perfection and their intrinsic properties [60].

Some of the processes could be used exclusively for synthesis of certain carbon-based nanofillers. For instance, high temperature evaporation of carbon is used for production of MWCNTs [61,62] while chemical vapor deposition (CVD) or catalytic growth process are used for both MWCNTs and SWNTs [63–65]. CVD and catalytic growth processes can also be used for production of CNFs [66]. As mentioned before, graphene can be synthesized using a simple mechanical cleavage technique also known as scotch tape method. However, this method lacks large scale production ability and can induce structural defects in graphite oxide monolayer which will be used later on to obtain graphene monolayer using chemical reduction process [67]. Therefore, other methods have been developed to solve these issues; for instance, Li *et al.* [68] have reported a method consisting of the exfoliation, reintercalation and expansion of graphite which can produce high-quality mono-layer graphene sheets. So far, the title of most common method for large-scale graphene production belongs to the CVD process either by thermal [69–72] or plasma [73–75]. Other methods such as chemical [76,77] and thermal reduction [76,78] of graphene oxide or unzipping of SWNT [79] have also been introduced as methods for graphene mono-layer production.

2.5 Polyetherimide nanocomposite foams

As the interest raises in development of polymeric foams, there are some issues that should be addressed. While foaming deliver various improvements in features such as weight reduction, damping properties, thermal and sound insulation, foamed materials suffer greatly from the loss of some mechanical properties. Addition of fillers can address this issue to some extent and also, introduce some functionalities for specific applications. The combination of functional fillers and foaming has a great potential to create new lightweight composite with high specific strength and multifunctionality [80]. Among various fillers available currently, carbon-based nanofillers such and graphene nanoplatelets and carbon nanotubes have attracted tremendous scientific and industrial attention, owing to their high aspect ratio (AR), outstanding mechanical and transport properties which have brought significant advantages over conventional fillers [49,81,82].

As mentioned before, the exceptional intrinsic mechanical and transport properties of carbon-based nanofillers makes them one of the most promising nanofillers for improving the specific strength of polymeric foams while enhancing other features such as their electrical properties. Combination of the these nanofiller’s functionality with foaming could counteract some of the loss in mechanical properties arose from foaming. The merging of foaming with nanofillers such as GnP and CNT could also result in synergic effects promoting both better dispersion of nanoparticles throughout the cellular structure and improve homogeneity of the cells which allows the development of foams with better properties when compared to conventional foams. Carbon-based nanoparticles have also shown that they can locally enhance the melt

strength of the polymer and therefore avoiding cells from collapsing and coalescing during foaming [25]. Moreover, the inherent layer-shape morphology of nanoparticles such as graphene has been reported to act as a barrier to escape of gases during foaming [83,84]. This particular platelet-like shape can also limit the escape of volatile gases during the thermal decomposition of foams, resulting in enhanced thermal stability [36,85].

Ling *et al.* [86], has presented water vapor induced phase separation (WVIPS) method as a proper way to obtain PEI-GnP nanocomposite foams. To do so, a proper solvent was chosen in order to obtain a homogenous solution of solvent/PEI/GnP, from which the cellular structure was formed through phase separation promoted by induction of a non-solvent (water vapor from air). The resultant foams were in microcellular range with a density of 0.3 g/cm^3 and an average cell diameter from 9.0-16.6 μm with a general descending trend with increasing the filler content. They have also analyzed the electrical conductivity and EMI shielding properties of this foams and showed that the foaming could result in better electronic properties of the foams by reducing the distance between particles and facilitating the orientation of them in cell walls (see Figure 2.14).

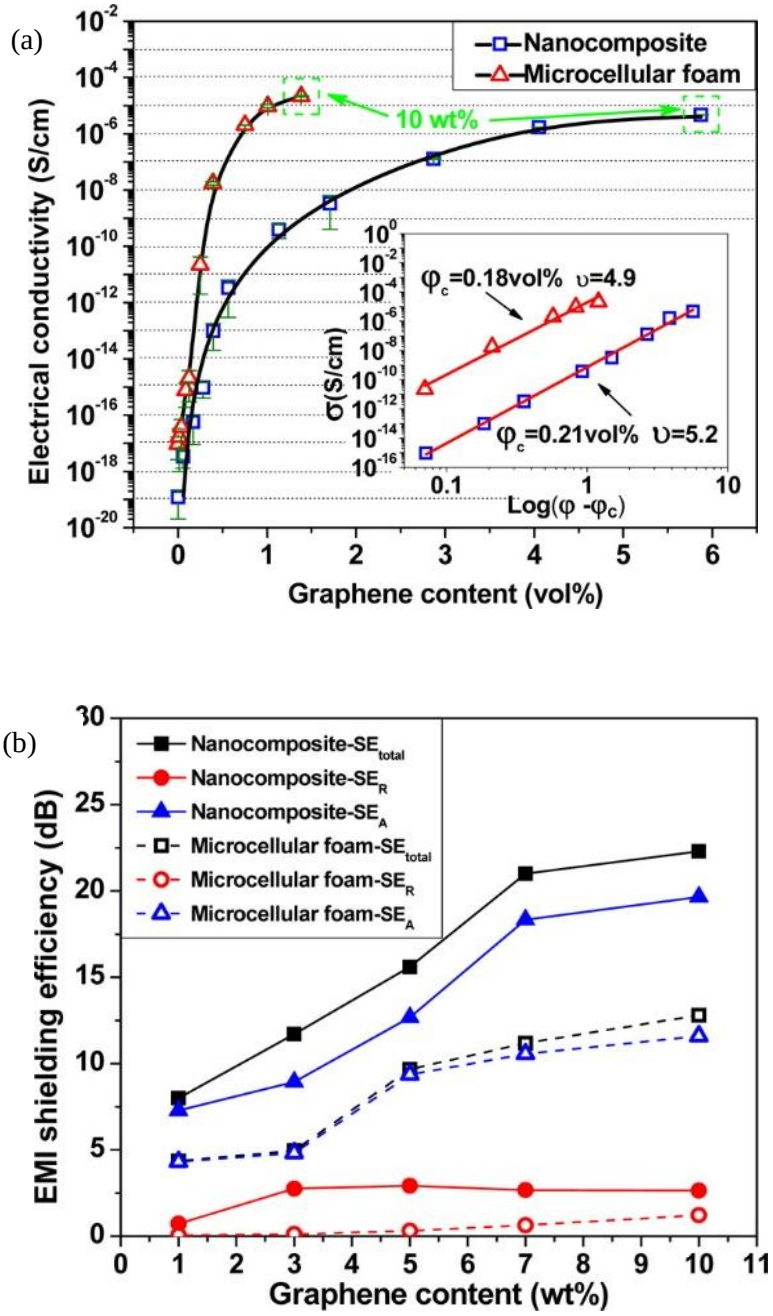

Figure 2.14 (a) Electrical conductivity and (b) EMI shielding efficiency of PEI-GnP foams. Adapted from [86].

However, the prepared foams by this group have shown a significant reduction in their tensile strength (up to half) by increasing the graphene content. contractively, the young modulus of the foams showed and increasing trend with addition of graphene up until 5 wt% (see Figure 2.15).

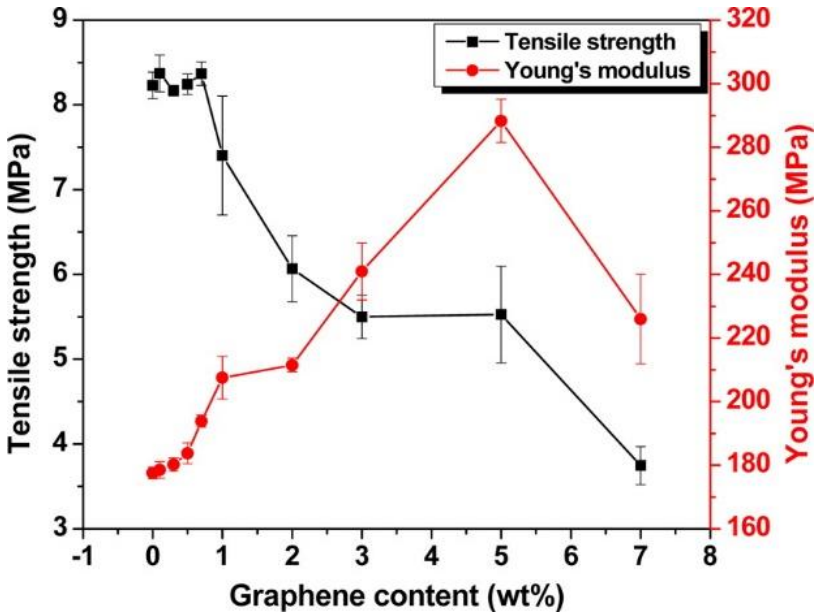

Figure 2.15 Tensile properties of PEI/graphene nanocomposite foams. Adapted from [86].

Goh *et al.* [87] have also prepared membranes based on PEI-MWCNTs using phase separation method. They reported that by using non-ionic Triton X100 as surfactant in MWCNT/NMP mixture, a better dispersion and stronger interfacial adhesion with PEI was achieved. They have also mentioned that the thermal and mechanical stability of these membranes were improved by the use of Triton X100 surfactant.

Another study by Kim and Li [88] has reported fabrication of PEI-based nanocomposite foams containing 0.5-3 wt% of MWCNTs using phase separation technique with a relative density of around 0.45. They also reported possible influences of residual solvent on mechanical properties on the foams. In terms of their electrical conductivity, they achieved a value of 10^{-7} S/cm at 2 wt% of MWCNTwhich is considerably lower than that of virgin PEI (10^{-13} S/cm). This study has also pointed out a reduction in electrical conductivity of the foams with reducing their relative density.

Shen *et al.* [89] have also carried out an investigation on multifunctional PEI/GnP@Fe_3O_4 nanocomposite foams, prepared via WVIPS method, with promising results in EMI shielding efficiency of the foams at various frequencies. They revealed that most of the applied microwave was absorbed rather than being reflected due to improved impedance matching, electromagnetic wave attenuation, and multiple reflections (see Figure 2.16).

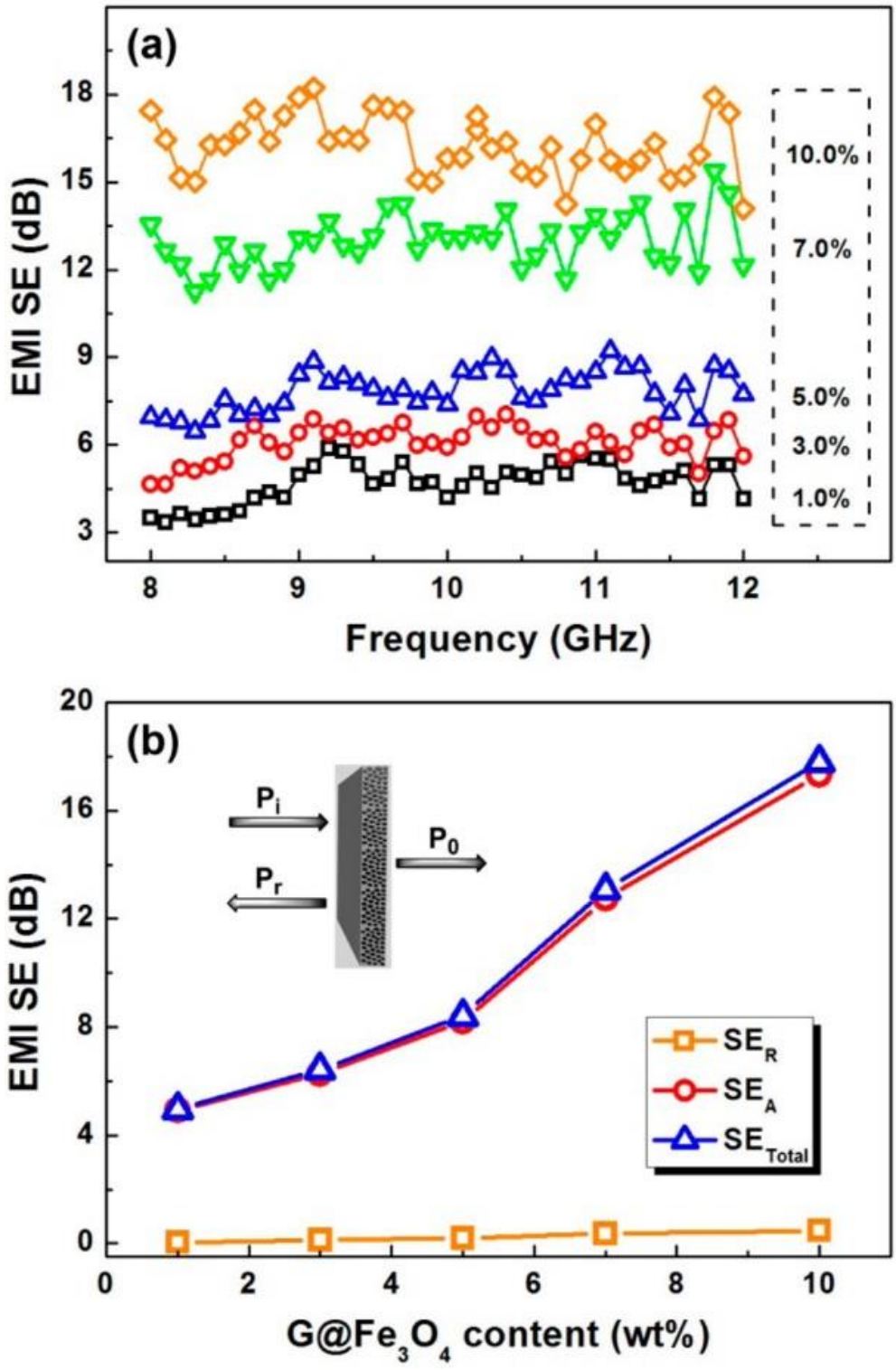

Figure 2.16 (a) EMI shielding performance as a function of frequency in the 8–12 GHz range of the PEI/GnP@Fe_3O_4; (b) total EMI shielding effectiveness (SE_{total}), microwave reflection (SE_R) and microwave absorption (SE_A) of microcellular foams at 9.6 GHz. Adapted from [89].

2.6 References

1. McKeen, L.W. Polyimides. In *PERMEABILITY PROPERTIES OF PLASTICS AND ELASTOMERS*; McKeen, L.W.B.T.-P.P. of P. and E. (Third E., Ed.; William Andrew Publishing: Oxford, 2012, 107–120.
2. Melton, G.H.; Peters, E.N.; Arisman, R.K. Engineering Thermoplastics. In *APPLIED PLASTICS ENGINEERING HANDBOOK*; Kutz, M.B.T.-A.P.E.H., Ed.; William Andrew Publishing: Oxford, 2011, 7–21.
3. Landis, A.L.; Lau, K.S.Y. High-Performance Polyimides and Related Thermoset Polymers: Past and Present Development, and Future Research Directions. In; Goodman, S.H.B.T.-H. of T.P. (Second E., Ed.; William Andrew Publishing: Westwood, NJ, 1998, 302–467 I.
4. Peters, E.N. Engineering Thermoplastic- Materials, Properties, Trends. In *APPLIED PLASTICS ENGINEERING HANDBOOK Processing, Materials, and Applications*; Kutz, M., Ed.; William Andrew: Oxford, UK, 2017, 03–26.
5. Bailey, W.J. 'Diels-Alder Polymerization. *Step growth Polym. Marcel Dekker. New York* 1972, *279*.
6. McKeen, L.W. Binders. In *Fluorinated Coatings and Finishes Handbook The Definitive User's Guide and Databook*; McKeen, L.W.B.T.-F.C. and F.H., Ed.; William Andrew Publishing: Norwich, NY, 2006, 45–58.
7. McKeen, L.W. Polyimides. In *FATIGUE AND TRIBOLOGICAL PROPERTIES OF PLASTICS AND ELASTOMERS*; McKeen, L.W.B.T.-F. and T.P. of P. and E. (Second E., Ed.; William Andrew Publishing: Oxford, 2010, 149–173.
8. McKeen, L. Polyimides. In *The Effect of Sterilization on Plastics and Elastomers*; McKeen, L.B.T.-T.E. of S. on P. and E. (Third E., Ed.; William Andrew Publishing: Boston, 2012, 169–182.
9. Smaoui, H.; Mzabi, N.; Guermazi, H.; Mlik, Y.; Agnel, S.; Toureille, A.; Schué, F. Characterisation of gamma-irradiated polyetherimide films with infrared spectroscopy and thermally stimulated current measurements. *Polym. Int.* 2006, *56*, 325–332.
10. Long Jr, E.R.; Long, S.A. *Spectroscopic Analysis of Radiation-Generated Changes in Tensile Properties of a Polyetherimide Film.*; NATIONAL AERONAUTICS AND SPACE ADMINISTRATION HAMPTON VA LANGLEY RESEARCH CEN TER, 1985;
11. Silindir, M.; Özer, A.Y. Sterilization methods and the comparison of e-beam sterilization with gamma radiation sterilization. *Fabad J. Pharm. Sci.* 2009, *34*, 43.
12. PEI Ultem 1000 product Guide, GE Plastics. *CYC-300D CA* 1997.
13. Serfaty, I.W. Polyetherimide: A Versatile, Processable Thermoplastic BT. In *Polyimides: Synthesis, Characterization, and Applications. Volume 1*; Mittal, K.L., Ed.; Springer US: Boston, MA, 1984, 149–161.
14. Lisa, G.; Hamciuc, C.; Hamciuc, E.; Tudorachi, N. Thermal and thermo-oxidative stability and probable degradation mechanism of some polyetherimides. *J. Anal. Appl. Pyrolysis* 2016, *118*, 144–

154.

15. Horner, A. *Aircraft Materials Fire Test Handbook.*; WILLIAM J HUGHES TECHNICAL CENTER ATLANTIC CITY NJ, 2000.
16. Zhang, H.-B.; Yan, Q.; Zheng, W.-G.; He, Z.; Yu, Z.-Z. Tough Graphene−Polymer Microcellular Foams for Electromagnetic Interference Shielding. *ACS Appl. Mater. Interfaces* 2011, *3*, 918–924.
17. Gedler, G.; Antunes, M.; Velasco, J.I.; Ozisik, R. Enhanced electromagnetic interference shielding effectiveness of polycarbonate/graphene nanocomposites foamed via 1-step supercritical carbon dioxide process. *Mater. Des.* 2016, *90*, 906–914.
18. Gedler, G.; Antunes, M.; Velasco, J.I.; Ozisik, R. Electromagnetic shielding effectiveness of polycarbonate/graphene nanocomposite foams processed in 2-steps with supercritical carbon dioxide. *Mater. Lett.* 2015, *160*, 41–44.
19. Miller, D.; Chatchaisucha, P.; Kumar, V. Microcellular and nanocellular solid-state polyetherimide (PEI) foams using sub-critical carbon dioxide I. Processing and structure. *Polymer.* 2009, *50*, 5576–5584.
20. Miller, D.; Kumar, V. Microcellular and nanocellular solid-state polyetherimide (PEI) foams using sub-critical carbon dioxide II. Tensile and impact properties. *Polymer.* 2011, *52*, 2910–2919.
21. Zhou, C.; Vaccaro, N.; Sundarram, S.S.; Li, W. Fabrication and characterization of polyetherimide nanofoams using supercritical CO_2. *J. Cell. Plast.* 2012.
22. Li, J.; Chen, Z.; Wang, X.; Liu, T.; Zhou, Y.; Luo, S. Cell morphology and mechanical properties of microcellular MuCell® injection molded polyetherimide and polyetherimide/fillers composite foams. *J. Appl. Polym. Sci.* 2013, *130*, 4171–4181.
23. Liu, T.; Lei, Y.; Chen, Z.; Wang, X.; Luo, S. Effects of processing conditions on foaming behaviors of polyetherimide (PEI) and PEI/polypropylene blends in microcellular injection molding process. *J. Appl. Polym. Sci.* 2014, *132*.
24. Antunes, M.; Gedler, G.; Velasco, J.I. Multifunctional nanocomposite foams based on polypropylene with carbon nanofillers. *J. Cell. Plast.* 2013, *49*, 259–279.
25. Antunes, M.; Velasco, J.I. Multifunctional polymer foams with carbon nanoparticles. *Prog. Polym. Sci.* 2014, *39*, 486–509.
26. Roy, N.; Sengupta, R.; Bhowmick, A.K. Modifications of carbon for polymer composites and nanocomposites. *Prog. Polym. Sci.* 2012, *37*, 781–819.
27. Zhang, S.; Lin, L.; Deng, H.; Gao, X.; Bilotti, E.; Peijs, T.; Zhang, Q.; Fu, Q. Dynamic percolation in highly oriented conductive networks formed with different carbon nanofillers. *Colloid Polym. Sci.* 2012, *290*, 1393–1401.
28. Novoselov, K.S.; Geim, A.K.; Morozov, S. V; Jiang, D.; Zhang, Y.; Dubonos, S. V; Grigorieva, I. V; Firsov, A.A. Electric field in atomically thin carbon films. *Science*, 2004, *306*, 666–669.
29. Novoselov, K.S.; Jiang, D.; Schedin, F.; Booth, T.J.; Khotkevich, V. V; Morozov, S. V; Geim, A.K. Two-dimensional atomic crystals. *Proc. Natl. Acad. Sci.* 2005, *102*, 10451–10453.

30. Salavagione, H.J.; Martínez, G.; Gómez, M.A. Synthesis of poly (vinyl alcohol)/reduced graphite oxide nanocomposites with improved thermal and electrical properties. *J. Mater. Chem.* 2009, *19*, 5027–5032.
31. Xu, Y.; Hong, W.; Bai, H.; Li, C.; Shi, G. Strong and ductile poly (vinyl alcohol)/graphene oxide composite films with a layered structure. *Carbon N. Y.* 2009, *47*, 3538–3543.
32. Villar-Rodil, S.; Paredes, J.I.; Martínez-Alonso, A.; Tascón, J.M.D. Preparation of graphene dispersions and graphene-polymer composites in organic media. *J. Mater. Chem.* 2009, *19*, 3591–3593.
33. Liu, N.; Luo, F.; Wu, H.; Liu, Y.; Zhang, C.; Chen, J. One-Step Ionic-Liquid-Assisted Electrochemical Synthesis of Ionic-Liquid-Functionalized Graphene Sheets Directly from Graphite. *Adv. Funct. Mater.* 2008, *18*, 1518–1525.
34. Bhadra, S.; Khastgir, D.; Singha, N.K.; Lee, J.H. Progress in preparation, processing and applications of polyaniline. *Prog. Polym. Sci.* 2009, *34*, 783–810.
35. Song, P.; Cao, Z.; Cai, Y.; Zhao, L.; Fang, Z.; Fu, S. Fabrication of exfoliated graphene-based polypropylene nanocomposites with enhanced mechanical and thermal properties. *Polymer.* 2011, *52*, 4001–4010.
36. Gedler, G.; Antunes, M.; Realinho, V.; Velasco, J.I. Thermal stability of polycarbonate-graphene nanocomposite foams. *Polym. Degrad. Stab.* 2012, *97*, 1297–1304.
37. Gedler, G.; Antunes, M.; Velasco, J.I. Effects of graphene nanoplatelets on the morphology of polycarbonate–graphene composite foams prepared by supercritical carbon dioxide two-step foaming. *J. Supercrit. Fluids* 2015, *100*, 167–174.
38. Wu, H.; Rook, B.; Drzal, L.T. Dispersion optimization of exfoliated graphene nanoplatelet in polyetherimide nanocomposites: Extrusion, precoating, and solid state ball milling. *Polym. Compos.* 2013, *34*, 426–432.
39. Breuer, O.; Sundararaj, U. Big returns from small fibers: a review of polymer/carbon nanotube composites. *Polym. Compos.* 2004, *25*, 630–645.
40. Sandler, J.; Shaffer, M.S.P.; Prasse, T.; Bauhofer, W.; Schulte, K.; Windle, A.H. Development of a dispersion process for carbon nanotubes in an epoxy matrix and the resulting electrical properties. *Polymer.* 1999, *40*, 5967–5971.
41. Sandler, J.K.W.; Kirk, J.E.; Kinloch, I.A.; Shaffer, M.S.P.; Windle, A.H. Ultra-low electrical percolation threshold in carbon-nanotube-epoxy composites. *Polymer.* 2003, *44*, 5893–5899.
42. Kilbride, B.E. ea; Coleman, J.N.; Fraysse, J.; Fournet, P.; Cadek, M.; Drury, A.; Hutzler, S.; Roth, S.; Blau, W.J. Experimental observation of scaling laws for alternating current and direct current conductivity in polymer-carbon nanotube composite thin films. *J. Appl. Phys.* 2002, *92*, 4024–4030.
43. Linares, A.; Canalda, J.C.; Cagiao, M.E.; García-Gutiérrez, M.C.; Nogales, A.; Martín-Gullón, I.; Vera, J.; Ezquerra, T.A.; García-Gutiérrez, M.C.; Nogales, A.; et al. Broad-Band Electrical Conductivity of High Density Polyethylene Nanocomposites with Carbon Nanoadditives: Multiwall

Carbon Nanotubes and Carbon Nanofibers. *Macromolecules* 2008, *41*, 7090–7097.

44. Al-Saleh, M.H.; Sundararaj, U. Microstructure, electrical, and electromagnetic interference shielding properties of carbon nanotube/acrylonitrile–butadiene–styrene nanocomposites. *J. Polym. Sci. Part B Polym. Phys.* 2012, *50*, 1356–1362.
45. Gao, D.L.; Zhan, M.S. Fabrication and electrical properties of CNT/PP conductive composites with low percolation threshold by solid state alloying. *Polym. Compos.* 2010, *31*, 1084–1090.
46. Lu, J.; Kumar, B.; Castro, M.; Feller, J.-F. Vapour sensing with conductive polymer nanocomposites (CPC): Polycarbonate-carbon nanotubes transducers with hierarchical structure processed by spray layer by layer. *Sensors Actuators B Chem.* 2009, *140*, 451–460.
47. Pötschke, P.; Bhattacharyya, A.R.; Janke, A. Melt mixing of polycarbonate with multiwalled carbon nanotubes: microscopic studies on the state of dispersion. *Eur. Polym. J.* 2004, *40*, 137–148.
48. Liu, T.; Tong, Y.; Zhang, W.-D. Preparation and characterization of carbon nanotube/polyetherimide nanocomposite films. *Compos. Sci. Technol.* 2007, *67*, 406–412.
49. Kostopoulos, V.; Vavouliotis, A.; Karapappas, P.; Tsotra, P.; Paipetis, A. Damage Monitoring of Carbon Fiber Reinforced Laminates Using Resistance Measurements. Improving Sensitivity Using Carbon Nanotube Doped Epoxy Matrix System. *J. Intell. Mater. Syst. Struct.* 2009, *20*, 1025–1034.
50. Tung, V.C.; Chen, L.-M.; Allen, M.J.; Wassei, J.K.; Nelson, K.; Kaner, R.B.; Yang, Y. Low-Temperature Solution Processing of Graphene−Carbon Nanotube Hybrid Materials for High-Performance Transparent Conductors. *Nano Lett.* 2009, *9*, 1949–1955.
51. Nguyen, D.D.; Tiwari, R.N.; Matsuoka, Y.; Hashimoto, G.; Rokuta, E.; Chen, Y.-Z.; Chueh, Y.-L.; Yoshimura, M. Low Vacuum Annealing of Cellulose Acetate on Nickel Towards Transparent Conductive CNT–Graphene Hybrid Films. *ACS Appl. Mater. Interfaces* 2014, *6*, 9071–9077.
52. Nguyen, D.D.; Tai, N.-H.; Chen, S.-Y.; Chueh, Y.-L. Controlled growth of carbon nanotube-graphene hybrid materials for flexible and transparent conductors and electron field emitters. *Nanoscale* 2012, *4*, 632–638.
53. Kim, S.H.; Song, W.; Jung, M.W.; Kang, M.-A.; Kim, K.; Chang, S.-J.; Lee, S.S.; Lim, J.; Hwang, J.; Myung, S.; et al. Carbon Nanotube and Graphene Hybrid Thin Film for Transparent Electrodes and Field Effect Transistors. *Adv. Mater.* 2014, *26*, 4247–4252.
54. Fan, Z.; Yan, J.; Zhi, L.; Zhang, Q.; Wei, T.; Feng, J.; Zhang, M.; Qian, W.; Wei, F. A Three-Dimensional Carbon Nanotube/Graphene Sandwich and Its Application as Electrode in Supercapacitors. *Adv. Mater.* 2010, *22*, 3723–3728.
55. Deng, J.; Zheng, R.; Zhao, Y.; Cheng, G. Vapor–Solid Growth of Few-Layer Graphene Using Radio Frequency Sputtering Deposition and Its Application on Field Emission. *ACS Nano* 2012, *6*, 3727–3733.
56. Kim, Y.-S.; Kumar, K.; Fisher, F.T.; Yang, E.-H. Out-of-plane growth of CNTs on graphene for supercapacitor applications. *Nanotechnology* 2012, *23*, 015301.
57. Hu, Y.; Li, X.; Wang, J.; Li, R.; Sun, X. Free-standing graphene–carbon nanotube hybrid papers

used as current collector and binder free anodes for lithium ion batteries. *J. Power Sources* 2013, *237*, 41–46.

58. Chen, S.; Yeoh, W.; Liu, Q.; Wang, G. Chemical-free synthesis of graphene–carbon nanotube hybrid materials for reversible lithium storage in lithium-ion batteries. *Carbon N. Y.* 2012, *50*, 4557–4565.
59. Zhong, S.K. and L.L.S. and S.C. and B.L. and W.W. and A.P. and R.G.M. and W.H. Dynamic synergy of graphitic nanoplatelets and multi-walled carbon nanotubes in polyetherimide nanocomposites. *Nanotechnology* 2010, *21*, 105702.
60. Shaffer, M.S.P.; Sandler, J.K.W. Carbon nanotube/nanofibre polymer composites. In *Processing and properties of nanocomposites*; World Scientific, 2007, 1–59.
61. Thess, A.; Lee, R.; Nikolaev, P.; Dai, H.; Petit, P.; Robert, J.; Xu, C.; Lee, Y.H.; Kim, S.G.; Rinzler, A.G. Crystalline ropes of metallic carbon nanotubes. *Science*, 1996, *273*, 483–487.
62. Cadek, M.; Murphy, R.; McCarthy, B.; Drury, A.; Lahr, B.; Barklie, R.C.; in het Panhuis, M.; Coleman, J.N.; Blau, W.J. Optimisation of the arc-discharge production of multi-walled carbon nanotubes. *Carbon N. Y.* 2002, *40*, 923–928.
63. Cheng, H.M.; Li, F.; Su, G.; Pan, H.Y.; He, L.L.; Sun, X.; Dresselhaus, M.S. Large-scale and low-cost synthesis of single-walled carbon nanotubes by the catalytic pyrolysis of hydrocarbons. *Appl. Phys. Lett.* 1998, *72*, 3282–3284.
64. Rao, C.N.R.; Govindaraj, A.; Sen, R.; Satishkumar, B.C. Synthesis of multi-walled and single-walled nanotubes, aligned-nanotube bundles and nanorods by employing organometallic precursors. *Mater. Res. Innov.* 1998, *2*, 128–141.
65. Andrews, R.; Jacques, D.; Rao, A.M.; Derbyshire, F.; Qian, D.; Fan, X.; Dickey, E.C.; Chen, J. Continuous production of aligned carbon nanotubes: a step closer to commercial realization. *Chem. Phys. Lett.* 1999, *303*, 467–474.
66. Merino, C.; Soto, P. Furnace for the manufacture of carbon fibres, procedure for obtaining using said furnace and the fibre thus obtained. *Eur. Pat. Appl.* 2004, *4381014*.
67. Becerril, H.A.; Mao, J.; Liu, Z.; Stoltenberg, R.M.; Bao, Z.; Chen, Y. Evaluation of Solution-Processed Reduced Graphene Oxide Films as Transparent Conductors. *ACS Nano* 2008, *2*, 463–470.
68. Li, X.; Zhang, G.; Bai, X.; Sun, X.; Wang, X.; Wang, E.; Dai, H. Highly conducting graphene sheets and Langmuir–Blodgett films. *Nat. Nanotechnol.* 2008, *3*, 538.
69. Somani, P.R.; Somani, S.P.; Umeno, M. Planer nano-graphenes from camphor by CVD. *Chem. Phys. Lett.* 2006, *430*, 56–59.
70. Bhaviripudi, S.; Jia, X.; Dresselhaus, M.S.; Kong, J. Role of Kinetic Factors in Chemical Vapor Deposition Synthesis of Uniform Large Area Graphene Using Copper Catalyst. *Nano Lett.* 2010, *10*, 4128–4133.
71. Chae, S.J.; Güneş, F.; Kim, K.K.; Kim, E.S.; Han, G.H.; Kim, S.M.; Shin, H.-J.; Yoon, S.-M.; Choi,

J.-Y.; Park, M.H.; et al. Synthesis of Large-Area Graphene Layers on Poly-Nickel Substrate by Chemical Vapor Deposition: Wrinkle Formation. *Adv. Mater.* 2009, *21*, 2328–2333.

72. Lee, S.; Lee, K.; Zhong, Z. Wafer Scale Homogeneous Bilayer Graphene Films by Chemical Vapor Deposition. *Nano Lett.* 2010, *10*, 4702–4707.
73. Wang, J.; Zhu, M.; Outlaw, R.A.; Zhao, X.; Manos, D.M.; Holloway, B.C. Synthesis of carbon nanosheets by inductively coupled radio-frequency plasma enhanced chemical vapor deposition. *Carbon N. Y.* 2004, *42*, 2867–2872.
74. Haesendonck, A.M. and R.V. and K.S. and A.V. and L.Z. and G.V.T. and A.V. and C. Van Synthesis of few-layer graphene via microwave plasma-enhanced chemical vapour deposition. *Nanotechnology* 2008, *19*, 305604.
75. Haesendonck, R.V. and A.M. and R.H.P. and R.K. and M.M. and A.V. and C. Van Initial stages of few-layer graphene growth by microwave plasma-enhanced chemical vapour deposition. *Nanotechnology* 2010, *21*, 95602.
76. Schniepp, H.C.; Li, J.-L.; McAllister, M.J.; Sai, H.; Herrera-Alonso, M.; Adamson, D.H.; Prud'homme, R.K.; Car, R.; Saville, D.A.; Aksay, I.A. Functionalized Single Graphene Sheets Derived from Splitting Graphite Oxide. *J. Phys. Chem. B* 2006, *110*, 8535–8539.
77. Gómez-Navarro, C.; Weitz, R.T.; Bittner, A.M.; Scolari, M.; Mews, A.; Burghard, M.; Kern, K. Electronic Transport Properties of Individual Chemically Reduced Graphene Oxide Sheets. *Nano Lett.* 2007, *7*, 3499–3503.
78. McAllister, M.J.; Li, J.-L.; Adamson, D.H.; Schniepp, H.C.; Abdala, A.A.; Liu, J.; Herrera-Alonso, M.; Milius, D.L.; Car, R.; Prud'homme, R.K.; et al. Single Sheet Functionalized Graphene by Oxidation and Thermal Expansion of Graphite. *Chem. Mater.* 2007, *19*, 4396–4404.
79. Jiao, L.; Zhang, L.; Wang, X.; Diankov, G.; Dai, H. Narrow graphene nanoribbons from carbon nanotubes. *Nature* 2009, *458*, 877.
80. Lee, L.J.; Zeng, C.; Cao, X.; Han, X.; Shen, J.; Xu, G. Polymer nanocomposite foams. *Compos. Sci. Technol.* 2005, *65*, 2344–2363.
81. Badamshina, E.; Estrin, Y.; Gafurova, M. Nanocomposites based on polyurethanes and carbon nanoparticles: preparation, properties and application. *J. Mater. Chem. A* 2013, *1*, 6509–6529.
82. Potts, J.R.; Dreyer, D.R.; Bielawski, C.W.; Ruoff, R.S. Graphene-based polymer nanocomposites. *Polymer.* 2011, *52*, 5–25.
83. Antunes, M.; Velasco, J.I.; Realinho, V. Polypropylene foams. Production, structure and properties. *Adv. Mater. Sci. Res.* 2011, *10*, 121–152.
84. Antunes, M. de S.P.; Velasco Perero, J.I. Foamed polypropylene for industrial applications. In *Polypropylene: synthesis, applications and environmental concerns*; Nova Science Publishers, 2013, 285–319.
85. Kim, H.; Macosko, C.W. Processing-property relationships of polycarbonate/graphene composites. *Polymer.* 2009, *50*, 3797–3809.

86. Ling, J.; Zhai, W.; Feng, W.; Shen, B.; Zhang, J.; Zheng, W. ge Facile Preparation of Lightweight Microcellular Polyetherimide/Graphene Composite Foams for Electromagnetic Interference Shielding. *ACS Appl. Mater. Interfaces* 2013, *5*, 2677–2684.

87. Goh, P.S.; Ng, B.C.; Ismail, A.F.; Aziz, M.; Sanip, S.M. Surfactant dispersed multi-walled carbon nanotube/polyetherimide nanocomposite membrane. *Solid State Sci.* 2010, *12*, 2155–2162.

88. Kim, Y.H.; Li, W. Multifunctional polyetherimide nanocomposite foam. *J. Cell. Plast.* 2013, *49*, 131–145.

89. Shen, B.; Zhai, W.; Tao, M.; Ling, J.; Zheng, W. Lightweight, Multifunctional Polyetherimide/Graphene@Fe_3O_4 Composite Foams for Shielding of Electromagnetic Pollution. *ACS Appl. Mater. Interfaces* 2013, *5*, 11383–11391.

2.7 Recent advances in carbon-based polymer nanocomposites

2.7.1 Abstract

Carbon-based nanofillers have gained massive popularity, as they are capable of creating polymer nanocomposites with improved properties, overcoming some limitations of polymers such as electrical conductivity which has a vast market in high demanding sectors of industries. Particularly, the protection of electronic components from electromagnetic radiation emitted by other devices or themselves. This section of this thesis considers the recent advances in carbon-based polymer nanocomposites for specifically electromagnetic interference (EMI) shielding applications as one of the functionalities that could be benefited from the incorporation of such nanoparticles among many others. In here, various types of carbon-based nanoparticles and respective polymer nanocomposites will be revised as well as possible preparation methods. Regarding the theoretical aspect explaining the shielding efficiency of the foams, various models would be studied which are categorized into those based on electrical conductivity, models based on the EMI shielding efficiency, on the so-called parallel resistor-capacitor model and those based on multiscale hybrids.

Recently, the studies of EMI shielding of polymeric nanocomposites reinforced with carbon-based nanoparticles are focused on the effects of nanofiller's aspect ratio, functionalization, dispersion and alignment during the processing stage alongside with the application of nanohybrids and 3D reinforcements

At the end of this section, the role of cellular nanocomposites in EMI shielding applications is discussed, focusing on how the eventual morphology and cellular structures could generate lightweight multifunctional nanocomposites with enhanced absorption-based EMI shielding properties.

2.7.2 Published review article (Journal of Progress in Materials Science,

Vol. 103, Page 319-373, 2019)

This section consists of reviewed studies regarding the carbon-based polymer nanocomposites for EMI shielding, the theoretical models explaining the phenomenon and cellular nanocomposites containing carbon-based nanofillers for EMI shielding applications. The article included in this chapter is titled **Recent advances in carbon-based polymer nanocomposites for electromagnetic interference shielding** published in **Progress in Materials Science** in **2019.**

ATTENTION¡¡
Pages 92 to 146 of the thesis, containing this article, are available at the editor's web
https://www.sciencedirect.com/science/article/pii/S0079642519300155
DOI: 10.1016/j.pmatsci.2019.02.003

Chapter 3

Materials and experimental procedure

Prior to the presentation of experimental results, this chapter will provide principal characteristics of materials used in study, as well as the description of foaming methods and testing procedures used for characterization of prepared foams.

3.1 Materials

3.1.1 Polyetherimide

Polyetherimide (PEI) used throughout this study was a commercial grade known as Ultem 1000 and was purchased from SABIC (Riyadh, Saudi Arabia and Sittard, Netherland). The chemical structure of the repeating unit is presented in Figure 3.1.

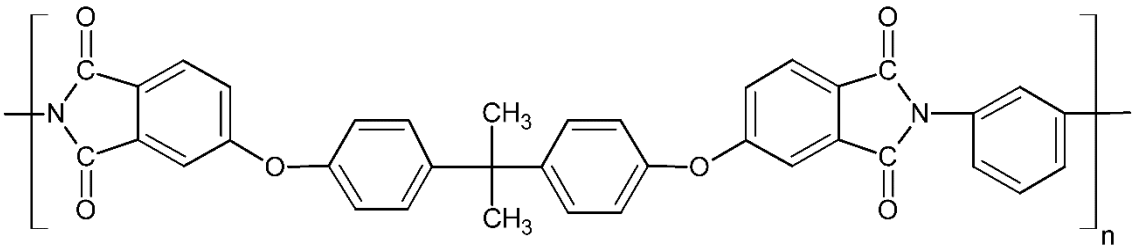

Figure 3.1 PEI Ultem 1000 repetitive unit.

Figure 3.2 PEI Ultem 1000 bar

Ultem 1000 is an amorphous grade of PEI with transparent amber color. Its high glass transition temperature (T_g) of 217 °C alongside with its chemical and thermal resistance, inherent flame retardancy, exceptional mechanical properties, dimensional stability and high use temperature provides numerous

possibilities for advanced applications [1]. The main characteristics of Ultem 1000 is presented in the following table:

Table 3.1 Properties of PEI (Ultem 1000). Modified from [2].

Properties	Value	Unit	Test method/standard
Physical			
Density	1.27	g/cm^3	ISO 1183
Water absorption, 23 °C/sat	1.25	%	ISO 62
Melt volume rate at 360 °C/5.0 kg	13	cm^3/10 min	ISO 1133
Mechanical			
Tensile Stress, yield, 50 mm/min	105	MPa	ISO 527
Tensile Stress, break, 50 mm/min	85	MPa	ISO 527
Tensile Strain, yield, 50 mm/min	6	%	ISO 527
Tensile Strain, break, 50 mm/min	60	%	ISO 527
Tensile modulus, 2 mm/min	3200	MPa	ISO 527
Hardness, H358/30	140	MPa	ISO 2039-1
Izod Impact, notched 80×10×4 @ +23 °C	6	kJ/m^2	ISO 180/1A
Izod Impact, notched 80×10×4 @ -30 °C	6	kJ/m^2	ISO 180/1A
Thermal			
T_g	217	°C	--
Melt temperature	370-410	°C	--
Thermal conductivity	0.24	W/m.°C	ISO 8302
Flame characteristics			
UL recognized, 94 V-2 class rating	0.4	mm	UL 94
UL recognized, 94 V-0 class rating	0.75	mm	UL 94
Electrical			
Volume resistivity	1.0×10^{15}	Ω.cm	IEC 60093

3.1.2 Polyamide-imide

The PAI used in this study was provided by Solvay (Klundert, Netherland) with a commercial name of Torlon 4203 in form on yellow-ochre color bars. Additionally, the PAI contained a 2.5 wt% of TiO_2 as added pigments. Its repeating unit is displayed in Figure 3.3.

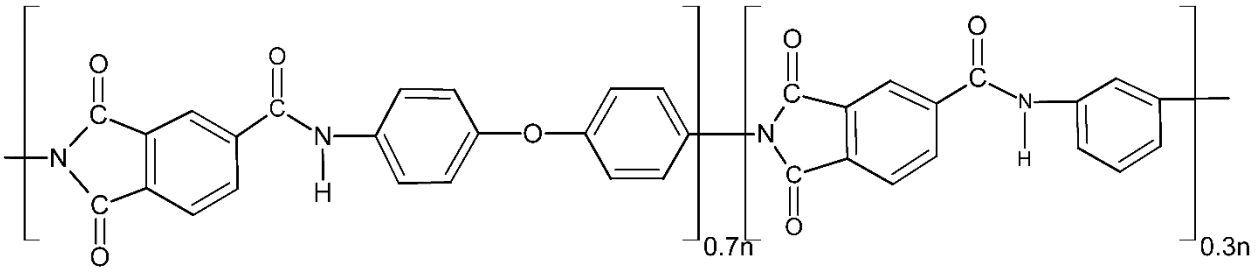

Figure 3.3 PAI Torlon 4206 repetitive unit.

Figure 3.4 PAI Torlon 4203 bar.

A summary of the basic characteristics of PAI Torlon 4203 is presented in Table 3.2

Table 3.2 Properties of PAI (Torlon 4203). Modified from [3].

Properties	Value	Unit	Test method/standard
Physical			
Density	1.42	g/cm^3	ASTM D792
Water absorption, 23 °C/after 24 h	0.33	%	ASTM D570
Mechanical			
Tensile Strength	152	MPa	ASTM D638
Tensile Stress	192	MPa	ASTM D1708
Tensile Strain	7.6	%	ASTM D638
Tensile Strain	15	%	ASTM D1708
Tensile modulus	4480	MPa	ASTM D638
Tensile modulus	4900	MPA	ASTM D1708
IZOD impact strength-unnotched	1062	J/m	ASTM D256
Thermal			
T_g	275	°C	--
Thermal conductivity	0.26	W/m.°C	ASTM D1708
Electrical			
Volume resistivity	2×10^{17}	Ω.cm	ASTM D257

3.1.3 Graphene nanoplatelets

As mentioned in the previous chapter, graphene is a 2-dimensional allotrope of carbon which consist of sp^2 hybridized carbon atoms tightly packed in a hexagonal lattice to form an atom-thick layer [4]. Exceptional mechanical properties of graphene *i.e.*, its Young modulus (≈ 1100 GPa) and fracture strength (125 GPa) [5] makes it a great candidate as nanofillers reinforcement for polymeric nanocomposites. Additionally, its transport properties such as thermal conductivity (≈ 5000 W/m. °C [6]) and electron mobility (as high as 200000 cm^2/Vs [7]) could offer multifunctionality to polymeric nanocomposites.

Graphene used throughout this study was acquired from XG science (Lansing, MI, USA) with the commercial name of xGnP M-15. The general characteristics are presented in Table 3.3.

Table 3.3 Characteristics of graphene powder (xGnP M-15). Adapted from [8].

Properties	Value		Unit
Physical			
Bulk density	2.2		g/cm^3
Residual acid content	< 0.5 wt%		%
Lateral size	15		μm
Average thickness	6-8		nm
Typical surface area	120-150		m^2/g
Mechanical			
Direction of measurement	Parallel to surface	Perpendicular to surface	
Tensile modulus	1000	NA	MPa
Tensile strength	5	NA	MPa
Thermal			
Thermal conductivity	3000	6	W/m.°C
Thermal expansion	$4 - 6 \times 10^{-6}$	$0.5 - 1.0 \times 10^{-6}$	m/m/°C
Electrical			
Electrical conductivity	10^7	10^2	S/m

3.1.4 Carbon nanotubes

Carbon nanotubes are referred to sheets of carbon atoms rolled in a cylindrical shape with diameters in scales on nanometers. These tube-like allotropes of carbon have been demonstrating exceptional properties mostly due to their symmetric structure. Although there are various reports on both experimental and theoretical measurements of their mechanical properties, all results have illustrated significantly high elastic modulus (> 1 TPa) [9]. In term of their transport properties, CNTs have estimated current carrying capacity of 10^9 A/cm^2 [10].

Multi-wall carbon nanotubes (MWCNTs) used in this study were purchased from Sigma Aldrich (Saint Louis, MO, USA) with a carbon content of > 95%, and dimensions of 6-9 nm × 5 μm. It is fair to mention that these CNTs were prepared by CVD method, using cobalt and molybdenum as catalysts.

3.1.5 Solvents

Initially *N*-methyl pyrrolidone (NMP) and *N,N′*-Dimethylformamide (DMF) were chosen as suitable solvents for the preparation of foams via WVIPS method. Although both are capable of dissolving PEI and PAI, NMP has shown higher solubility values at lower temperatures. Additionally, the proper dispersion of GnP prior to dissolving the polymers in NMP proved that it was the best choice when compared to other solvents such as acetone, tetrahydrofuran (THF), benzene, toluene, dichlorobenzene or

DMF [11] as can also be seen in Figure 3.5. Since the presence of high interfacial tension results in poor dispersion of the solid in the liquid due to the high energy value of work of cohesion and restacking, solvent selection was highly dependent on the interfacial tension between GnP and NMP [12]. Therefore, NMP was chosen since its surface tension was 40 mJ/m^2 (similar to that of GnP) and the second runner up was DMF with the value of 37.1 mJ/m^2 [13].

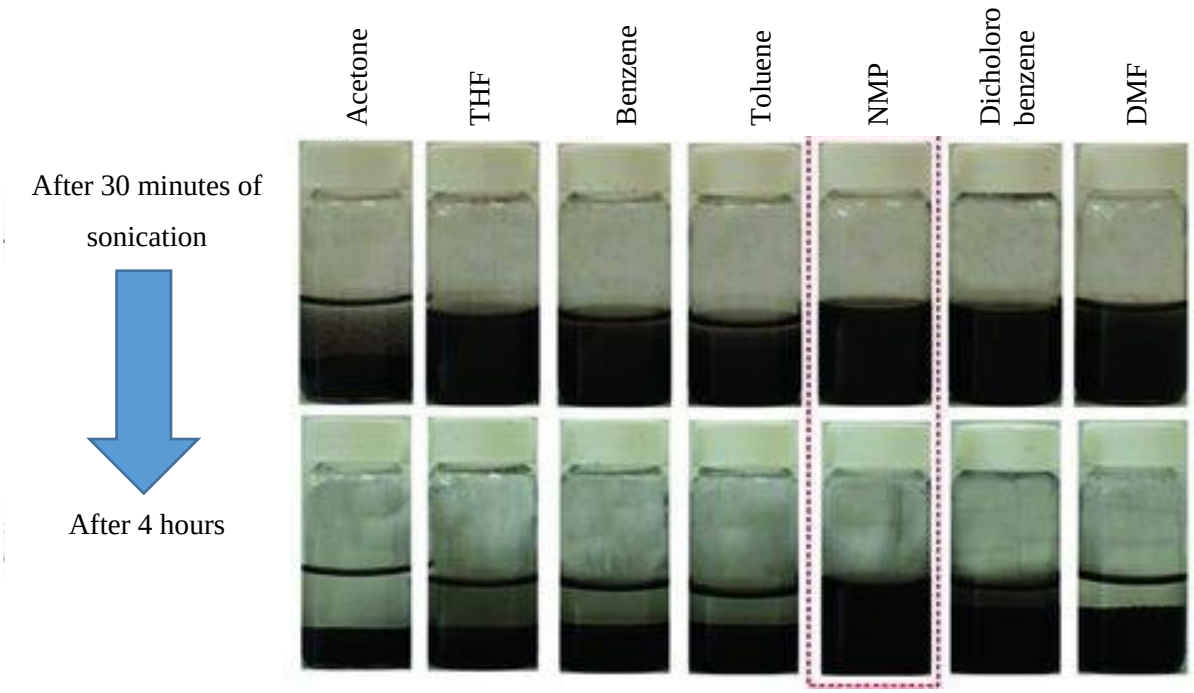

Figure 3.5 Visual comparison of GnP dispersion in organic solvents. Modified from [11].

The NMP used throughout this study was purchased from Panreac Química SA (Barcelona, Spain). NMP characteristics is presented in Table 3.4.

Table 3.4 Characteristics of N-methyl pyrrolidone (NMP). Adapted from [14].

Properties	Value	Unit
color	Clear colorless	
Miscibility with water	yes	
Hygroscopic	yes	
Melting point	-23	°C
Boiling point	202	°C
Flash point	95	°C
Ignition temperature	269	°C
pH	8.5-10	
Viscosity @ 20 °C	1.67	mPa.s
Purity	99	%

3.1.6 Carbon dioxide

As explained in previous chapters, CO_2 and N_2 are foaming agents used vastly due to their low environmental impact. CO_2 in particular is abundant, cheap, nontoxic, and has an easily achievable critical point (T_c = 31.1°C, P_c = 7.38 MPa or 73.8 bars) [15]. Numerous works have been carried out regarding the production of microcellular foams using supercritical CO_2 ($scCO_2$) [16–19] since its diffusion properties could be tuned easily by changing its pressure and temperature. The CO_2 used during this study was in form of liquid purchased from Carburos Metálicos (Barcelona, Spain).

3.2 Sample preparation

3.2.1 Polymer dissolution

Polymer dissolution in NMP was carried out using a magnetic stirrer with heating control (MBG056E BasicMagMix, OVAN; Barcelona, Spain). The condition of mixing is explained in following sections for each series of foams and masterbatch.

3.2.2 Ultrasonication

Liquid-phase exfoliation has raised a lot of attention in past years due to its potential industrial scalability [13]. The exfoliation of GnP stacks and MWCNTs in liquid medium can be carried out by the application of ultrasounds and, as mentioned before, choosing a proper solvent with low interfacial tension could be used in order to avoid re-stacking of graphene nanoparticles and CNTs. Here, we have used two equipment in order to realize this task; Bransonic 3510E DTH ultrasonication bath (Danbury, CT, USA)

and Fisher Scientific FB-705 high-power ultrasonication probe (Hampton, NH, USA). Details such as duration, frequency and amplitude of ultrasonication processes are explained for each series of samples.

3.2.3 Melt compounding

In order to obtain various compositions, a masterbatch of PEI and GnP was previously prepared in form a solution with NMP and was washed and dried in order to achieve a masterbatch enriched with 40 wt% of GnP. The GnP/NMP suspension was previously subjected to ultrasonication for 30 minutes using a FB-705 ultrasonic probe processor at maximum amplitude in order to achieve a decent dispersion and force the GnP stacks to exfoliate. The prepared masterbatch was then physically mixed with pure PEI and fed to the Brabender mixing chamber.

Melt mixing of materials was carried out using a twin screw Brabender Plastic-Corder W50 EHT (Brabender GmbH & Co.; Duisburg, Germany) with a chamber capacity of 50 cm^3, maximum torque of 200 N.m and maximum service temperature of 500 °C. The polymer and masterbatch were dried prior to mixing in a vacuum drier at 140 °C for at least 7 hours in order to minimize the water content. The condition of mixing is explained in the corresponding chapter. This step was done prior to molding the precursor and foaming.

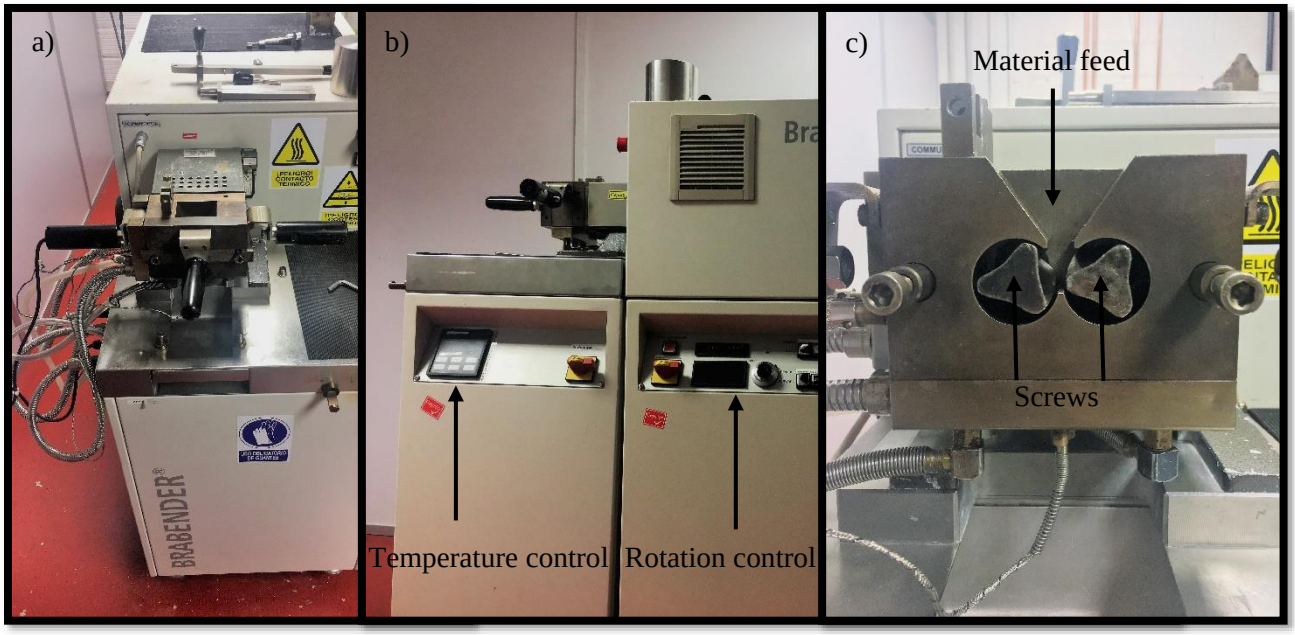

Figure 3.6 Photograph of the melt mixing equipment (Brabender Plastic-Corder W50 EHT) a) General view, b) Temperature and rotation speed/direction control and c) chamber.

3.2.4 Compression molding

Once the nanocomposites were prepared in the Brabender and grinded into small manipulable pieces, they were used in order to prepare solid precursors which were used subsequently for foaming. Compression molding was used to prepare the precursors of both pure PEI and nanocomposites. To do so, IQAP LAP PL-15 hot-plate press (IQAP Masterbatch Group S.L.; Barcelona, Spain) with electrical resistance heaters was used. In both case of pure polymer and nanocomposite molding, the materials were dried using a vacuum dried at 140 °C for at least 7 hours.

3.2.5 Foaming methods

3.2.5.1 Water vapor induced phase separation (WVIPS)

The water vapor induced phase separation method is a common process for obtaining asymmetric cellular structure. Generally speaking, this process consists of casting a polymer-solvent dissolution into a desired recipient or flat surface and following by its exposure to a non-solvent, *e.g.*, water, to induce the phase inversion. This process has been widely used for membrane preparation [20–24].

The schematic of water vapor induced phase separation of this study is presented in Figure 3.7. As can be seen in this figure, the preparation starts with dissolution of the polymer (PEI or PAI) in NMP. The specification (such as concentration, temperature, time and rpm) of this step is explained for each series of foams in the following chapters. The concentration of polymer in solvent plays a key role in defining the final average cell size and the density of the foams (as explained in Chapter 5). For foams containing nanoparticles, the nanofillers were dispersed in solvent prior to addition of the polymer (explained in Ultrasonication).

Subsequent to complete dissolution of the polymer in NMP, the solution was casted and left at room temperature in order to initiate the phase exchange between NMP and water vapor. The duration of this step depends on the thickness to surface ratio of casted dissolution.

The formed cellular structure was then emerged in water/ethanol in order to remove the excess of solvent. The following step consist of drying in vacuum which is explained for each series of foams in the following chapters.

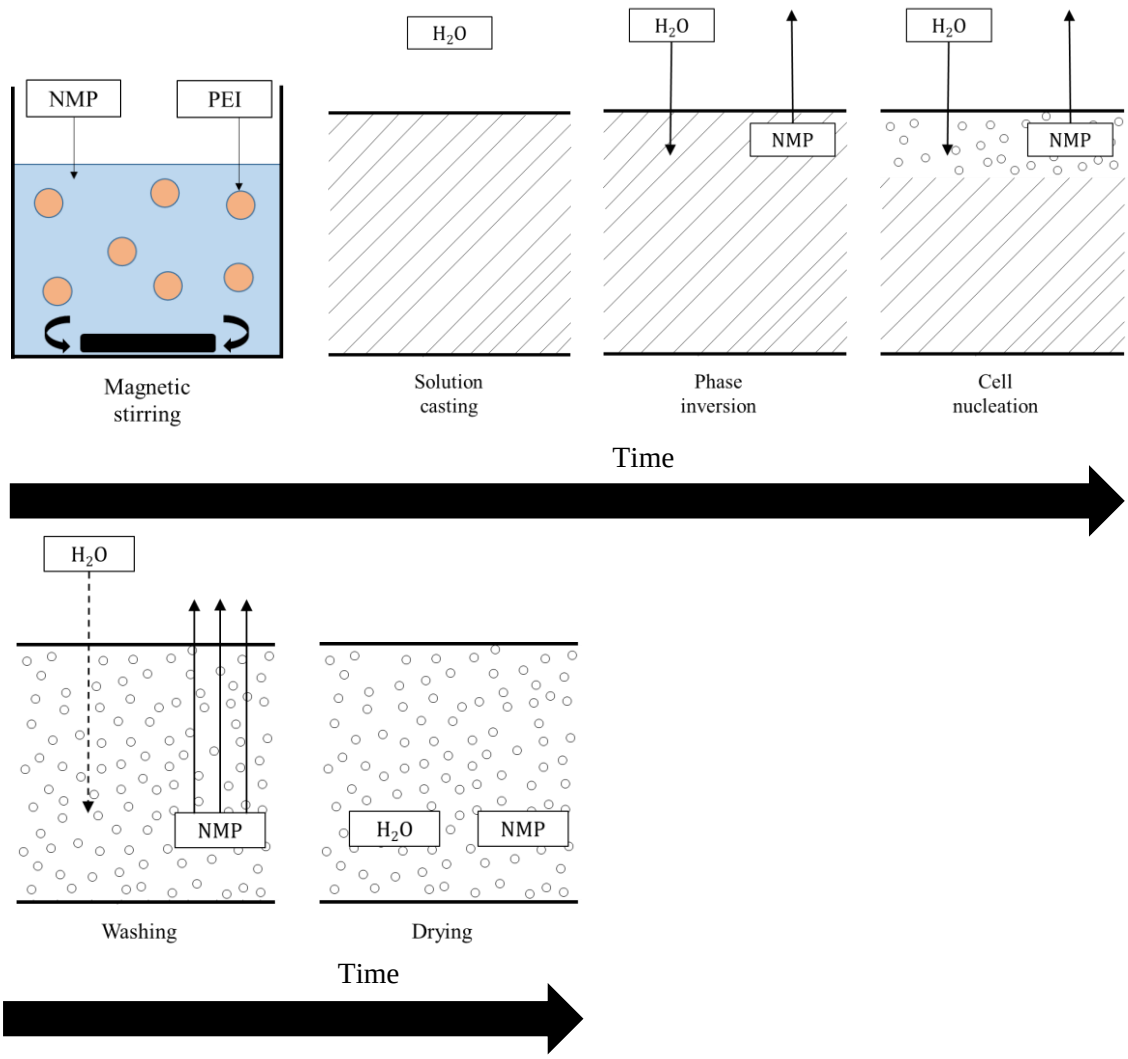

Figure 3.7 Schematic of WVIPS foaming process.

3.2.5.2 One-step supercritical CO_2 dissolution

One-step foaming process has characteristics similar to that of industrial scale productions. This method consists of dissolving a gas (normally a non-reactive gas such as CO_2 or N_2) in polymer in solid or semi-solid state followed by a sudden depressurization at a temperature equal to that of polymer's T_g. This would induce a thermodynamic instability in the system resulting in reduced miscibility of gas in the polymer and therefore, promoting cell nucleation as a second phase from a metastable polymer/gas dissolution followed by a cell growth due to diffusion of gas molecules from the polymer to the nucleated gas phase [25]. Subsequently, the formed cellular structure is stabilized due to rise of viscosity during the cooling and solidification stage.

Here, the dissolution of supercritical CO_2 ($scCO_2$) was carried out using a CH-8610 Büchiglasuster high pressure vessel (Uster, Switzerland). The dissolution was achieved by simultaneously increasing the

temperature and pressure of the vessel to 230 °C and 180-210 bar, respectively, and maintaining this condition for 5 hours. Subsequently, the expansion took place by applying a sudden depressurization (≈ 0.3 MPa/s) and moderate controlled cooling of the vessel using a water cooling system. Figure 3.8 depicts both stages of pressurization/heating and depressurization/cooling.

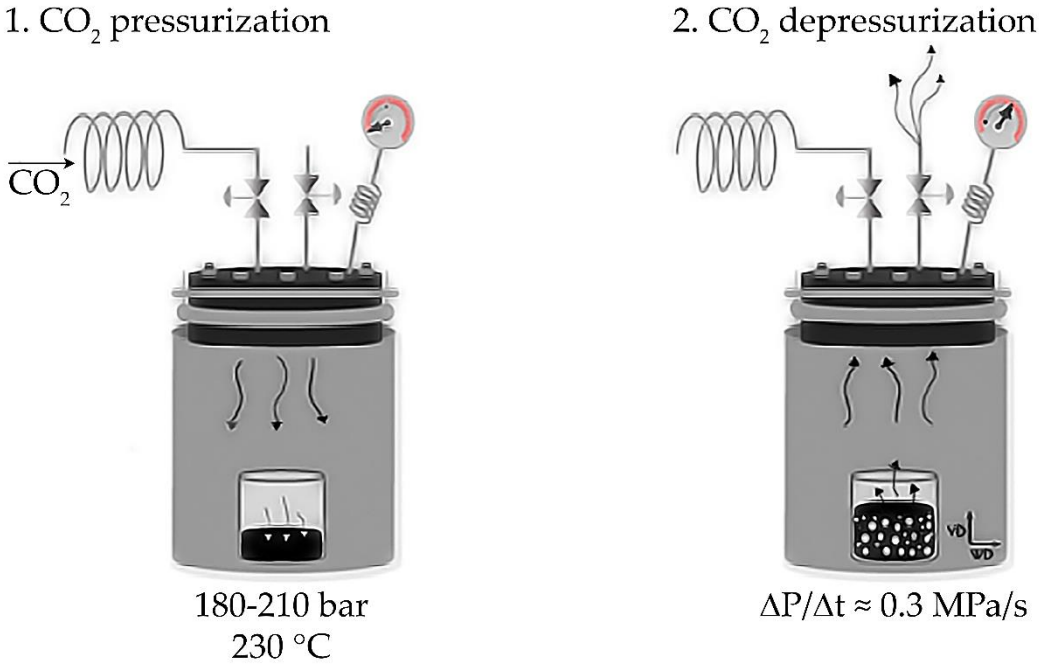

Figure 3.8 Schematic of one-step foaming using $scCO_2$ dissolution. Adapted from [26].

3.3 Characterization procedures

3.3.1 Density measurements

The densities of foams were measured according to ISO 845. A minimum of five samples were tested for each series of foams and the specimens were kept at standard atmosphere for 16 hours prior to measurement. The samples were cut into rectangular cuboid shape in order to facilitate the dimension measurements and 3 separate values were taken for each dimension. The samples were then weighted with high precision weighing scale. The density was then given by:

$$\rho = \frac{m}{V} \tag{3.1}$$

Where ρ is the density (g/cm^3), m is the mass in grams and V is the volume in cubic centimeters. Due to the particular foam preparation process of foams, the non-cellular nanocomposites were not available at any stage of the preparation and, therefore, the values of unfoamed composite density (ρ_s) could only be theoretically calculated using the density values of the polymer and GnP and their respective fractions.

3.3.2 Scanning electron microscopy (SEM)

The morphology of the foams was analyzed using JEOL JSM-5610 (Tokyo, Japan) scanning electron microscope (SEM) (see Figure 3.10). Foams were brittle fractured in liquid nitrogen and then a thin layer of gold was sputter deposited onto their surface using a BAL-TEC SCD005 (Los Angeles, CA, USA) sputter coater under argon atmosphere (see Figure 3.9).

Figure 3.9 Photograph of sputter coater used for sample preparation prior to SEM.

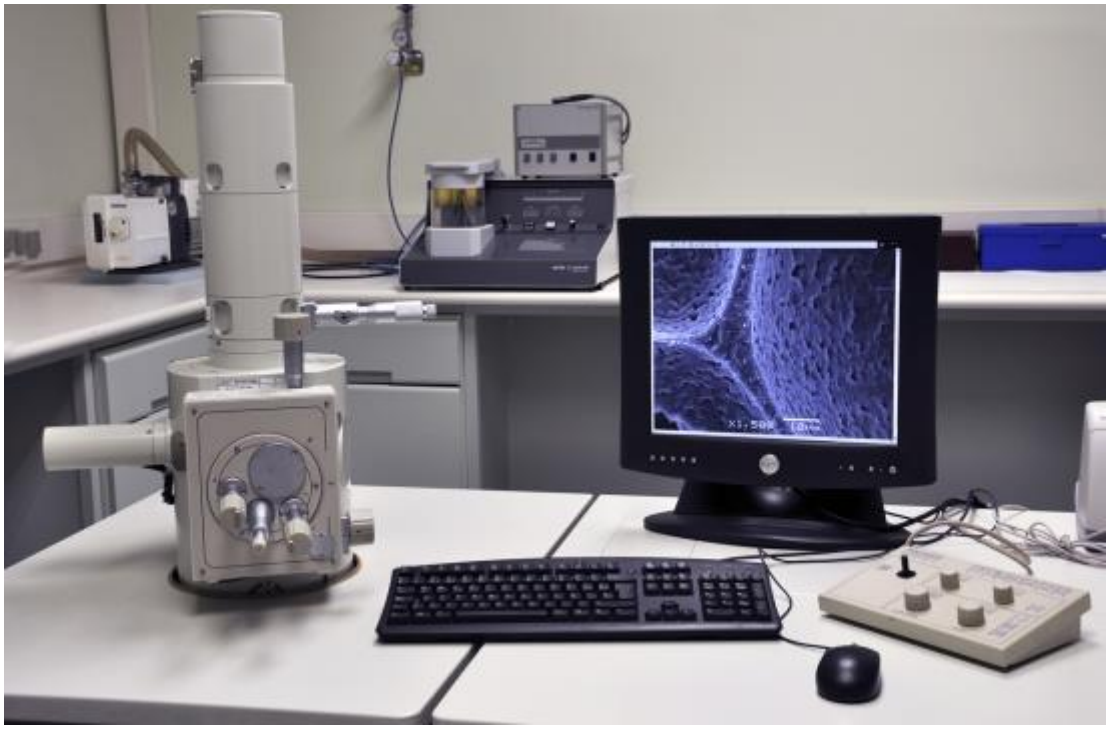

Figure 3.10 Photograph of scanning electron microscope used for morphological analysis.

In order to obtain the average cell size (Φ) value of the foams, the intercept counting method [27] was used. Micrographs with proper magnifications were analyzed for this purpose. Additionally, the cell nucleation density and cell density (N_0 and N_f, respectively) were calculated assuming an isotropic distribution of spherical cells according to equations below:

$$N_0 = \left(\frac{n}{A}\right)^{3/2}\left(\frac{\rho_s}{\rho}\right) \tag{3.2}$$

$$N_f = \frac{6}{\pi\Phi^3}\left(1-\frac{\rho}{\rho_s}\right) \tag{3.3}$$

Where n and A are the number of cells counted and area in cm^2, respectively in the chosen micrograph. In here, N_0 and N_f represent the number of cells per volume of unfoamed and foamed material respectively.

Qualitative information such as, cell shape and distribution as well as particle dispersion in the cellular structure was also gathered from different micrograph magnifications.

3.3.3 Wide angle X-ray scattering (WAXS)

Wide angle X-ray scattering (WAXS) was carried out by a PANalytical X'Pert PRO MPD Alpha1 diffractometer (Almelo, The Netherlands) operating with CuKα radiation (λ = 0.154 nm) at 40-45 kV and 40 mA. Samples were stuck with silicon paste on glass plates of 25 × 25 mm and 2 mm of thickness, that were mounted in standard sample holders for bulk samples of thickness ≤ 7 mm (PW1812/00) by means of plasticizer. Scans were taken from 2° to 60° using a 0.033° scan step and measuring time of 200 seconds per step and sample spinning 2 revolutions per second. Variable automatic divergence slit was used to get an illuminated length in the beam direction of 10 millimeters. Incident and diffracted beam were received by a X'Celerator detector with active length of 2.122º.

Figure 3.11 Photograph of X-ray diffraction equipment.

Analyzing the diffraction results would give a comparative spectrum of how the carbon-based nanofillers are dispersed throughout the cellular structure by studying the intensity of the peak corresponding to (002) crystal diffraction plane located at $2\theta = 26.5°$. The WAXS analysis would also reveal any eventual presence of crystallinity of the matrix.

3.3.4 Differential scanning calorimetry (DSC)

DSC was carried out in order to assess the possible occurrence of crystallinity and also eventual effects of the filler on the glass transition temperature of the matrix. Additionally, the DSC test during the preparation foams suing WVIPS method would assure the absence of solvent at the final drying stage. For this purpose, two DSC machines were used during the development of this study. Firstly, a Perkin Elmer Pyris 1 calorimeter (Waltham, MA, USA) with a glycol-based Perkin Elmer Intracooler IIP and secondly, a Q2000 from TA instruments (New Castle, DE, USA) with refrigerated cooling systems (RCS 90).

The Perkin Elmer DSC's heat flow measurements was based on the power compensation principle that assumes contributions by the sample and the reference sensors to the total measured heat flow nulling each other out which requires the subtraction of the previously recorded baseline. Therefore, in this equipment the sample and reference are located in two separated furnaces in order to measure the heat flow in and out of a sample, directly (see Figure 3.12). Meanwhile the heat-flux based DSC machine by TA instruments, measures the resistance and capacitance of the sensors and utilizes these values to obtain the heat flow. In this case (see Figure 3.13) both the sample and reference are placed in a single chamber and the heat flow is calculated by measuring the temperature differences between the two and process the results through calibration data.

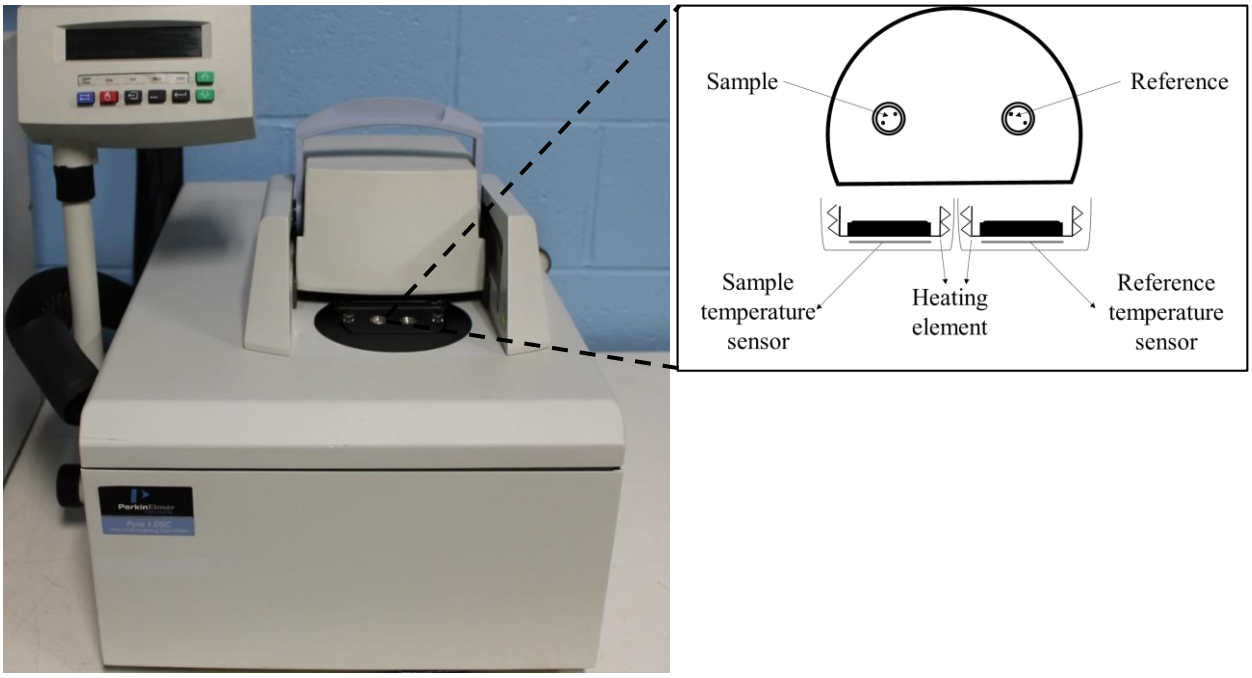

Figure 3.12 Double-furnace differential scanning calorimetry equipment.

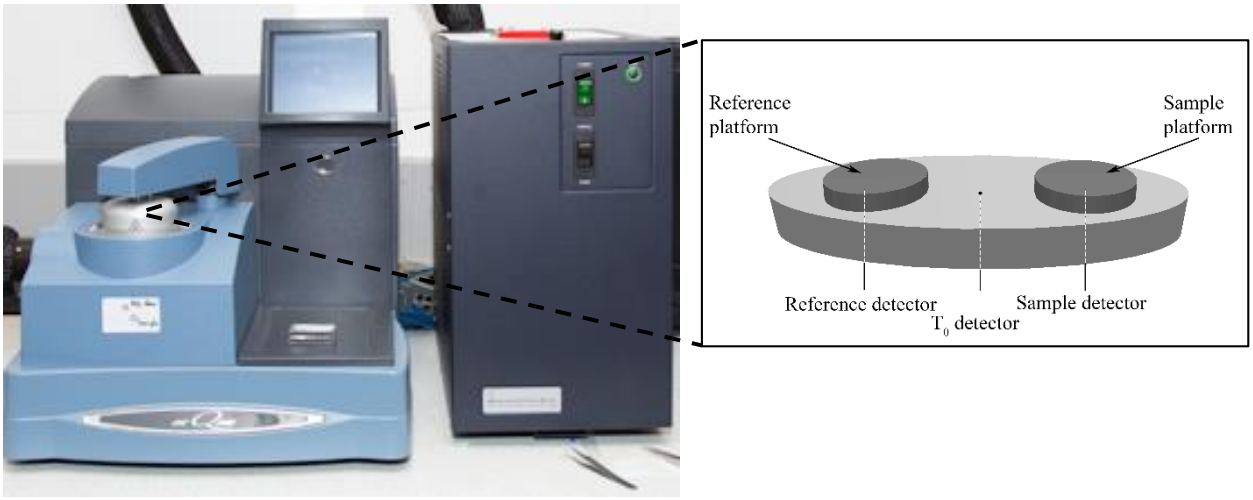

Figure 3.13 Single-furnace differential scanning calorimetry equipment.

The glass transition temperature (T_g) and the melting temperature (T_m) were determined using the inflection point in the heat flow curve and maximum temperature of the endothermic melting peak, respectively.

3.3.5 Thermogravimetric analysis (TGA)

The thermogravimetric analysis was carried out using a TGA/DSC 1 Mettler Toledo (Columbus, OH, USA) STAR System analyzer in order to investigate the thermal stability of the materials and the effect of both foaming and composition of the nanocomposite foams on their thermal degradation behaviour. The TGA tests were performed by heating a sample (5-10 mg) from 30 to 1000 °C at a rate of 10 °C/min under a constant flow of nitrogen (30 ml/min).

Figure 3.14 Photograph of thermogravimetric equipment used for thermal degradation analysis.

3.3.6 Dynamic mechanical thermal analysis (DMTA)

DMTA was used in order to study the influence of composition including nanofillers and polymer blends, density and cellular structure on the viscoelastic properties of the foams as a function of temperature. This machine simply functions as a sinusoidal oscillating force applied to a sample while analyzing its respond to the said force during a temperature window. The response could be translated into storage modulus which is the capacity of the material to respond to the applied force (elastic component) and the loss modulus which is the energy absorbed by the material through molecular mobility (viscous /imaginary component). Together they represent the complex modulus which is the ratio between the dynamic tension and the deformation.

$$E^* = E' + E'' \tag{3.4}$$

Where E^* is the complex modulus, E' is the storage modulus, and E'' is the loss modulus. E' and E'' are calculated using following expressions [28]:

$$E' = \left(\frac{f_0}{bk}\right) cos\,\delta \tag{3.5}$$

and

$$E'' = \left(\frac{f_0}{bk}\right) sin\,\delta \tag{3.6}$$

where δ is the phase angle, b is the sample geometry term, f_0 is the force applied at the peak of the sine wave, and k is the sample displacement at peak.

Another parameter which expresses the efficiency of the material in losses of energy due to molecular mobility and internal friction is *tan* δ. It is calculated as the ratio of the loss and storage modulus.

$$tan\,\delta = \frac{E''}{E'} \tag{3.7}$$

In DMTA curves, the glass transition temperature appears at the maximum of the loss modulus curve since the materials capacity to absorb energy increases by incrementing the molecular chain mobility and consequently, the temperature corresponding to the maximum of the transition peak in the *tan* δ curve could be also translated as the T_g of the material. DMA Q800 from TA instruments (New Castle, DE, USA) were used to carry out the measurements in this study. The clamps were set in a single cantilever configuration (see Figure 3.16) to analyze samples in an introduced temperature ramp with a rate of 2 °C/min while applying a dynamic strain of 0.02% at frequency of 1 Hz.

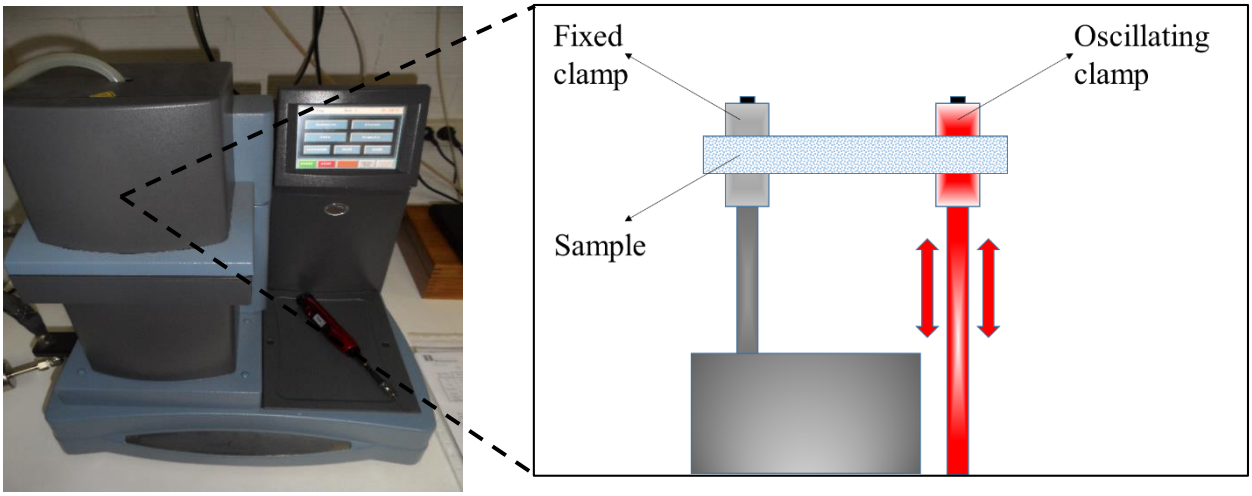

Figure 3.15 Dynamic mechanical thermal analysis equipment with single cantilever configuration.

3.3.7 Electrical conductivity measurements

The electrical conductivity measurements were carried out using a 4140B model Hewlett Packard (Palo Alto, CA, USA) pA meter/dc voltage source with a two-probe set. A thin layer of conductive colloidal silver paint was used to cover the surfaces of the samples in contact with the copper electrode pads, which had an electrical resistance between 0.01 Ω/cm^2 and 0.1 Ω/cm^2. This was done in order to ensure a perfect electrical contact between the sample and the copper pads. A direct current voltage was applied with a range of 0–20 V, voltage step of 0.05 V, hold time of 10 s, and step delay time of 5 s. The electrical conductivity (σ, in S/m) was calculated using:

$$\sigma = \frac{1}{\rho_v} \tag{3.8}$$

and

$$\rho_v = \frac{RA_{E.C}}{d} \tag{3.9}$$

where ρ_v (Ω·m) is the electrical volume resistivity, R the electrical resistance of the sample (in Ω), $A_{E.C}$ the area of the surface in contact with the electrode (in m^2), and d the distance between the electrodes (in m). A correction was applied to the measured values of electrical conductivity considering that porosity could affect the surface area in contact with the electrode. Cell size and cell density of foams were used in order to obtain the corrected value of electrical conductivity (σ_{corr}) by taking into account variations in the effective surface area as follows:

$$\sigma_{corr} = \frac{d}{R(A_{non-cell} + A_{cell-hemisphere})} \tag{3.10}$$

where $A_{non\text{-}cell}$ is the $A_{E.C}$ with the cell section excluded and

$$A_{cell-hemisphere} = \left(\frac{n}{A}\right) A_{E.C}\left(2\pi\frac{\Phi^2}{4}\right) \tag{3.11}$$

and therefore:

$$A_{non-cell} + A_{cell-hemisphere} = A_{E.C} + \left(\left(\frac{n}{A}\right) A_{E.C}\left(\pi\frac{\Phi^2}{4}\right)\right) \tag{3.12}$$

the values of n, A, and Φ were obtained from the previously analyzed SEM micrographs, and represent the number of cells, the corresponding area of the micrograph, and average cell size, respectively.

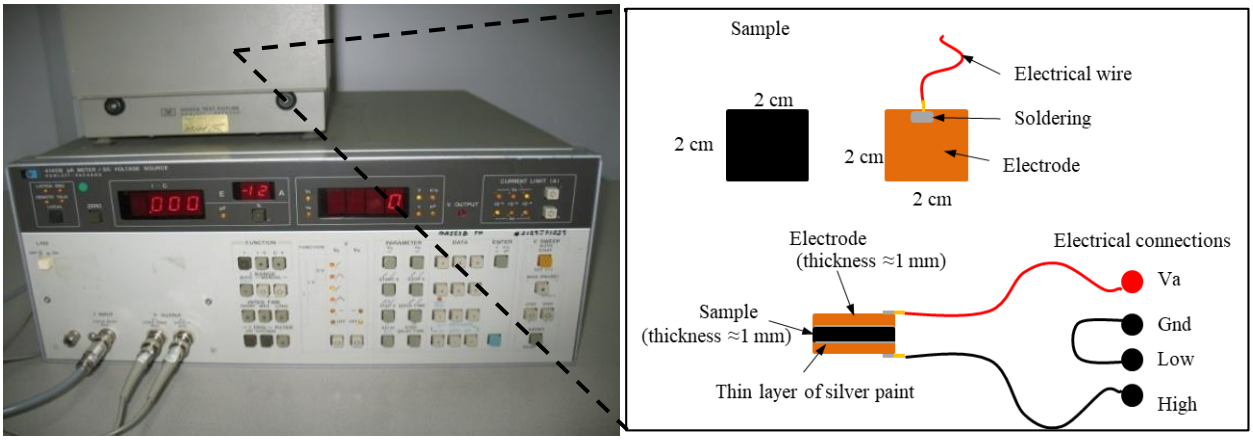

Figure 3.16 Voltage source and sample configuration used for electrical conductivity measurements.

3.4 References

1. McKeen, L.W. Polyimides. In *PERMEABILITY PROPERTIES OF PLASTICS AND ELASTOMERS*; McKeen, L.W.B.T.-P.P. of P. and E. (Third Ed.; William Andrew Publishing: Oxford, 2012, 107–120.
2. SABIC, *PEI Ultem 1000 data sheet*; Revision: 2018.
3. Solvay Engineering Plastic Products, *PAITorlon 4203 data sheet*; Revision: 2011.
4. Park, S.; Ruoff, R.S. Chemical methods for the production of graphenes. *Nat. Nanotechnol.* 2009, *4*, 217–224.
5. Lee, C.; Wei, X.; Kysar, J.W.; Hone, J. Measurement of the elastic properties and intrinsic strength of monolayer graphene. *Science*, 2008, *321*, 385–388.
6. Balandin, A.A.; Ghosh, S.; Bao, W.; Calizo, I.; Teweldebrhan, D.; Miao, F.; Lau, C.N. Superior thermal conductivity of single-layer graphene. *Nano Lett.* 2008, *8*, 902–907.
7. Bolotin, K.I.; Sikes, K.J.; Jiang, Z.; Klima, M.; Fudenberg, G.; Hone, J.; Kim, P.; Stormer, H.L. Ultrahigh electron mobility in suspended graphene. *Solid State Commun.* 2008, *146*, 351–355.
8. XG Science *xGnP M-15 date sheet*, Revision: 2019.
9. Thostenson, E.T.; Ren, Z.; Chou, T.-W. Advances in the science and technology of carbon nanotubes and their composites: a review. *Compos. Sci. Technol.* 2001, *61*, 1899–1912.
10. Collins, P.G.; Avouris, P. Nanotubes for electronics. *Sci. Am.* 2000, *283*, 62–69.
11. Zaman, I.; Kuan, H.-C.; Meng, Q.; Michelmore, A.; Kawashima, N.; Pitt, T.; Zhang, L.; Gouda, S.; Luong, L.; Ma, J. A Facile Approach to Chemically Modified Graphene and its Polymer Nanocomposites. *Adv. Funct. Mater.* 2012, *22*, 2735–2743.
12. Bonaccorso, F.; Lombardo, A.; Hasan, T.; Sun, Z.; Colombo, L.; Ferrari, A.C. Production and processing of graphene and 2d crystals. *Mater. Today* 2012, *15*, 564–589.
13. Wu, H.; Rook, B.; Drzal, L.T. Dispersion optimization of exfoliated graphene nanoplatelet in

polyetherimide nanocomposites: Extrusion, precoating, and solid state ball milling. *Polym. Compos.* 2013, *34*, 426–432.

14. PanReac AppliChem *1-Methyl-2-Pyrrolidone data sheet*; Revision: 2011.
15. Urbanczyk, L.; Calberg, C.; Detrembleur, C.; Jérôme, C.; Alexandre, M. Batch foaming of SAN/clay nanocomposites with $scCO_2$: A very tunable way of controlling the cellular morphology. *Polyme.* 2010, *51*, 3520–3531.
16. Jacobs, L.J.M.; Kemmere, M.F.; Keurentjes, J.T.F. Sustainable polymer foaming using high pressure carbon dioxide: a review on fundamentals, processes and applications. *Green Chem.* 2008, *10*, 731–738.
17. Tomasko, D.L.; Burley, A.; Feng, L.; Yeh, S.-K.; Miyazono, K.; Nirmal-Kumar, S.; Kusaka, I.; Koelling, K. Development of CO_2 for polymer foam applications. *J. Supercrit. Fluids* 2009, *47*, 493–499.
18. Ibeh, C.C.; Bubacz, M. Current trends in nanocomposite foams. *J. Cell. Plast.* 2008, *44*, 493–515.
19. Lee, L.J.; Zeng, C.; Cao, X.; Han, X.; Shen, J.; Xu, G. Polymer nanocomposite foams. *Compos. Sci. Technol.* 2005, *65*, 2344–2363.
20. Khare, V.P.; Greenberg, A.R.; Krantz, W.B. Vapor-induced phase separation—effect of the humid air exposure step on membrane morphology: Part I. Insights from mathematical modeling. *J. Memb. Sci.* 2005, *258*, 140–156.
21. Hołda, A.K.; Vankelecom, I.F.J. Understanding and guiding the phase inversion process for synthesis of solvent resistant nanofiltration membranes. *J. Appl. Polym. Sci.* 2015, *132*, 42130.
22. Thomas, R.; Guillen-Burrieza, E.; Arafat, H.A. Pore structure control of PVDF membranes using a 2-stage coagulation bath phase inversion process for application in membrane distillation (MD). *J. Memb. Sci.* 2014, *452*, 470–480.
23. Hendrix, K.; Koeckelberghs, G.; Vankelecom, I.F.J. Study of phase inversion parameters for PEEK-based nanofiltration membranes. *J. Memb. Sci.* 2014, *452*, 241–252.
24. Garcia-Ivars, J.; Alcaina-Miranda, M.-I.; Iborra-Clar, M.-I.; Mendoza-Roca, J.-A.; Pastor-Alcañiz, L. Enhancement in hydrophilicity of different polymer phase-inversion ultrafiltration membranes by introducing PEG/Al_2O_3 nanoparticles. *Sep. Purif. Technol.* 2014, *128*, 45–57.
25. Di Maio, E.; Mensitieri, G.; Iannace, S.; Nicolais, L.; Li, W.; Flumerfelt, R.W. Structure optimization of polycaprolactone foams by using mixtures of CO_2 and N_2 as blowing agents. *Polym. Eng. Sci.* 2005, *45*, 432–441.
26. Gedler, G.; Antunes, M.; Realinho, V.; Velasco, J.I. Novel polycarbonate-graphene nanocomposite foams prepared by CO_2 dissolution. In Proceedings of the IOP Conference Series: Materials Science and Engineering; IOP Publishing, 2012; *31*, 012008.
27. Sims, G.L.A.; Khunniteekool, C. Cell-size measurement of polymeric foams. *Cell. Polym.* 1994, *13*, 137–146.
28. Menard, K.P. *Dynamic mechanical analysis: a practical introduction*; CRC press, 2008.

Chapter 4

The WVIPS foaming method: PEI, PEI-GnP and PEI/PAI microcellular foams

4.1 Graphene nanoplatelets-reinforced polyetherimide foams prepared by water vapor-induced phase separation

4.1.1 Abstract and conclusions

This chapter focuses on the preparation and characterization of nanocomposite foams based on WVIPS method using high-performance thermoplastic polyetherimide and graphene nanoplatelets. Foams were prepared with various amounts of GnP (1-10 wt%) and were characterized using SEM, WAXS (XRD), DSC, TGA, DMTA and electrical conductivity measurements.

The idea of preparing a multifunctional nanocomposite foam with functionalities such as electrical conductivity that could be regulated by controlling the amount of nanofillers would provide numerous possibilities in cutting edge applications of industries such as electronics and aerospace. Various parameters should be considered regarding the modification of foams' properties and functionalities. For instance, foams with different densities and cellular structures would result in changes of their final properties. As mentioned before in equation (1.3) by Gibson and Ashby [1] in chapter 1, most physical properties of the foams could be estimated based on characteristics of their respective unfoamed materials and their final densities.

Since foaming would particularly affect the mechanical properties of the materials, in a manner that by decreasing the density foams tend to lose their stiffness, specific nanofillers could contradict this loss due to contribution of their intrinsic high mechanical properties. Among these nano-scale reinforcements, the use of carbon-based fillers in foams was increased drastically due to their exceptional mechanical properties [2,3]. Furthermore, carbon-based nanofillers such as GnP and CNT could provide additional functionalities for cellular materials. For this purpose, the use of carbon-based nanofillers were considered in this study. Since the addition of fillers would affect various aspects of the foams, such as their foaming process and final characteristics of the foams, thorough characterization of the products is essential to have a better understanding of these materials.

This study was developed in order to cover various objective points. Firstly, preparing a PEI-based foam using WVIPS method and study the structure and morphology of the foam. Secondly, introducing various amounts of graphene nanoparticles and investigate its effects on structure and morphology of the foams as well as their thermal stability, dynamic-mechanical-thermal properties and electrical conductivity.

The following conclusions could be extracted from this chapter:

1. Through WVIPS foaming process, homogenous microcellular PEI foams were obtained. These foams did not exhibit any sign of crystallinity according to XRD and DSC results.

2. The morphological aspects of the foams were affected by the thickness of the films during the preparation of the foams. Particularly, foams with lower thickness showed higher values of relative density with relatively smaller average cell size value.
3. The addition of GnP also resulted in slightly higher values of average cell size, showing that the presence of GnP could mildly affect the phase separation process.
4. Although the nanocomposite foams showed a good dispersion level of nanoparticles, the full exfoliation of graphene stacks was not achieved throughout the process.
5. The addition of graphene improved the thermal stability of the foams resulting in higher onset decomposition temperatures.
6. Both foaming and GnP addition had very little effect on the glass transition temperature of the polymer.
7. The specific storage modulus of the foams had an increment in value by increasing the amount of GnP.
8. The addition of GnP resulted in a mild increase of the foam's electrical conductivity reaching 1.8×10^{-7} S/m at 2.2 vol% GnP (10 wt%). This obtained results showed a formation of conductive network. The foam's obtained electrical conductivity is sufficient for applications such as EMI shielding.

4.1.2 References

1. Gibson, L. J.; Ashby, M. F. Cellular solids: structure and properties; Cambridge university press, 1999. 2. Young, R. J.; Kinloch, I. A.; Gong, L.; Novoselov, K. S. The mechanics of graphene nanocomposites: a review. Compos. Sci. Technol. 2012, 72, 1459–1476.

3. Lee, C.; Wei, X.; Kysar, J. W.; Hone, J. Measurement of the elastic properties and intrinsic strength of monolayer graphene. Science, 2008, 321, 385–388.

4.1.3 Published article (Journal of eXPRESS Polymer Letters, Vol. 9, Page 412-423, 2015)

This chapter displays the preparation and characterization of first series of PEI-GnP foams prepared via WVIPS foaming. The article included in this chapter is titled **Graphene nanoplatelets-reinforced polyetherimide foams prepared by water vapor-induced phase separation** and was published in **eXPRESS Polymer Letters** in **2015**

ATTENTION¡¡
Pages 176 to 187 of the thesis, containing this article, are available at the editor's web
http://www.expresspolymlett.com/index.html?tartalom=content.php&year=2015&number=1&kodnumber=1
DOI: 10.3144/expresspolymlett.2015.40

4.2 Influence of polyamide–imide concentration on the cellular structure and thermo-mechanical properties of polyetherimide/polyamide–imide blend foams

4.2.1 Abstract and conclusions

In this chapter the possibility of preparing foams using WVIPS method with addition of PAI to PEI-based foams is investigated. Differences in kinetics of the PEI and PAI during foaming were observed, and the changes in cellular structure of the foams and consequently, variation in the foams' properties were characterized through SEM, WAXS, DSC, TGA and DMTA.

The aim behind polymeric blends is to create new materials with tunable properties without chemical modification while achieving a significant reduction in cost. Various researchers have investigated numerous possibilities of PEI-based polymer blends including PEI/PEEK [1–3], PEI/PC [4,5], PEI/amorphous polyamide (a-PA) [6], PEI/liquid crystalline polymer (LCP) [7–10], PEI/polyethylene terephthalate (PET) [11–13], and PEI/ polytrimethylene terephthalate (PTT) [14].

In case of this study, high glass transition temperature of polyamide-imide (PAI) and its mechanical properties were the reasons behind the preparation of these blends. As it was mentioned before, PEI is one of high performance polymers with relatively high temperature service and this aspect of PEI could be improved by addition of PAI since it possesses even higher stability due to its elevated T_g.

This study was developed in order to cover various objective points. Firstly, preparing a PEI/PAI foam using WVIPS method and study the structure, and physical properties of the foams. Secondly, investigate the effect of PAI amount on the structure and morphology of the foams as well as their thermal stability and dynamic-mechanical-thermal properties.

The following conclusions could be extracted from this chapter:

1. Through WVIPS foaming process, homogenous medium-density polyetherimide (PEI)/polyamide–imide (PAI) blend foams were prepared containing 0, 25, 50 and 100 wt% PAI.
2. These foams did not exhibit any sign of crystallinity according to XRD and DSC results.
3. The morphological aspects of the foams were strongly affected by the addition of PAI. Particularly, foams with 50 wt% of PAI presented a dual cellular structure where the bigger cells were initially formed from a PAI-rich phase and secondary smaller cells formed by the remaining PEI-rich solution.
4. The addition of PAI resulted in a decrease in temperature corresponding to the onset of the thermal decomposition but its presence delayed the secondary stage of the degradation resulting in higher values of char residual.

5. Owing to the high stiffness of PAI compared to PEI, blend foams demonstrated a general increasing trend of the storage modulus when compared to pure PEI foams.
6. The particularly fine microcellular structure of foams containing 25 wt% of PAI was responsible for the highest specific modulus among blend foams, similar to that of pure PAI foam, in spite of the relatively low content of PAI. On the contrary, albeit having a higher amount of PAI, 50/50 blend foam displayed a comparatively lower specific storage modulus due to its dual cellular morphology, particularly the presence of considerably bigger cells.
7. The appeared peaks in loss modulus and tan delta curves showed a certain level of miscibility in the blend foams. Specifically, foams with only 25 wt% PAI demonstrated a disappearance of the second peak in loss modulus and *tan* δ curves related to the T_g of PAI which could be taken as a proof of the miscibility of the PAI in PEI.

4.2.2 References

1. Jenkins, M.J. Crystallisation in miscible blends of PEEK and PEI. *Polymer.* 2001, *42*, 1981–1986.
2. Jenkins, M.J. Relaxation behaviour in blends of PEEK and PEI. *Polymer.* 2000, *41*, 6803–6812.
3. Bicakci, S.; Cakmak, M. Development of structural hierarchy during uniaxial drawing of PEEK/PEI blends from amorphous precursors. *Polymer.* 2002, *43*, 149–157.
4. Zhang, M.; Choi, P.; Sundararaj, U. Molecular dynamics and thermal analysis study of anomalous thermodynamic behavior of poly (ether imide)/polycarbonate blends. *Polymer.* 2003, *44*, 1979–1986.
5. Chun, Y.S.; Lee, H.S.; Kim, W.N.; Oh, T.S. Thermal properties and morphology of blends of poly (ether imide) and polycarbonate. *Polym. Eng. Sci.* 1996, *36*, 2694–2702.
6. Ramiro, J.; Eguiazábal, J.I.; Nazábal, J. Structure and mechanical properties of blends of poly (ether imide) and an amorphous polyamide. *Eur. Polym. J.* 2006, *42*, 458–467.
7. Hatui, G.; Malas, A.; Bhattachaya, P.; Dhibar, S.; Kundu, M.K.; Das, C.K. Effect of Expanded Graphite and PEI- co-Silicon Rubber on the Thermo Mechanical, Morphological as well as Rheological properties of in situ composites based on poly (ether imide) and liquid crystalline polymer. *J. Alloys Compd.* 2015, *619*, 709-718.
8. Nayak, G.C.; Rajasekar, R.; Das, C.K. Effect of SiC coated MWCNTs on the thermal and mechanical properties of PEI/LCP blend. *Compos. Part A Appl. Sci. Manuf.* 2010, *41*, 1662–1667.
9. Hong, S.; Gil, Y.S.; Hwang, S.S.; Hong, S.M. Effect of poly (esterimide) s as compatibilizers on the physical properties of poly (etherimide)/thermotropic liquid crystalline polymer in-situ composites. *Polym. J.* 2004, *36*, 271–283.
10. Bastida, S.; Eguiazábal, J.I.; Nazábal, J. Effects of mixing procedure on the morphology and properties of poly(ether imide)/thermotropic copolyester blends. *Eur. Polym. J.* 1999, *35*, 1661–1669.
11. Ruvolo-Filho, A.; de Fátima Barros, A. Correlation between thermal properties and conformational

changes in poly (ethylene terephthalate)/poly (ether imide) blends. *Polym. Degrad. Stab.* 2001, *73*, 467–470.

12. Chen, H.-L.; Hwang, J.C.; Chen, C.-C. Multiple melting and crystal annealing of poly (ethylene terephthalate) in its blends with poly (ether imide). *Polymer.* 1996, *37*, 5461–5467.
13. Martínez, J.M.; Eguiazábal, J.I.; Nazábal, J. Miscibility level and properties of poly(ether imide)/poly(ethylene terephthalate) blends. *J. Appl. Polym. Sci.* 1996, *62*, 393–408.
14. Supaphol, P.; Dangseeyun, N.; Thanomkiat, P.; Nithitanakul, M. Thermal, crystallization, mechanical, and rheological characteristics of poly(trimethylene terephthalate)/poly(ethylene terephthalate) blends. *J. Polym. Sci. Part B Polym. Phys.* 2004, *42*, 676–686.

4.2.3 Published article (Journal of European Polymer Journal, Vol. 69, Page 273-283, 2015)

This chapter displays the preparation and characterization of PEI/PAI foams prepared via WVIPS foaming. The article included in this chapter is titled **Influence of polyamide–imide concentration on the cellular structure and thermo-mechanical properties of polyetherimide/polyamide–imide blend foams** and was published in **European Polymer Journal** in **2015.**

ATTENTION¡¡
Pages 192 to 202 of the thesis, containing this article, are available at the editor's web
https://www.sciencedirect.com/science/article/abs/pii/S0014305715003183
DOI: 10.1016/j.eurpolymj.2015.06.014

Chapter 5

Improving the microstructure through solution concentration and GnP ultrasonication

5.1 Enhancing the electrical conductivity of polyetherimide-based foams by simultaneously increasing the porosity and graphene nanoplatelets dispersion

5.1.1 Abstract and conclusions

Following the successful preparation and characterization of PEI foams containing GnP, which was explained previously, this chapter focuses on various ways to modify the foaming process in order to achieve a path in which the maximum potential of the nanofillers and foams could be extracted. Similarly, in this chapter, various amounts of GnP (1-10 wt%) were used and the resultant foams were characterized through SEM, WAXS, TGA, DMTA and electrical conductivity measurements.

The final properties of nanocomposites are highly affected by the distribution and orientation of the nanofillers. Therefore, one way to optimize the performance of nanocomposites is through improved dispersion of nanofillers throughout the matrix [1]. Liquid-phase exfoliation has been introduced and investigated as a solution to tackle agglomeration of filler mainly due to its simplicity and potential for industrial scalability [2]. For carbon-based nanoparticles such as GnP, ultrasonication could be applied to a mixture of the nanofillers and a proper liquid in order to promote the exfoliation of GnP stacks. This type of exfoliation is achieved by hydrodynamic shear-forces corresponding to cavitation, which is the formation, growth and collapse of microbubbles within a liquid substance which are formed due to pressure fluctuations [3,4]. In order to stabilize the inter-particle attractive forces and avoid re-agglomeration of the GnP, a proper solvent should be used which is highly dependent in the interfacial tension between the solvent and the nanoparticles surface. In order to achieve good dispersion, restacking should be avoided by choosing a solvent which would minimize the value of interfacial tension. In case of high interfacial tension between the GnP and a solvent, after the application of ultrasound, the nanoparticles tend to adhere to one another and the work of cohesion is high between them. Consequently, organic solvents with a surface close to 40 mJ/m^2 would be the suitable solution for graphene dispersion. *N*-methyl pyrrolidone (NMP) is one of the solvents with this characteristic which is also able to dissolve PEI therefore, a suitable option of the objective of this study.

Additionally, foaming has shown to improve the electrical conductivity of nanocomposites by reducing the inter-particular distance between the conductive nanofillers and assist the formation of a conductive network throughout the cell struts. Various works have been published emphasizing on the positive effect of foaming and/or increased porosity on the electrical conductivity of the nanocomposite foams due to repositioning of the nanoparticles and promoting the probability of electrical conduction by mechanisms such as tunneling [5–7].

This section of the study focuses on the improvement of already existing foaming process for PEI-GnP nanocomposite in order to obtain foams with higher electrical conductivity through ultrasonication

and increased porosity. From the results and analysis of the prepared foams the following conclusions could be extracted in this chapter:

1. Through WVIPS foaming process, homogenous microcellular PEI foams were obtained and these foams did not exhibit any sign of crystallinity according to XRD and DSC results.
2. Compared with the previous chapter, here, the foams were prepared with lower concentration of polymer in the casting solution, resulting in lower density values and higher average cell sizes.
3. In here, the cellular structure demonstrated no influence from the previously ultrasonicated GnP amounts in the system. Compared with previous results, the better dispersion facilitated by the ultrasonication seem to reduce the effect of nanoparticles amount on the foaming process, resulting in formation of foams with similar densities and microstructures.
4. The foams prepared in this chapter have shown and improved thermal stability with increasing the amount of GnP.
5. The foams prepared in this section have shown improved mechanical properties by incrementing the GnP amount. The GnP addition has resulted in significant improvements in both series of foams. In series 1 foams (25wt% PEI in solution and higher resultant density values), the specific storage modulus rose from 1335.6 to 1718.2 MPa.cm^3/g for 1 and 10 wt% of GnP respectively, and in case of series 2 foams (lower densities), the specific storage modulus increased from 1110.9 to 1476.2 MPa.cm^3/g for similar amounts of GnP nanoparticles.
6. Most importantly, the ultrasonication and increased porosity resulted in significant increase in electrical conductivity of the foams prepared in this chapter. The reduction of the distance between conductive GnP particles resulted in increases as high as six orders of magnitude. The results fitted the tunnel conduction model which demonstrated the presence of a 3D random network in sonicated PEI-GnP foams as a consequence of improved dispersion of GnP. Said results suggest that a full GnP exfoliation would not be essential to achieve high electrical conductivities in these foams.

5.1.2 References

1. Wu, H.; Rook, B.; Drzal, L. T. Dispersion optimization of exfoliated graphene nanoplatelet in polyetherimide nanocomposites: Extrusion, precoating, and solid state ball milling. *Polym. Compos.* 2013, *34*, 426–432.
2. Bonaccorso, F.; Lombardo, A.; Hasan, T.; Sun, Z.; Colombo, L.; Ferrari, A. C. Production and processing of graphene and 2d crystals. *Mater. Today* 2012, *15*, 564–589.
3. Young, F. R. *Cavitation*; World Scientific, 1999.
4. Mason, T. J.; Peters, D. An introduction to the uses of power ultrasound in chemistry.

Sonochemistry, *Oxford Univ. Press New York* 1999.

5. Maxian, O.; Pedrazzoli, D.; Manas-Zloczower, I. Conductive polymer foams with carbon nanofillers - Modeling percolation behavior. *Express Polym. Lett.* 2017, *11*, 406–418.
6. Gedler, G.; Antunes, M.; Velasco, J. I. Enhanced electrical conductivity in graphene-filled polycarbonate nanocomposites by microcellular foaming with sc-CO_2. *J. Adhes. Sci. Technol.* 2016, *30*, 1017–1029.
7. Ryvkina, N.; Tchmutin, I.; Vilčáková, J.; Pelíšková, M.; Sáha, P. The deformation behavior of conductivity in composites where charge carrier transport is by tunneling: theoretical modeling and experimental results. *Synth. Met.* 2005, *148*, 141–146

5.1.3 Published article (Journal of Polymer Composites, Vol. 40, Page E1416-E1425, 2019)

This chapter displays the modification of WVIPS process parameters, particularly by addition of ultrasonication step and tuning the polymer concentration in order to improve the properties of PEI-based foams, specifically in terms of their electrical conductivity. The article included in this chapter is titled **Enhancing the electrical conductivity of polyetherimide-based foams by simultaneously increasing the porosity and graphene nanoplatelets dispersion** published in **Polymer Composites** in Wiley online library **2018.**

ATTENTION¡¡
Pages 209 to 218 of the thesis are available at the editor's web
https://onlinelibrary.wiley.com/doi/abs/10.1002/pc.25029

Chapter 6

PEI foams with enhanced electrical conductivity through an optimized hybrid nanofillers system

6.1 Effects of carbon nanotubes/graphene nanoplatelets hybrid systems on the structure and properties of polyetherimide-based foams

6.1.1 Abstract and conclusions

Following the optimization of the PEI-based foams, in this chapter we are focusing on the preparation of PEI foams containing carbon nanotubes (0.1-2.0 wt%) and carbon nanotube/graphene hybrid nanofillers with total amount of 2 wt%. foams were prepared using the WVIPS method and were characterized by SEM, WAXS, TGA, DMTA and electrical conductivity measurements.

CNT/GnP hybrid reinforcement was chosen with the objective of simultaneous improvement of electrical conductivity and mechanical properties of the foams. Maxian *et al.* [1] have conducted a study on a new numerical model considering the distribution of nanofillers in polymeric foams. Their model predicted that the electrical percolation threshold would decrease in a foam containing 1D-carbon nanotubes and 2D-graphene nanoplatelets by increasing the porosity due to repositioning of the conductive nanoparticles as a result of foaming. This model was in agreement with experimental results produced by Gedler *et al.* [2] showing the increment of electrical conductivity and decrease in percolation threshold of foamed PC-GnP nanocomposite when compared to that of unfoamed nanocomposite. Sensitivity analysis showed that the electrical percolation behavior of the porous polymer incorporating 1D- and 2D-nanofillers was significantly under influence of four main factors:

i. Porosity level
ii. Type of filler
iii. Filler alignment
iv. Filler aspect ratio (AR)

The type of filler and its AR played the most important roles in establishing the percolation threshold [1].

Various studies have focused on the applications of CNT/GnP hybrid based materials. Tung *et al.* [3] have reported the preparation of a nanocomposite consisting in chemically converted graphene and CNT without the use of any surfactant while maintaining the intrinsic electrical and mechanical properties of the carbon-based components. Their results have shown successful preparation of hybrid materials for high-performance transparent conductors. Nguyen *et al.* [4] have also reported a successful preparation of CNT/GnP hybrid material for transparent conductive films using versatile method based on low vacuum annealing of cellulose acetate on nickel's surface resulting in transparent films with tunable properties. Another study [5] also reported a versatile preparation process based on rapid heating and cooling during a CVD-based method for CNT/GnP hybrid growth. The graphene stack thickness and the density of CNTs were properly monitored. Based on this method, the opto-electronic and field emission properties of

57. Yang, Y.; Gupta, M.C.; Dudley, K.L.; Lawrence, R.W. A comparative study of EMI shielding properties of carbon nanofiber and multi-walled carbon nanotube filled polymer composites. *J. Nanosci. Nanotechnol.* **2005**, *5*, 927–931. [CrossRef] [PubMed]
58. Verdejo, R.; Bernal, M.M.; Romasanta, L.J.; Lopez-Manchado, M.A. Graphene filled polymer nanocomposites. *J. Mater. Chem.* **2011**, *21*, 3301–3310. [CrossRef]

Chapter 7

Enhancing the electrical conductivity through high pressure scCO_2 dissolution process

7.1 Polyetherimide foams filled with low content of graphene nanoplatelets prepared by $scCO_2$ dissolution

7.1.1 Abstract and conclusions

This chapter focuses of PEI-based foams with graphene nanoplatelets (GnP) prepared by supercritical carbon dioxide ($scCO_2$) dissolution and their characterization through SEM, WAXS, TGA, DMTA and electrical conductivity measurements.

Since the PEI-GnP nanocomposite foams prepared by WVIPS method showed promising results in terms of their significant enhancement of mechanical and electrical properties, another foaming method with characteristics closer to that of industrial processes was considered. This method involves dissolution of a gas in polymeric precursor in a semi-solid state and subsequent foaming by sudden drop of pressure [1] (one-step or solid-state foaming) or increasing the temperature of gas-saturated precursor [2] (two-step foaming) at low pressure in order to induce foaming. Both pathways have been used vastly in order to obtain homogenous microcellular foams using vast number of polymers.

The first series of foams prepared by dissolution of CO_2 in this study contains 0-2 wt% of GnP. The objective of preparing such foams was to analyze the foaming parameters on the cellular structure of the foams as well as their physical properties. Additionally, the addition of GnP was considered in order to counteract the negative effect of foaming on the mechanical properties of the foams and provide foams with increased electrical conductivity.

The following conclusions arose after thorough analysis of prepared foams:

1. In terms of cellular structure, PEI-GnP foams presented a microcellular closed-cell structure with similar cell sizes and cell densities independent from the amount of GnP.
2. The X-ray diffraction analysis showed that the combination of ultrasonication, melt-mixing and sudden expansion using depressurization of $scCO_2$ promoted enhanced dispersion and partial exfoliation of GnP in the foams.
3. The addition of GnP did not seem to improve the thermal stability of the foams, particularly at the onset of the decomposition process.
4. The mechanical properties of the foams were mainly controlled by their respective density. The addition of GnP in foams with similar densities resulted in increased stiffness due to intrinsic mechanical properties of graphene nanoplatelets.
5. The electrical conductivity of the foams improved significantly with the addition of GnP following a tunneling conduction model.

7.1.2 References

1. Gedler, G.; Antunes, M.; Realinho, V.; Velasco, J.I. Novel polycarbonate-graphene nanocomposite foams prepared by CO2 dissolution. I*n Proceedings of the IOP Conference Series: Materials Science and Engineering*; IOP Publishing, 2012; *31*, 2008.
2. Gedler, G.; Antunes, M.; Velasco, J.I. Effects of graphene nanoplatelets on the morphology of polycarbonate–graphene composite foams prepared by supercritical carbon dioxide two-step foaming. *J. Supercrit. Fluids* 2015, *100*, 167–17

7.1.3 Published article (Journal of Polymers, Vol. 11, Page 328, 2019)

This chapter displays the preparation and characterization of first series of PEI-GnP foams prepared via one-step foaming by $scCO_2$ dissolution. The article included in this chapter is titled **Polyetherimide foams filled with low content of graphene nanoplatelets prepared by $scCO_2$ dissolution** and was published in **Polymers** in **2019.**

polymers

MDPI

Article

Polyetherimide Foams Filled with Low Content of Graphene Nanoplatelets Prepared by $scCO_2$ Dissolution

Hooman Abbasi, Marcelo Antunes * and José Ignacio Velasco

Centre Català del Plàstic, Departament de Ciència dels Materials i Enginyeria Metal lúrgica, Universitat Politècnica de Catalunya (UPC Barcelona Tech), C/Colom 114, E-08222 Terrassa, Barcelona, Spain; hooman.abbasi@upc.edu (H.A.); jose.ignacio.velasco@upc.edu (J.I.V.)

* Correspondence: marcelo.antunes@upc.edu; Tel.: +34937837022

Received: 8 January 2019; Accepted: 11 February 2019; Published: 13 February 2019

Abstract: Polyetherimide (PEI) foams with graphene nanoplatelets (GnP) were prepared by supercritical carbon dioxide ($scCO_2$) dissolution. Foam precursors were prepared by melt-mixing PEI with variable amounts of ultrasonicated GnP (0.1–2.0 wt %) and foamed by one-step $scCO_2$ foaming. While the addition of GnP did not significantly modify the cellular structure of the foams, melt-mixing and foaming induced a better dispersion of GnP throughout the foams. There were minor changes in the degradation behaviour of the foams with adding GnP. Although the residue resulting from burning increased with augmenting the amount of GnP, foams showed a slight acceleration in their primary stages of degradation with increasing GnP content. A clear increasing trend was observed for the normalized storage modulus of the foams with incrementing density. The electrical conductivity of the foams significantly improved by approximately six orders of magnitude with only adding 1.5 wt % of GnP, related to an improved dispersion of GnP through a combination of ultrasonication, melt-mixing and one-step foaming, leading to the formation of a more effective GnP conductive network. As a result of their final combined properties, PEI-GnP foams could find use in applications such as electrostatic discharge (ESD) or electromagnetic interference (EMI) shielding.

Keywords: polyetherimide foams; graphene; multifunctional foams; ultrasonication; $scCO_2$; electrical conductivity

1. Introduction

Polyetherimide (PEI) is a high-performance thermoplastic that has proven to be a viable candidate in advanced applications in cutting edge sectors, such as aerospace, due to its outstanding properties, including, but not limited to, high mechanical performance, high chemical and inherently high flame resistance, thermal and dimensional stability, low smoke generation, and transparency [1]. Weight reduction by means of foaming has been proven as one of the most promising strategies for cost reduction and for attaining functional characteristics for applications such as EMI shielding [2]. The properties of PEI-based nanocomposite foams prepared using water vapour-induced phase separation (WVIPS) have been investigated in depth and the effect of carbon-based nanoparticles on the physical properties of these foams has been studied, showing promising results in terms of simultaneously enhancing the mechanical properties and electrical conductivity [3–7].

Another foaming technique with characteristics closer to that of industrial foaming processes involves the dissolution of a gas in a polymer precursor in a semisolid-state, i.e., below its melting temperature (semicrystalline polymers) or below its glass transition temperature

(amorphous polymers) and subsequent foaming by either applying a sudden drop of pressure (called one-step or solid-state batch foaming) or heating the gas-saturated precursor above its glass transition temperature after a slow decompression. Both methods have been used to prepare various foams with homogeneous microcellular structures using polymers such as acrylonitrile–butadiene–styrene (ABS) [8], polymethylmethacrylate (PMMA) [9], poly(styrene-co-acrylonitrile) (SAN)/chlorinated polyethylene (CPE) blend [10], polycarbonate (PC) [11] or polyethylene terephthalate (PET) [12]. PEI-based foams have also been prepared in this way using sub–critical CO_2 as the blowing agent [13,14].

Carbon-based nanoparticles (carbon nanotubes, CNT; graphene and graphene-based materials; and carbon nanofibres, CNF) have recently received significant attention due to their outstanding combination of mechanical, thermal, and electrical properties [15,16]. Particularly, graphene and graphene-based materials, such as graphene oxide, reduced graphene oxide, or graphene nanoplatelets, offer great possibilities in terms of improving multiple aspects of polymers due to their high aspect ratio and exceptional mechanical, thermal and electrical characteristics [17–19]. For instance, the addition of GnP/CNT hybrids to PEI-based foams prepared using WVIPS led to significant improvements of their electrical conductivity, reaching values as high as 8.8×10^{-3} S/m for 1 wt % of each filler [5]. Our previous study showed that by achieving a proper GnP dispersion through ultrasonication, the electrical conductivity value of PEI-based nanocomposites foamed via WVIPS could reach as high as 1.7×10^{-1} S/m for foams containing 10 wt % GnP.

Although the preparation and characterization of PEI foams using sub–critical and supercritical CO_2 ($scCO_2$) have been carried out [13,14,20], not many studies have considered the investigation of PEI-based nanocomposite foams. Carbon-based nanoparticles in particular, have presented promising results in the creation of multifunctional foams. The combination of high-performance polymers with these functional nanoparticles could result in outstanding nanocomposite foams with enhanced specific properties. Additionally, $scCO_2$ foaming has shown promising results in improving the dispersion level of nanoparticles throughout the polymer matrix after foaming. Recent studies on PC-based foams containing GnP have shown that foaming could improve their electrical conductivity and EMI shielding effectiveness by inducing a better exfoliation of graphene stacks and reducing the effective inter-particle distance [21]. Another study on PC-based foams [22] suggests that the electrical conductivity of foams prepared by $scCO_2$ dissolution could be enhanced and surpass their respective unfoamed nanocomposites due to improved homogenous dispersion of GnP after foaming.

Furthermore, studies have suggested that the addition of nano-sized particles, such as carbon nanotubes and graphene, to foams prepared by CO_2 dissolution could improve cellular structure homogeneity, increase cell density, reduce cell size and, at the same time, reinforce the matrix [23,24].

This article considers investigating the effects of foaming by $scCO_2$ on the cellular structure, thermal, mechanical, and electrical properties of PEI foams containing variable concentrations of GnP (0.1–2.0 wt %), with the objective of developing novel lightweight materials for advanced applications, such as EMI shielding, ESD, and fuel cells.

2. Materials and Methods

Polyetherimide (PEI), commercially known as Ultem 1000, was purchased from Sabic (Riyadh, Saudi Arabia). PEI Ultem 1000 is a thermoplastic with a density of 1.27 g/cm^3 and a glass transition temperature (T_g) of 217 °C. Graphene nanoplatelets (GnP), with the commercial name of xGnP M-15, were supplied by XG Sciences (Lansing, MI, USA). These nanoparticles have a density of 2.2 g/cm^3 and are formed by stacks of individual graphene nanoplatelets. These stacks have an average thickness of 6–8 nm, a lateral size of 15 µm and a surface area of 120–150 m^2/g. As reported by the manufacturer, the electrical conductivities of GnP measured parallel and perpendicular to the surface are 10^7 and 10^2 S/m, respectively. *N*-methyl pyrrolidone (NMP), with a purity of 99%,

a boiling point of 202 °C, and a flash point of 95 °C, was obtained from Panreac Química SA (Barcelona, Spain).

PEI-GnP foams were prepared containing 0.1–2.0 wt % GnP using $scCO_2$ dissolution. To do so, prior preparation of a set of foam precursors with various GnP concentrations was carried out. The preparation of said foam precursors began with obtaining a GnP-rich PEI-GnP masterbatch. For that, a solution of NMP-GnP was ultrasonicated for 30 min using a FB-705 ultrasonic processor (Fisher Scientific, Hampton, NH, USA) at maximum amplitude with a 12 mm solid tip probe and 20 kHz operating frequency, and maintained at constant temperature of 50 °C using an ice-bath. PEI was added to the solution and dissolved at 75 °C while stirring using a magnetic stirrer at 450 rpm during 24 h. The resulting solution was filtered and rinsed with distilled water and, later, dried under vacuum at 140 °C (maximum vacuum drier temperature) for a week to remove any trace of the solvent. The final PEI-GnP masterbatch contained a GnP amount of 40 wt %.

PEI-GnP nanocomposites with variable concentrations of GnP (0.1–2.0 wt % GnP) were prepared by melt-mixing pure PEI with the PEI-GnP masterbatch using a Brabender Plastic-Corder (Brabender GmbH and Co., Duisburg, Germany). The procedure consisted in feeding 48 g of previously physically-mixed pure PEI and PEI-GnP masterbatch to the Brabender mixing chamber and initially melt-mixing for 6 min at 250 °C using a constant rotation speed of 30 rpm. Mixing continued for another 6 min at the same conditions in order to guarantee homogeneity of the mix, monitoring the temperature and torque values to confirm the stability of the process and the absence of possible degradation. Nanocomposites were then extracted from the mixing chamber and compression-molded into circular-shaped discs (foam precursors) with a nominal thickness of 3 mm and a diameter of 74 mm using a hot-plate press (PL15, IQAP LAP, IQAP Masterbatch Group S.L., Barcelona, Spain) at 300 °C and 70 bar during 4–5 min.

Foaming was carried out by placing the foam precursors inside a high pressure vessel (CH-8610 Uster/Schweiz, Büchiglasuster, Switzerland) using a one-step $scCO_2$ dissolution process. Firstly, $scCO_2$ dissolution was achieved by simultaneously raising the temperature and pressure of the vessel to 230 °C and 180–210 bar, respectively, and maintaining the temperature and pressure conditions for 5 h. Foaming took place by applying a sudden depressurization at a rate around 0.3 MPa/s and moderate controlled cooling of the vessel using a water cooling system. Figure 1 shows both steps of CO_2 pressurization/heating and CO_2 depressurization/cooling used in order to obtain PEI-GnP foams. Thin skin layers formed on both top and bottom of the resulting foams were carefully removed before characterization.

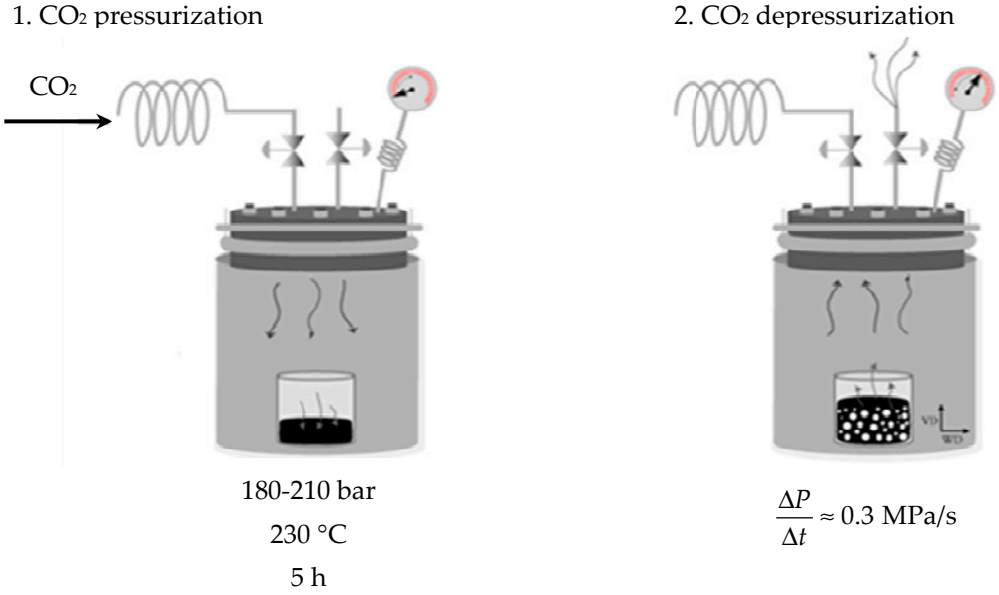

Figure 1. Scheme of the one-step $scCO_2$ foaming process.

Samples coded as PEI correspond to pure PEI foams and the ones coded as GnP to PEI-GnP nanocomposite foams. In the case of the second, the number placed before GnP represents the amount of GnP in weight percentage; for instance, 0.1 GnP corresponds to PEI-GnP foam containing 0.1 wt % GnP.

The foam's density values were measured using the ISO-845 standard procedure. The porosity values were directly calculated from the density values of the foam and respective unfoamed material according to the following expression:

$$\text{Porosity } (\%) \; = \; \left(1 - \frac{\rho}{\rho_s}\right) \times 100 \tag{1}$$

where ρ and ρ_s are the density of the foam and density of the respective unfoamed material, respectively (ρ/ρ_s is the so-called relative density). The cellular structure of the foams was analysed using a JEOL (Tokyo, Japan) JSM-5610 scanning electron microscope (SEM) applying a voltage of 10 kV and a working distance of 40 mm. Samples were brittle-fractured using liquid nitrogen and later coated with a thin layer of gold by sputter deposition using a BAL-TEC (Los Angeles, CA, USA) SCD005 sputter coater under an argon atmosphere. The values of the average cell size (Φ) were measured using the intercept counting method, explained in detail in [25]. Five ×300 magnification SEM micrographs were used for each sample. Cell nucleation density (N_0, in cells/cm^3) was calculated assuming an isotropic distribution of spherical cells according to:

$$N_0 \; = \; \left(\frac{n}{A}\right)^{3/2} \left(\frac{\rho_s}{\rho}\right) \tag{2}$$

where n is the number of cells counted in each SEM micrograph and A is the area of the SEM image in cm^2.

Wide-angle X-ray diffraction was used to evaluate the characteristic (002) diffraction plane of GnP and the possible crystallinity of PEI by a PANalytical diffractometer (Almelo, The Netherlands) running with CuKα (λ = 0.154 nm) at 40 kV and 40 mA. The scanning range was from 2° to 60° using a scan step of 0.033°.

The study of the thermal stability of the foams was done using a TGA/DSC 1 Mettler Toledo (Columbus, OH, USA) STAR System analyser with samples of around 10.0 mg, applying a heating ramp from 30 to 1000 °C at 10 °C/min under a nitrogen atmosphere (constant flow of 30 mL/min). The weight loss evolution with temperature was analysed using the STAR Evolution Software (Mettler Toledo Columbus, OH, USA).

The study of the viscoelastic behaviour of the foams was performed using dynamic-mechanical-thermal analysis. Particularly, the foam's storage and loss moduli (E' and E'', respectively) were measured as a function of temperature, and PEI's glass transition temperature (T_g) was determined. A DMA Q800 from TA Instruments (New Castle, DE, USA) was used in a single cantilever configuration. Samples were analysed by heating at a rate of 2 °C/min from 30 to 300 °C while applying a dynamic strain of 0.02% and frequency of 1 Hz. Rectangular-shaped specimens used in this test had a length of 35.5 ± 1.0 mm, width of 12.5 ± 1.0 mm, and thickness of 3.0 ± 0.5 mm. Three different measurements were performed for each sample (error < 5%).

The electrical conductivity measurements were performed on 20 × 20 × 1 mm samples using a 4140B model HP pA meter/dc voltage source with a two-probe set. A thin layer of colloidal silver conductive paint was used to cover the surfaces of the samples in contact with the copper electrode pads, which had an electrical resistance between 0.01 and 0.1 Ω/cm^2 to ensure perfect electrical contact. A direct current voltage was applied with a range of 0–20 V, voltage step of 0.05 V, hold time of 10 s and step delay time of 5 s. The electrical conductivity (σ, in S/m) was calculated using:

$$\sigma \; = \; 1/\rho_v \tag{3}$$

and

$$\rho_v = RA_{E.C}/d \quad (4)$$

where ρ_v (Ω·m) is the electrical volume resistivity, R is the electrical resistance of the sample (in Ω), $A_{E.C}$ is the area of the surface in contact with the electrode (in m^2), and d is the distance between the electrodes (in m). A correction was applied to the measured values of electrical conductivity considering that porosity could affect the effective surface area in contact with the electrode. The average cell size and the cell density of foams were used in order to obtain the corrected value of electrical conductivity (σ_{corr}) by taking into account variations in the effective surface area as follows:

$$\sigma_{corr} = \frac{d}{R(A_{non-cell} + A_{cell-hemisphere})} \quad (5)$$

where $A_{non\text{-}cell}$ is the $A_{E.C}$ with the cell section area excluded and

$$A_{cell-hemisphere} = \left(\frac{n}{A}\right) A_{E.C} \left(2\pi \frac{\Phi^2}{4}\right) \quad (6)$$

Therefore:

$$A_{non-cell} + A_{cell-hemisphere} = A_{E.C} + \left(\left(\frac{n}{A}\right) A_{E.C} \left(\pi \frac{\Phi^2}{4}\right)\right) \quad (7)$$

The values of n, A, and Φ were obtained from the previously analysed SEM micrographs, and represent the number of cells, the corresponding area of the micrograph, and the average cell size, respectively.

3. Results

3.1. Cellular Structure of the Foams

The composition of PEI-GnP nanocomposite foams, their respective relative densities and main cellular structure characteristics are presented in Table 1.

Table 1. Composition, relative densities, and cellular structure characteristics of PEI and PEI-GnP nanocomposite foams.

Sample	GnP (wt %)	GnP (vol%)	Relative Density	Φ (μm) [1]	N_0 (cells/cm^3)
PEI	0.0	0.00	0.44	14.0 (5.0)	5.1×10^8
0.1 GnP	0.1	0.03	0.48	11.7 (4.2)	5.6×10^8
0.4 GnP	0.4	0.11	0.49	13.6 (4.4)	3.9×10^8
0.7 GnP	0.7	0.17	0.42	5.4 (2.3)	6.5×10^9
1.0 GnP	1.0	0.27	0.46	9.5 (3.3)	1.1×10^9
1.5 GnP	1.5	0.35	0.40	10.0 (4.0)	1.2×10^9
2.0 GnP	2.0	0.57	0.49	7.5 (2.9)	1.6×10^9

[1] Standard deviation of the average cell size is presented between parentheses.

Foams presented densities between 0.52 and 0.63 g/cm^3 (relative densities between 0.40 and 0.49). Although the foam containing 2 wt % of GnP presented the highest relative density, no direct correlation was found between the relative density and the amount of GnP present in PEI-GnP foams. The porosity

values were between 51.0% and 59.6%, with the minimum corresponding to 0.4 GnP and 2.0 GnP foams and the maximum to 1.5 GnP foam.

Digital photographs showing the sample before (foam precursor) and after foaming and characteristic SEM images showing the microcellular structure of PEI-GnP foams are respectively presented in Figures 2 and 3. As can be seen, the addition of GnP seemed to induce the formation of cellular structures with slightly smaller cells.

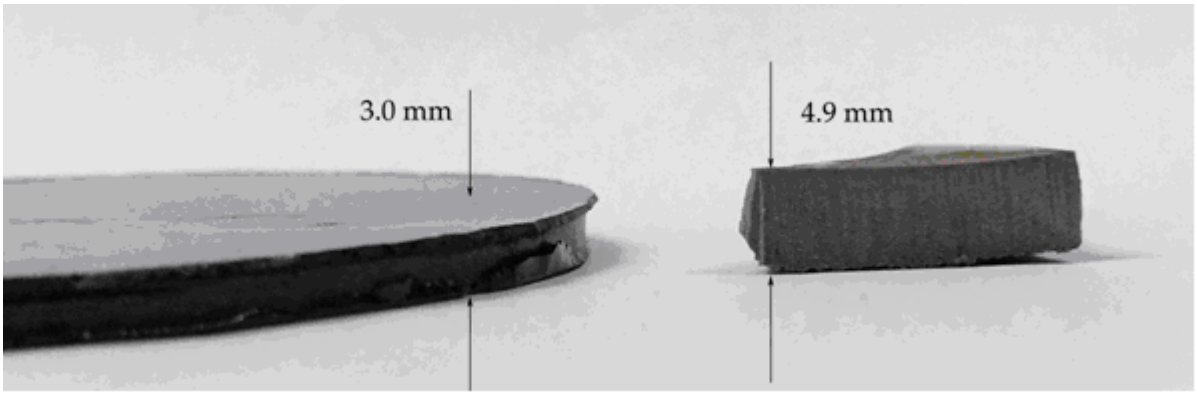

Figure 2. Digital photographs showing the sample before foaming (foam precursor, **left**) and after foaming (**right**).

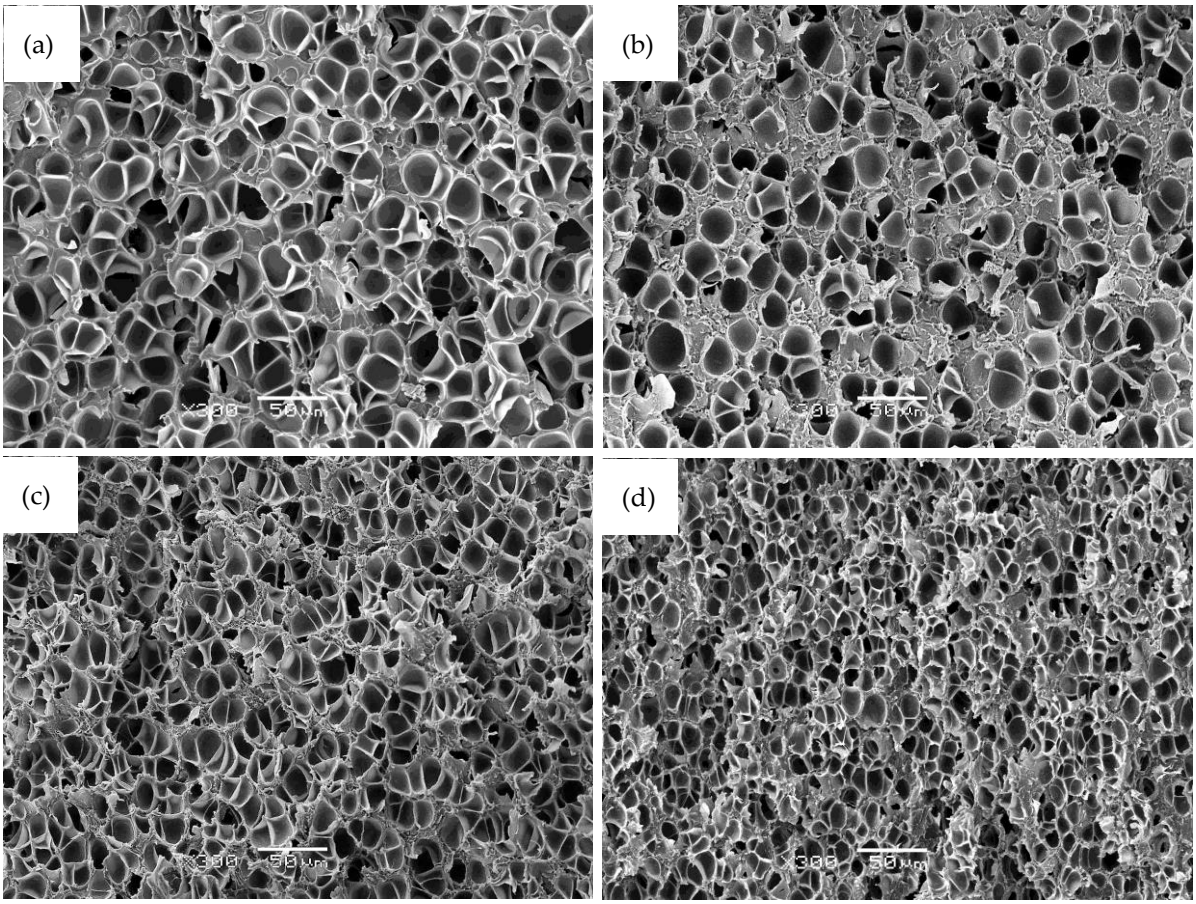

Figure 3. SEM micrographs at ×300 magnification illustrating the microcellular structure of (**a**) pure PEI; (**b**) 0.4 GnP; (**c**) 1.0 GnP; and (**d**) 2.0 GnP foams.

The microcellular foams obtained in this process had an approximate average cell size around 10 μm, with the smallest cells corresponding to 0.7 GnP foam (5.4 μm) and the largest corresponding to pure PEI (14.0 μm). A slight reduction in the average cell size was observed between pure PEI and PEI-GnP foams, showing that the presence of GnP slightly affected the cellular structure of the resulting foams. Consequently, the highest cell nucleation density value corresponded to 0.7 GnP foam (7.0×10^9 cells/cm^3) and the lowest to PEI (3.9×10^8 cells/cm^3).

The peak intensity and full width at half maximum (FWHM) values of X-ray diffraction spectra related to the (002) characteristic diffraction plane of GnP found at $2\theta = 26.5^\circ$ are presented in Table 2. The low and stretched (002) peak formation shows that by applying ultrasonication, melt-mixing, and foaming through $scCO_2$, a significant improvement in dispersion of GnP in foams containing up to 1.5 wt % of GnP could be achieved.

Table 2. Intensity and FWHM values of the characteristic (002) crystal diffraction plane of GnP in PEI and PEI-GnP nanocomposite foams.

Sample	Intensity (a.u.)	FWHM (°)
PEI	-	-
0.1 GnP	-	-
0.4 GnP	350.5	0.23
0.7 GnP	481.2	0.35
1.0 GnP	505.4	0.30
1.5 GnP	483.5	0.40
2.0 GnP	1716.6	0.29

Disappearance and/or significant reduction in intensity of the (002) characteristic diffraction plane of GnP for foams containing up to 1.5 wt % of GnP (see Figure 4) showed that the ultrasonication process was effective and provided a better dispersion and partial exfoliation of GnP stacks. Additionally, melt-mixing and sudden depressurization during foaming could have promoted further dispersion due to shear forces applied during these steps. Nevertheless, the GnP's (002) diffraction plane peak was clearly visible in the 2.0 GnP foam, which was related to the not full dispersion of GnP nanoplatelets, as at such high GnP concentration the ultrasonication, melt-mixing and foaming stages were not enough to guarantee a proper dispersion of the nanoplatelets throughout the polymer matrix.

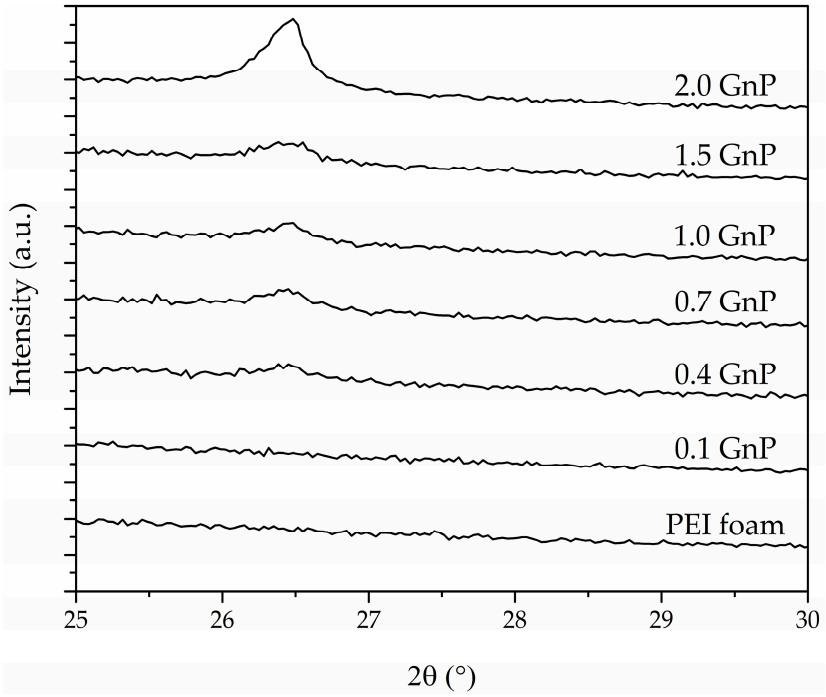

Figure 4. X-ray spectra of PEI and PEI-GnP nanocomposite foams illustrating the disappearance or reduction in intensity of GnP's (002) characteristic diffraction plane.

This high level of GnP dispersion was possible through the combination of ultrasonication, melt-mixing and one-step foaming of PEI-GnP nanocomposites. In the primary stages of foam precursor preparation, GnP stacks were forced to separate by applying ultrasonication. Afterwards, during melt-mixing, high shear forces were applied, favouring GnP distribution and dispersion throughout the polymer matrix. The ultimate stage of one-step $scCO_2$ foaming could have further induced GnP dispersion and partial exfoliation.

3.2. Thermal Analysis

Typical thermogravimetric curves (TGA) of decomposition of all foams are displayed with their respective first derivative (dTG) in Figure 5. The values of the temperature corresponding to a 5% weight loss ($T_{5\%\ \text{weight loss}}$), the temperature at maximum velocity of degradation ($T_{\max}$), the temperature corresponding to a 35% weight loss ($T_{35\%\ \text{weight loss}}$), the char residue ($CR$, in wt %), and the limiting oxygen index (LOI), calculated based on Van Krevelen and Hoftyzer [26] equation:

$$\text{LOI}(\%) = 17.5 + 0.4CR \quad (8)$$

are presented in Table 3. Results indicate a characteristic two-step thermal degradation of PEI, with the first step being related to the decomposition of the aliphatic part of PEI followed by the degradation of the aromatic part in a second step [4,5].

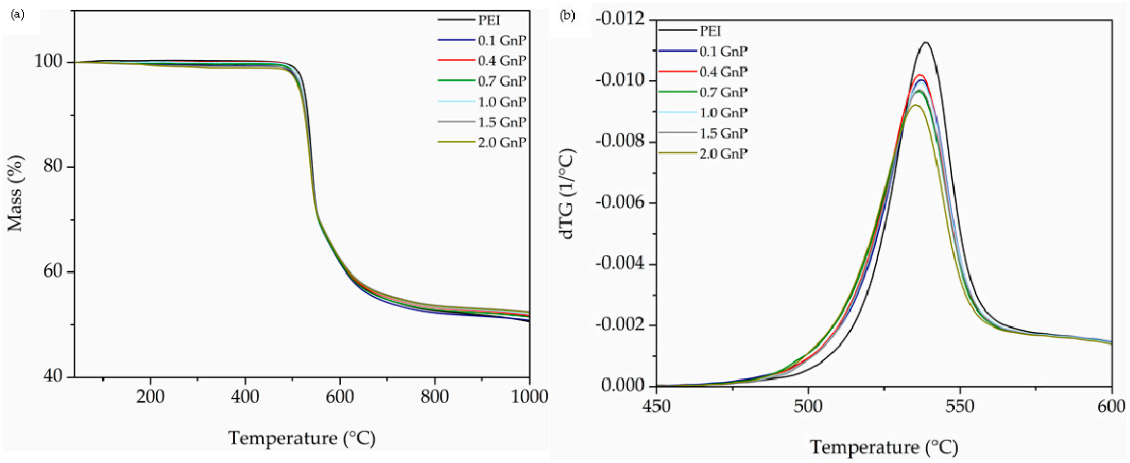

Figure 5. (**a**) TGA and (**b**) dTG thermograms of pure PEI and PEI-GnP nanocomposite foams.

Table 3. TGA results of pure PEI and PEI-GnP nanocomposite foams.

Sample	Decomposition Temperature (°C)			*CR* (wt %)	LOI (%)
	$T_{5\%\ \text{weight loss}}$	T_{max}	$T_{35\%\ \text{weight loss}}$		
PEI	523.4	538.7	580.9	50.5	37.7
0.1 GnP	516.8	537.3	578.3	50.8	37.8
0.4 GnP	518.7	536.9	580.4	51.7	38.2
0.7 GnP	516.2	536.5	579.3	51.5	38.1
1.0 GnP	519.0	537.0	583.0	51.9	38.3
1.5 GnP	517.4	536.6	582.9	52.4	38.5
2.0 GnP	513.9	535.3	581.7	52.3	38.4

As can be seen in Table 3 and Figure 5, there were minor changes in the degradation behaviour of foams regarding the addition of GnP. It has been reported that the addition of carbon-based nanoparticles, especially platelet-like, such as graphene nanoplatelets, could result in improved thermal stability of nanocomposites through a better physical barrier effect, hindering the escape of volatile gasses during pyrolysis [27]. On the other hand, the high thermal conductivity of GnP could promote a higher heat transfer velocity through the foamed structure, thus resulting in a faster degradation [6]. As can be seen, at the first stage of decomposition there was a slight general decreasing trend in $T_{5\%\ \text{weight loss}}$ and T_{max} with increasing GnP amount, suggesting an accelerating effect of GnP on the degradation behaviour; however, as the degradation process approached the second stage, a reversed relation was observed, resulting in a delay in the values of $T_{35\%\ \text{weight loss}}$ and a rise in *CR*. This behaviour is the result of the mentioned contradictory factors, one being the barrier effect of GnP and the other the enhanced heat transfer, which simultaneously affect the thermal degradation, their importance varying in the different stages of decomposition. This could be verified by the calculated values of LOI presented in Table 3, which showed an increasing trend with incrementing the amount of GnP.

3.3. Dynamic-Mechanical-Thermal Behavior

The results of the dynamic-mechanical-thermal analysis (DMTA) of all foams are presented in Table 4. For comparative purposes, the DMTA results of PEI-based nanocomposite foams previously prepared by the WVIPS method are also presented [5,6]. As with PEI-GnP foams prepared by one-step $scCO_2$ foaming, the prefix number represents the amount of nanoparticle in wt %, followed by the type of nanoparticle (GnP or CNT) and the letters S and NS, representing whether ultrasonication was applied or not, respectively.

Table 4. DMTA results of pure PEI and PEI-GnP nanocomposite foams.

Sample	Relative Density	E' at 30 °C (MPa)	E'_{spec} (MPa·cm^3/g)	Glass Transition (°C)	
				Max E''	Max tanδ
		$scCO_2$ foams			
PEI	0.44	738.6	1295.8	212.0	220.9
0.1 GnP	0.48	702.8	1171.3	212.1	224.4
0.4 GnP	0.49	884.3	1426.3	212.5	221.4
0.7 GnP	0.42	630.7	1168.0	212.6	224.0
1.0 GnP	0.46	751.6	1273.9	212.8	218.2
1.5 GnP	0.40	642.3	1235.2	213.0	224.2
2.0 GnP	0.49	922.1	1463.7	210.9	226.5
		WVIPS foams [1]			
1.0 GnP NS	0.44	742.6	1335.6	218.0	225.0
2.0 GnP NS	0.39	568.1	1147.7	218.4	226.7
1.0 GnP S	0.26	370.4	1110.9	223.1	229.8
2.0 GnP S	0.26	385.3	1170.5	223.3	228.6
2.0 CNT S	0.44	442.9	776.5	221.5	227.1

[1] PEI-based nanocomposite foams prepared by water vapour induced phase separation (WVIPS) [5,6].

The results indicate that two main factors could have affected the viscoelastic response of foams: Their relative density and the amount of GnP. The foam's glass transition temperature (T_g) was obtained from the temperatures corresponding to the maximum of the loss modulus (Max E'') and tanδ (Max tanδ) curves. The storage modulus (E') was obtained from the DMTA curves at 30 °C. The specific storage modulus values (E'_{spec}) of foams were calculated by dividing E' obtained at 30 °C by their respective density.

As can be seen in Figure 6a, foams showed and increasing trend of the normalized modulus (E'_{norm}), defined as the quotient between the storage modulus of the foam and the storage modulus of the respective unfoamed material (E'_s), i.e., $E'_{norm} = E'/E'_s$, with increasing relative density. Additionally, Figure 6b illustrates the effect of GnP weight percentage on the specific modulus of the foams, where a general increasing trend was observed with incrementing the amount of GnP.

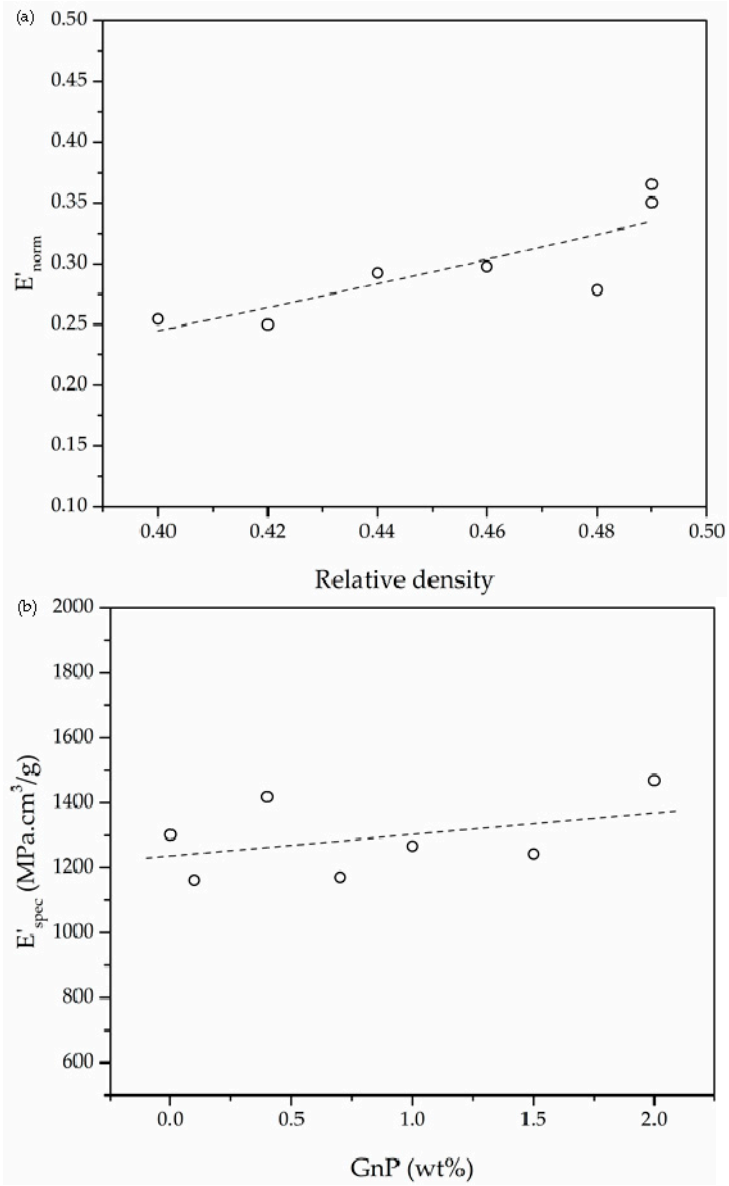

Figure 6. (**a**) Effect of relative density on the normalized storage modulus of PEI and PEI-GnP nanocomposite foams and (**b**) enhancement of the specific modulus with increasing GnP content.

Regarding the viscous part, on the one hand the temperature corresponding to the maximum value of the loss modulus did not change significantly with increasing the amount of GnP. On the other hand, a general increasing trend was observed for the temperature corresponding to the maximum of tanδ with incrementing GnP's concentration, rising 5 °C for the 2.0 GnP foam compared to that of pure PEI foam. Graphene has proven capable of hindering the molecular mobility in multiple study cases of nanocomposites [28–30] due to possible strong interfacial interaction and/or chemical bonding between graphene and the polymeric matrix. Hence, the increase in the temperature corresponding to the maximum of tanδ could be related to an improved interaction of the polymer with graphene nanoplatelets, broadening the glass transition temperature window.

It is commonly known that density, and hence relative density, plays a key role in the mechanical performance of foams. Here, as can be seen in Table 4, relative density appears to have a clear impact on the storage modulus of foams. For instance, the storage modulus increased significantly from 630.7 MPa to 922.1 MPa with increasing relative density from 0.42 to 0.49. Gibson and Ashby [31]

introduced a model that represents the relation of the elastic modulus with density for closed-cell foams assuming foams as a cubic array of individual units:

$$\frac{E}{E_s} \approx C\left(\frac{\rho}{\rho_s}\right)^n \quad (9)$$

where ρ and E are respectively the density and the elastic modulus of the foams and ρ_s and E_s correspond to those of the respective unfoamed material. In this equation C represents the geometry constant of proportionality and is commonly assumed to be equal to 1 [31].

As presented in Figure 6a, with a power fit of the normalized storage modulus (E'_{norm}) obtained at 30 °C as a function of relative density, the value of exponent n could be calculated. This value is related to the efficiency of foaming, with values around 1 representing a smoother decrease in the normalized elastic modulus with reducing density, typical of homogenous closed-cell foams with relatively small cell sizes [32]. Values close to 2 represent a faster decrease of E'_{norm} with reducing density. The n value in this series of foams was equal to 1.53, somewhat close to homogeneous closed-cell structure with few interconnectivities and irregularities. However, this model does not take into account the eventual effects of an additional component, in this case GnP, on the mechanical properties of the foams, nor its secondary effects on the cellular morphology of the foams. Therefore, in order to address the effects of GnP on the mechanical performance of the foams, the specific storage modulus (E'_{spec}) was calculated and represented as a function of GnP content (Figure 6b). As expected based on the inherently high elastic modulus of GnP, a general increasing tendency was observed with the addition of GnP.

Interestingly, PEI-GnP foams containing 1.0 and 2.0 wt % GnP showed higher values of E'_{spec} when compared to their counterparts prepared using WVIPS method containing the same amount of GnP [6]. Additionally, PEI-GnP foams presented much higher values of both E' and E'_{spec} for similar relative densities at lower GnP amounts when compared to foams containing 2.0 wt % of CNT prepared by the WVIPS method [5] (in both cases, compare values presented in Table 4). This could suggest that a more effective reinforcing effect could be achieved by adding GnP when compared to CNT and guaranteeing a more homogeneous microcellular structure via $scCO_2$ foaming when compared to WVIPS method.

3.4. Electrical Conductivity

It has been suggested that mainly two factors affect the electrical conductivity of polymer-based foams containing conductive carbon-based nanoparticles: Firstly and most importantly, the dispersion level of the conductive nanoparticles; and secondly, the porosity level of the foams.

As can be seen in Table 5 and Figure 7, the addition of increasingly higher GnP amounts up until 1.5 wt % GnP led to foams with increasingly higher electrical conductivities, related to the formation of a more effective conductive network attained by the higher amount of GnP and proper GnP dispersion throughout the cell walls after foaming. Nevertheless, comparatively 2.0 GnP foam displayed a lower conductivity than 1.0 GnP or 1.5 GnP foams, which was related to a certain GnP aggregation at the highest added GnP concentration (2.0 wt % GnP) after foaming, as previously demonstrated by the intense (002) GnP crystal diffraction plane in 2.0 GnP foam (see Figure 4).

Table 5. Electrical conductivity and corrected electrical conductivity values of pure PEI and PEI-GnP nanocomposite foams.

Sample	GnP (wt %)	GnP (vol %)	Porosity (%)	σ (S/m)	σ_{corr} (S/m) [1]
PEI	0.0	0.00	55.3	7.18×10^{-16}	4.60×10^{-16} (9.92×10^{-17})
0.1 GnP	0.1	0.03	52.4	2.70×10^{-13}	1.88×10^{-13} (4.03×10^{-14})
0.4 GnP	0.4	0.11	51.0	3.17×10^{-11}	2.27×10^{-11} (4.10×10^{-12})
0.7 GnP	0.7	0.17	57.7	7.16×10^{-11}	4.99×10^{-11} (1.25×10^{-11})
1.0 GnP	1.0	0.27	53.5	3.76×10^{-10}	1.86×10^{-10} (4.00×10^{-11})
1.5 GnP	1.5	0.35	59.6	5.12×10^{-10}	3.45×10^{-10} (8.67×10^{-11})
2.0 GnP	2.0	0.57	51.0	1.12×10^{-10}	7.70×10^{-11} (1.53×10^{-11})

σ_{corr} represents the electrical conductivity corrected according to Equation (7). [1] Standard deviation of the corrected electrical conductivity is presented between parentheses.

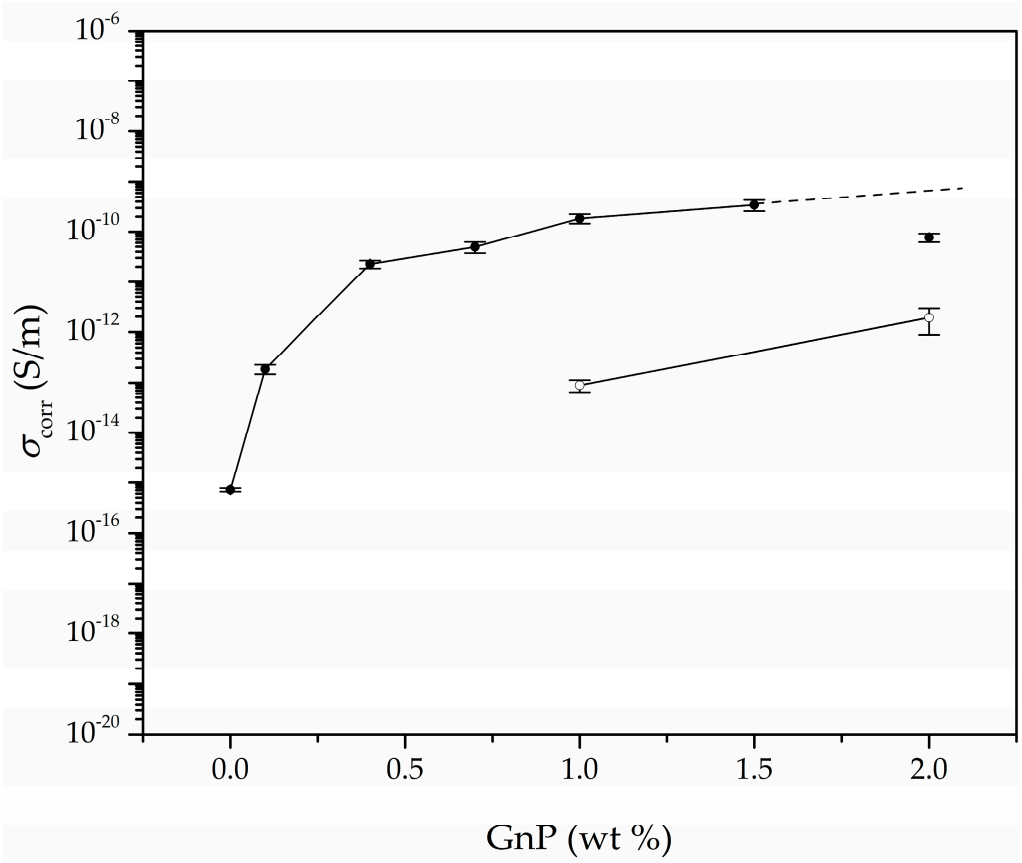

Figure 7. Electrical conductivity enhancement of PEI and PEI-GnP nanocomposite foams with increasing GnP amount. Black circles represent the electrical conductivity values corresponding to foams prepared by one-step $scCO_2$ foaming and white circles correspond to the electrical conductivity of foams prepared by WVIPS [6].

As mentioned before, ultrasonication was used in the preparation of the PEI-GnP masterbatch in order to promote a high level of GnP dispersion. This method has proven worthy in enhancing the electrical conductivity of foams by reducing particle agglomeration [6,33–36].

Ultrasonication, combined with melt-mixing and sudden pressure drop applied during foaming were responsible for promoting the dispersion and partial exfoliation of GnP in PEI, as previously experienced in foams prepared via $scCO_2$ foaming [21].

Moreover, the porosity of foams could play a key role in the inter-particle distance between GnP nanoparticles, enhancing their electrical conductivity by forming a more compact network of conductive nanoparticles. In this sense, by increasing the porosity GnP nanoparticles present in the continuous polymer phase of the foam would be pushed closer together, favouring the formation of an electrical pathway, as shown in Figure 8.

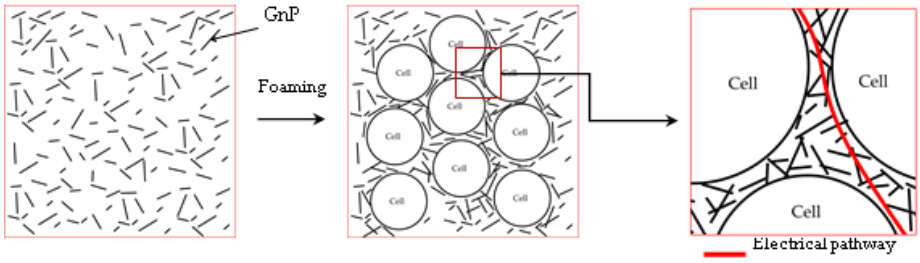

Figure 8. Detail of GnP dispersion showing the microstructural changes in a polymer foam containing GnP with foaming and the effects in electrical conduction.

As can be seen, the electrical conductivity of the foams increased by six orders of magnitude, reaching 3.45×10^{-10} S/m with the addition of only 1.5 wt % (0.35 vol %) GnP. Interestingly, this value was clearly higher than those obtained for foams containing the same amount of GnP prepared by WVIPS method [6]. Since ultrasonication was used in both cases, this result could indicate an enhanced dispersion of GnP nanoparticles via melt-mixing and formation of a more effective conductive network throughout the foam using one-step $scCO_2$ foaming.

In terms of electrical conductivity models, a tunnelling mechanism seemed more accurate compared to a percolative model. Although the percolative model has been used vastly to explain the conductivity behaviour in various studies of nanocomposites containing carbon nanotubes [5,37–39] and graphene [40–43], this model is applicable only when the concentration of the conductive filler is above the critical volume fraction (ϕ_c), also known as the percolation threshold. The percolative model is based on the physical contact between conductive nanoparticles in order to form a pathway for the electrical conduction and is expressed as:

$$\sigma \propto (\phi - \phi_c)^{\nu} \tag{10}$$

where the electrical conductivity value (σ) is proportional to the volume fraction of the conductive filler (ϕ) and the percolation threshold (ϕ_c), and ν is the percolation exponent [43]. Nevertheless, a tunnel conduction model was preferred, as it has been proven to be a more accurate model to anticipate the electrical conductivity behaviour of nanocomposite foams containing conductive carbon-based nanoparticles. As mentioned in some of our previous works [4,6], this model was assumed as the main conduction mechanism in this series of foams due to two main reasons: Firstly, GnP's concentration was below the percolation threshold, resulting in absolute electrical conductivities clearly below what would be expected assuming physical contact between conductive nanoparticles. Secondly, the percolation model does not consider that these nanocomposite foams have already achieved a certain level of electrical conductivity for GnP concentrations below the critical value.

According to quantum mechanics, a tunnelling mechanism indicates that when there is an absence of physical contact between conductive particles the electrons still have the possibility to penetrate through a potential barrier. The crossing of electrons in a tunnelling model could occur when the applied electric field possesses enough potential so that the electron wave function could penetrate

the barrier [44]. Assuming a tunnel-like mechanism, the dc electrical conductivity can be expressed as [45–47]:

$$\sigma \propto \exp(-Ad) \tag{11}$$

where A and d are the tunnel parameter and tunnel distance, respectively.

The phi^{-n} presented in Figure 9 (assuming $n = 1/5$) is directly proportional to the tunnel distance (d), where the value of n is related to the geometry of the conductive fillers and their distribution. Particularly, the value of n for randomly distributed spherical-shaped particles has been proposed to be equal to 1/3 [48], while the value of $n = 1$ corresponds to a 3D random fibre network [49]. We have shown in our previous works [4,6] that assuming a tunnel-like approach for PEI-GnP foams prepared using WVIPS led to a value of n equal to 1/5, which, according to Krenchel [50] and Fisher et al. [51], could confirm the existence of a conductive network formed by GnP with a 3D random distribution. Similarly, in this work the best fit was obtained using an n value of 1/5 (see fitting representation in Figure 9). As shown in previous works, the combination of ultrasonication and increased porosity due to foaming promoted GnP dispersion and led to enhanced electrical conductivity values. In this work it was observed that using one-step $scCO_2$ foaming the electrical conductivity could be improved by a few orders of magnitude for low GnP amounts (<2 wt %), explained on the basis of the already mentioned improved dispersion of GnP.

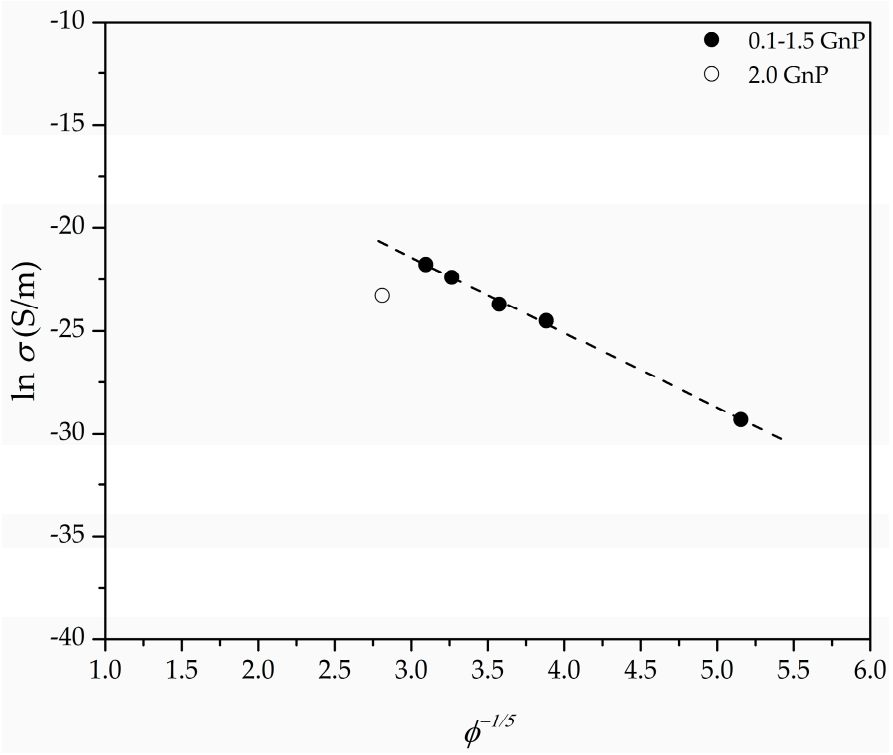

Figure 9. Representation of the fitting results of the electrical conductivity versus $\Phi^{-1/5}$, demonstrating the tunnel conduction characteristic of a 3D random particle distribution system formed by conductive GnP nanoparticles.

4. Conclusions

In terms of cellular structure, PEI-GnP foams presented a microcellular closed-cell structure with similar cell sizes and cell densities independently of the amount of GnP.

The X-ray diffraction analysis showed that the combination of ultrasonication, melt-mixing, and sudden expansion using depressurization of $scCO_2$ promoted enhanced dispersion and partial exfoliation of GnP in the foams.

The addition of GnP has shown to have opposed influences on the thermal degradation behaviour of the foams. On the one hand, the char residue resulting from burning increased with incrementing the amount of GnP while, on the other hand, the value of T_{max} experienced a minor decrease with augmenting GnP content. These behaviours could relate to both the barrier effect of platelet-like GnP, hindering the escape of volatile gases, and the increase in heat transfer due to the presence of the highly conductive GnP, resulting in a faster degradation.

The dynamic-mechanical-thermal performance of PEI-GnP foams was globally controlled by their relative density, as they displayed increasingly higher specific storage moduli with increasing relative density independently of GnP's content. Only for similar relative densities the addition of higher GnP amounts led to stiffer foams. Comparatively, PEI-GnP foams prepared by $scCO_2$ dissolution presented much higher storage moduli at lower GnP concentrations than foams containing 2 wt % CNT prepared by WVIPS method [5], explained mainly by their more homogeneous microcellular structure.

The electrical conductivity of foams increased significantly with incrementing GnP's content, following a tunnel-like conduction mechanism. Foams showed greater values when compared to foams previously prepared using WVIPS method. This increase is believed to be a consequence of the enhanced dispersion of GnP by the combination of ultrasonication, melt-mixing and sudden pressure drop applied during one-step $scCO_2$ foaming, confirmed by X-ray diffraction results. One-step $scCO_2$ foaming could have also promoted increases in the electrical conductivity by decreasing the effective distance between conductive nanoparticles for electrical conduction, as the growth of cells pushed GnP nanoparticles closer to each other within the continuous PEI matrix.

The foams prepared and analysed in this work could be used in cutting-edge sectors, such as aerospace or telecommunications, for applications involving ESD or EMI shielding due to their combination of medium-low density and enhanced electrical conductivity.

Author Contributions: Formal analysis: H.A., M.A., and J.I.V.; investigation: H.A., M.A., and J.I.V.; methodology: H.A., and M.A.; writing—original draft: H.A., M.A., and J.I.V.; writing—review and editing: H.A., M.A., and J.I.V.

Funding: Research funded by the Spanish Ministry of Economy, Industry and Competitiveness, Government of Spain (project MAT2017-89787-P).

Conflicts of Interest: The authors declare no conflict of interest.

References

1. McKeen, L.W. Polyimides. In *Permeability Properties of Plastics and Elastomers*; William Andrew Publishing: Oxford, UK, 2012; pp. 107–120. ISBN 978-1-4377-3469-0.
2. Gedler, G.; Antunes, M.; Velasco, J.I.; Ozisik, R. Enhanced electromagnetic interference shielding effectiveness of polycarbonate/graphene nanocomposites foamed via 1-step supercritical carbon dioxide process. *Mater. Des.* **2016**, *90*, 906–914. [CrossRef]
3. Ling, J.; Zhai, W.; Feng, W.; Shen, B.; Zhang, J.; Zheng, W. Ge Facile Preparation of Lightweight Microcellular Polyetherimide/Graphene Composite Foams for Electromagnetic Interference Shielding. *ACS Appl. Mater. Interfaces* **2013**, *5*, 2677–2684. [CrossRef] [PubMed]
4. Abbasi, H.; Antunes, M.; Velasco, J.I. Graphene nanoplatelets-reinforced polyetherimide foams prepared by water vapor-induced phase separation. *eXPRESS Polym. Lett.* **2015**, *9*, 412–423. [CrossRef]
5. Abbasi, H.; Antunes, M.; Velasco, J. Effects of Carbon Nanotubes/Graphene Nanoplatelets Hybrid Systems on the Structure and Properties of Polyetherimide-Based Foams. *Polymers* **2018**, *10*, 348. [CrossRef]
6. Abbasi, H.; Antunes, M.; Velasco, J.I. Enhancing the electrical conductivity of polyetherimide-based foams by simultaneously increasing the porosity and graphene nanoplatelets dispersion. *Polym. Compos.* **2018**. [CrossRef]
7. Shen, B.; Zhai, W.; Tao, M.; Ling, J.; Zheng, W. Lightweight, Multifunctional Polyetherimide/Graphene@Fe_3O_4 Composite Foams for Shielding of Electromagnetic Pollution. *ACS Appl. Mater. Interfaces* **2013**, *5*, 11383–11391. [CrossRef]

8. Nadella, K.; Kumar, V. Tensile and flexural properties of solid-state microcellular ABS panels. In *Experimental Analysis of Nano and Engineering Materials and Structures*; Springer: Berlin/Heidelberg, Germany, 2007; pp. 765–766.
9. Martín-de León, J.; Bernardo, V.; Rodríguez-Pérez, M.Á. Low Density Nanocellular Polymers Based on PMMA Produced by Gas Dissolution Foaming: Fabrication and Cellular Structure Characterization. *Polymers* **2016**, *8*, 265. [CrossRef]
10. Zhang, H.-C.; Yu, C.-N.; Liang, Y.; Lin, G.-X.; Meng, C. Foaming Behavior and Microcellular Morphologies of Incompatible SAN/CPE Blends with Supercritical Carbon Dioxide as a Physical Blowing Agent. *Polymers* **2019**, *11*, 89. [CrossRef]
11. Kumar, V.; VanderWel, M.; Weller, J.; Seeler, K.A. Experimental Characterization of the Tensile Behavior of Microcellular Polycarbonate Foams. *J. Eng. Mater. Technol.* **1994**, *116*, 439–445. [CrossRef]
12. Shimbo, M.; Higashitani, I.; Miyano, Y. Mechanism of Strength Improvement of Foamed Plastics Having Fine Cell. *J. Cell. Plast.* **2007**, *43*, 157–167. [CrossRef]
13. Miller, D.; Chatchaisucha, P.; Kumar, V. Microcellular and nanocellular solid-state polyetherimide (PEI) foams using sub-critical carbon dioxide I. Processing and structure. *Polymer* **2009**, *50*, 5576–5584. [CrossRef]
14. Miller, D.; Kumar, V. Microcellular and nanocellular solid-state polyetherimide (PEI) foams using sub-critical carbon dioxide II. Tensile and impact properties. *Polymer* **2011**, *52*, 2910–2919. [CrossRef]
15. Badamshina, E.; Estrin, Y.; Gafurova, M. Nanocomposites based on polyurethanes and carbon nanoparticles: Preparation, properties and application. *J. Mater. Chem. A* **2013**, *1*, 6509–6529. [CrossRef]
16. Kostopoulos, V.; Vavouliotis, A.; Karapappas, P.; Tsotra, P.; Paipetis, A. Damage Monitoring of Carbon Fiber Reinforced Laminates Using Resistance Measurements. Improving Sensitivity Using Carbon Nanotube Doped Epoxy Matrix System. *J. Intell. Mater. Syst. Struct.* **2009**, *20*, 1025–1034. [CrossRef]
17. Potts, J.R.; Dreyer, D.R.; Bielawski, C.W.; Ruoff, R.S. Graphene-based polymer nanocomposites. *Polymer* **2011**, *52*, 5–25. [CrossRef]
18. Wang, H.; Robinson, J.T.; Diankov, G.; Dai, H. Nanocrystal growth on graphene with various degrees of oxidation. *J. Am. Chem. Soc.* **2010**, *132*, 3270–3271. [CrossRef]
19. Kuilla, T.; Bhadra, S.; Yao, D.; Kim, N.H.; Bose, S.; Lee, J.H. Recent advances in graphene based polymer composites. *Prog. Polym. Sci.* **2010**, *35*, 1350–1375. [CrossRef]
20. Zhou, C.; Vaccaro, N.; Sundarram, S.S.; Li, W. Fabrication and characterization of polyetherimide nanofoams using supercritical CO_2. *J. Cell. Plast.* **2012**, *48*, 239–255. [CrossRef]
21. Gedler, G.; Antunes, M.; Velasco, J.I. Enhanced electrical conductivity in graphene-filled polycarbonate nanocomposites by microcellular foaming with sc-CO_2. *J. Adhes. Sci. Technol.* **2016**, *30*, 1017–1029. [CrossRef]
22. Ma, H.-L.; Zhang, H.-B.; Li, X.; Zhi, X.; Liao, Y.-F.; Yu, Z.-Z. The effect of surface chemistry of graphene on cellular structures and electrical properties of polycarbonate nanocomposite foams. *Ind. Eng. Chem. Res.* **2014**, *53*, 4697–4703. [CrossRef]
23. Yang, C.; Zhao, Q.; Xing, Z.; Zhang, W.; Zhang, M.; Tan, H.; Wang, J.; Wu, G. Improving the Supercritical CO_2 Foaming of Polypropylene by the Addition of Fluoroelastomer as a Nucleation Agent. *Polymers* **2019**, *11*, 226. [CrossRef]
24. Ventura, H.; Sorrentino, L.; Laguna-Gutierrez, E.; Rodriguez-Perez, M.A.; Ardanuy, M. Gas Dissolution Foaming as a Novel Approach for the Production of Lightweight Biocomposites of PHB/Natural Fibre Fabrics. *Polymers* **2018**, *10*, 249. [CrossRef]
25. Sims, G.L.A.; Khunniteekool, C. Cell-size measurement of polymeric foams. *Cell. Polym.* **1994**, *13*, 137–146.
26. Van Krevelen, D.W.; Hoftyzer, P.J. *Properties of Polymers: Their Estimation and Correlation with Chemical Structure*; Elsevier: New York, NY, USA, 1976.
27. Realinho, V.; Haurie, L.; Antunes, M.; Velasco, J.I. Thermal stability and fire behaviour of flame retardant high density rigid foams based on hydromagnesite-filled polypropylene composites. *Compos. Part B Eng.* **2014**, *58*, 553–558. [CrossRef]
28. Yoon, O.J.; Jung, C.Y.; Sohn, I.Y.; Kim, H.J.; Hong, B.; Jhon, M.S.; Lee, N.-E. Nanocomposite nanofibers of poly(D,L-lactic-co-glycolic acid) and graphene oxide nanosheets. *Compos. Part A Appl. Sci. Manuf.* **2011**, *42*, 1978–1984. [CrossRef]
29. Ji, X.; Xu, Y.; Zhang, W.; Cui, L.; Liu, J. Review of functionalization, structure and properties of graphene/polymer composite fibers. *Compos. Part A Appl. Sci. Manuf.* **2016**, *87*, 29–45. [CrossRef]

30. Wang, B.; Chen, Z.; Zhang, J.; Cao, J.; Wang, S.; Tian, Q.; Gao, M.; Xu, Q. Fabrication of PVA/graphene oxide/TiO_2 composite nanofibers through electrospinning and interface sol–gel reaction: Effect of graphene oxide on PVA nanofibers and growth of TiO_2. *Colloids Surf. A Physicochem. Eng. Asp.* **2014**, *457*, 318–325. [CrossRef]
31. Gibson, L.J.; Ashby, M.F. *Cellular Solids: Structure and Properties*; Cambridge University Press: Cambridge, UK, 1999; ISBN 131602542X.
32. Kumar, V.; Nadella, K.V. Microcellular Foams. In *Handbook of Polymer Foams*; Eaves, D., Ed.; Rapa Technology Limited: Shawbury, UK, 2004; Volume 25, pp. 243–268.
33. Zhou, J.; Yao, Z.; Chen, Y.; Wei, D.; Xu, T. Fabrication and mechanical properties of phenolic foam reinforced with graphene oxide. *Polym. Compos.* **2014**, *35*, 581–586.
34. Yang, H.; Li, F.; Shan, C.; Han, D.; Zhang, Q.; Niu, L.; Ivaska, A. Covalent functionalization of chemically converted graphene sheets via silane and its reinforcement. *J. Mater. Chem.* **2009**, *19*, 4632–4638. [CrossRef]
35. Chen, L.; Jin, H.; Xu, Z.; Shan, M.; Tian, X.; Yang, C.; Wang, Z.; Cheng, B. A design of gradient interphase reinforced by silanized graphene oxide and its effect on carbon fiber/epoxy interface. *Mater. Chem. Phys.* **2014**, *145*, 186–196. [CrossRef]
36. Zhang, W.; Wang, S.; Ji, J.; Li, Y.; Zhang, G.; Zhang, F.; Fan, X. Primary and tertiary amines bifunctional graphene oxide for cooperative catalysis. *Nanoscale* **2013**, *5*, 6030–6033. [CrossRef] [PubMed]
37. Hou, S.; Su, S.; Kasner, M.L.; Shah, P.; Patel, K.; Madarang, C.J. Formation of highly stable dispersions of silane-functionalized reduced graphene oxide. *Chem. Phys. Lett.* **2010**, *501*, 68–74. [CrossRef]
38. Lin, Y.; Jin, J.; Song, M. Preparation and characterisation of covalent polymer functionalized graphene oxide. *J. Mater. Chem.* **2011**, *21*, 3455–3461. [CrossRef]
39. Fang, M.; Wang, K.; Lu, H.; Yang, Y.; Nutt, S. Covalent polymer functionalization of graphene nanosheets and mechanical properties of composites. *J. Mater. Chem.* **2009**, *19*, 7098–7105. [CrossRef]
40. Boukhvalov, D.W.; Katsnelson, M.I. Chemical functionalization of graphene with defects. *Nano Lett.* **2008**, *8*, 4373–4379. [CrossRef] [PubMed]
41. Gao, X.; Jang, J.; Nagase, S. Hydrazine and thermal reduction of graphene oxide: Reaction mechanisms, product structures, and reaction design. *J. Phys. Chem. C* **2009**, *114*, 832–842. [CrossRef]
42. Iqbal, M.Z.; Katsiotis, M.S.; Alhassan, S.M.; Liberatore, M.W.; Abdala, A.A. Effect of solvent on the uncatalyzed synthesis of aminosilane-functionalized graphene. *RSC Adv.* **2014**, *4*, 6830–6839. [CrossRef]
43. Stankovich, S.; Dikin, D.A.; Dommett, G.H.B.; Kohlhaas, K.M.; Zimney, E.J.; Stach, E.A.; Piner, R.D.; Nguyen, S.T.; Ruoff, R.S. Graphene-based composite materials. *Nature* **2006**, *442*, 282–286. [CrossRef]
44. Chiu, F.-C. A review on conduction mechanisms in dielectric films. *Adv. Mater. Sci. Eng.* **2014**, *2014*. [CrossRef]
45. Antunes, M.; Mudarra, M.; Velasco, J.I. Broad-band electrical conductivity of carbon nanofibre-reinforced polypropylene foams. *Carbon N. Y.* **2011**, *49*, 708–717. [CrossRef]
46. Sichel, E.K. *Carbon Black-Polymer Composites: The Physics of Electrically Conducting Composites*; Marcel Dekker Inc.: New York, NY, USA, 1982; Volume 3, ISBN 0824716736.
47. Ryvkina, N.; Tchmutin, I.; Vilčáková, J.; Pelíšková, M.; Sáha, P. The deformation behavior of conductivity in composites where charge carrier transport is by tunneling: Theoretical modeling and experimental results. *Synth. Met.* **2005**, *148*, 141–146. [CrossRef]
48. Hull, D.; Clyne, T.W. *An Introduction to Composite Materials*; Cambridge University Press: Cambridge, UK, 1996; ISBN 0521388554.
49. Allaoui, A.; Hoa, S.V.; Pugh, M.D. The electronic transport properties and microstructure of carbon nanofiber/epoxy composites. *Compos. Sci. Technol.* **2008**, *68*, 410–416. [CrossRef]
50. Krenchel, H. *Fibre Reinforcement*; Ademisk forlag: Copenhagen, Denmark, 1964.
51. Fisher, F.T.; Bradshaw, R.D.; Brinson, L.C. Fiber waviness in nanotube-reinforced polymer composites—I: Modulus predictions using effective nanotube properties. *Compos. Sci. Technol.* **2003**, *63*, 1689–1703. [CrossRef]

Chapter 8

General discussion, conclusions and future studies

8.1 General discussion

In this chapter a general discussion of the results obtained during the research will be presented and compared in terms of their foaming process and the composition of the foams and their relative effects on the properties of the nanocomposites.

8.1.1 The effects of carbon-based nanofillers

The incorporation of **carbon-based nanofillers** had the following effects on the **cellular structure** of the foams.

The cellular structure of the PEI foams prepared using WVIPS method containing GnP showed slight changes in the size of cells by increasing the amount non-ultrasonicated GnP content. The slight increase in cell size observed in these series of foams could have been related to changes in solvent/non-solvent exchange velocity due to a higher barrier to diffusion promoted by the GnP. However, the application of ultrasonication using a probe sonicator seems to achieve improved dispersion level and smaller GnP stacks and thus nullifying their barrier effect during the phase separation process. The cellular structure of foams prepared with applied ultrasonication did not show any significant sensitivity to the amount of GnP.

The addition of CNT on the other hand, has strongly affected the cellular structure of the foams prepared by WVIPS method. These changes could be a consequence of two main simultaneous effects of CNT during the formation and growth of cells. Firstly, the CNT seems to have interfered with solvent/non-solvent exchange, reducing its velocity and therefore resulting in slower cell nucleation rate, which led to increased cell size. Secondly, due to a strong interaction between CNT and PEI, increasing the CNT amount restricted the mobility of the polymer in the casted solution resulting in formation of inter-connected cells/porous structure. Due to this effect, the inter-connected cell structure of the foams prepared by WVIPS increased with the CNT content up until 2 wt% of CNT. In particular case of the foams containing 2 wt% of CNT, the high restriction to polymer mobility prevented the formation of close-cells, resulting in a generalized inter-connected porous structure. In this case, the solvent exchange with water was not confined within the cells but rather expelled from the foam through the formed porous structure. The foam's porosity decreased with increasing CNT and, as mentioned before, the foam's density increased with increasing CNT content. The cause behind the elevated density and decreased porosity of the foams containing the higher CNT concentrations (1 wt % CNT and 2 wt % CNT) seems to be due to a collapse of the inter-connected cell structure.

The foams prepared by WVIPS containing hybrid reinforcement of GnP and CNT displayed increased cellular structure homogeneity by decreasing the concentration of CNT, which coincides with the results obtained for similar foams prepared in this series containing only CNT. Within the Hybrid series foams, the ones with a higher concentration of CNT showed a dual cell size distribution because of two different cell nucleation steps. Additionally, a comparison between the SEM images of the Hybrid series and foams containing similar

amount of CNT (0.5/1.5 and 1/1 wt% CNT/GNP hybrids with 0.5 and 1 wt% CNT), showed that the addition of GnP provided further cellular structure homogeneity.

Regarding the foams prepared by one-step $scCO_2$ dissolution process, the presence of GnP did not seem to significantly affect the density of the foams up until 2 wt%. Characteristic SEM images showed that the microcellular structure of PEI-GnP foams could be affected by the addition of GnP resulting in the formation of a cellular structures with slightly smaller cells.

Regarding the effects of **nanofillers** addition on the **thermal stability** of the prepared foams, the following changes were observed.

The thermal stability of the foams was affected by the presence of GnP. Two competitive effects corresponding to presence of GnP seem to influence the thermal decomposition of the foams. On the one hand, the layer-shaped graphene nanoparticles seem to have an effective physical barrier effect, delaying the escape of volatile gases arose from the pyrolysis, typical behaviour of platelet-like morphologies [1–3]. On the other hand, due to significantly higher thermal conductivity of graphene, by incrementing their concentration in the foams, the rate of heat transfer throughout the matrix would increase, thus accelerating the thermal decomposition of the foams.

Additionally, the size of GnP stacks could influence both mentioned aspects. The results of foams containing ultrasonicated GnP showed a significant reduction of GnP's area which resulted in softening their barrier effect and simultaneously increasing their thermal conductivity through better dispersion. Therefore, the foams containing exfoliated GnP (through ultrasonication) showed lower decomposition temperatures.

In terms of foams prepared by the dissolution of $scCO_2$, the addition of GnP resulted in a faster degradation process during the primary stages of the degradation followed by a reverse relation during the second stage. This behaviour could be related to the mentioned contradictory factors (the barrier effect of GnP and enhanced heat transfer) simultaneously affecting the decomposition process with varying importance in different stages of the degradation.

Similarly, the presence of CNT in foams prepared via WVIPS had a delaying effect on thermal decomposition of the nanocomposite foams. Although CNT is not recognized as a layer-shaped particle, it could still promote a barrier effect by increasing the tortuosity and delaying the discharge of combustible gases, even though not as effective as graphene nanoplatelets. However, the high thermal conductivity of the CNT could act similar to that of GnP, increasing the heat transfer throughout the solid phase and therefore, accelerating the decomposition process. Additionally, the influence of CNT on the morphology of the foams could have also had an effect on altering the velocity of decomposition by increasing the surface area of the cells and their interconnectivity. As mentioned before, the addition of CNT showed significant influence on cell formation behaviour of PEI, resulting in formation of inter-connected and open-cells. This could also be a factor in speeding up the degradation.

The effects of **nanofillers** on the **dynamic-mechanical-thermal properties** of the foams could be explained and below.

Regarding the effect of nanofillers on viscoelastic behaviour of the foams prepared by WVIPS, a general increasing trend was observed with incrementing the GnP content related to significantly higher stiffness of graphene. Ultrasonication of GnP nanoparticles had slightly weakened this effect which could be due to smaller GnP area size after the application of probe ultrasound.

Investigating the effects of GnP on the elastic behaviour of foams prepared by $scCO_2$ dissolution, showed a general increasing trend in the values of specific modulus with incrementing the amount of GnP. Interestingly, these foams containing 1.0 and 2.0 wt% of GnP showed higher values of specific storage modulus when compared to their counterparts prepared using WVIPS method containing the same amounts of graphene nanoparticles. Additionally, $scCO_2$ foams presented much higher values of both storage modulus and specific storage modulus for similar relative densities at lower GnP amounts when compared to foams containing 2.0 wt% of CNT prepared by the WVIPS method. This could suggest that a more effective reinforcing effect could be achieved by adding GnP when compared to CNT and guaranteeing a more homogeneous microcellular structure via one-step $scCO_2$ foaming when compared to the WVIPS method.

Considering the reinforcement effect of CNT aside, the side effect of its addition on density of the foams seems to have had an effect on the storage modulus of these foams. As mentioned before, by increasing the amount of CNT, foams resulted in higher values of density and hence improved elastic behaviour of the foams.

In terms of foams prepared by WVIPS containing hybrid mixture of CNT and GnP, the addition of GnP and its mentioned effect on the cellular structure in the Hybrid series foams resulted in higher values of the specific storage modulus, opening up a possible strategy to exploit the mechanical enhancement effects of these carbon nanoparticles for these type of foams.

With respect to the viscous response of foams prepared by WVIPS, results suggested that nanofillers could have opposing effects on the viscous behavior of the foams. On the one hand, a lubricating effect facilitated the mobility of PEI molecules surrounding the nanofillers and, on the other, there is a restrictive element to molecular mobility due to an enhanced surface interaction with the PEI molecules. For foams containing GnP, the maximum temperature of loss modulus and *tan δ* resulted in slightly higher values for foams with assisted ultrasonication, reaching 8 °C of difference for foams containing 10 wt% GnP. Considering that the maximum temperatures of *E″* and *tan δ* reflect the glass transition temperature of the polymer, the appearance of measured differences indicates a greater interaction between the sonicated particles and the polymer and, as a consequence, a greater restriction to molecular mobility in these foams.

WVIPS foams containing CNT showed a 1–3 °C decrease in the maximum temperatures of both *tan δ* and *E″* by increasing the amount of CNT from 0.1 to 2.0 wt%. This decline seems to be related to

higher molecular mobility by increasing the concentration of CNT which suggests that CNT could have a self-lubricating property, as they are formed by sp^2 bonded cylindrical layers that can easily slide and move upon each other as inter-layer interaction is controlled by weak Van der Waals forces.

Regarding the viscous part of foams prepared by $scCO_2$, on the one hand, the temperature corresponding to the maximum value of the loss modulus did not change significantly with increasing the amount of GnP. On the other hand, a general increasing trend was observed for the temperature corresponding to the maximum of *tan δ* with incrementing GnP's concentration, rising 5 °C for the foams containing 2 wt% of GnP compared to that of pure PEI foam. As mentioned before, graphene has proven capable of hindering the molecular mobility to some extend in multiple study cases of nanocomposites.

The addition of **carbon-based nanofillers** had a significant impact on **electrical conductivity** of the foams. Great efforts have been invested in improving the electrical conductivity of PEI-based foams during this study. Firstly, the addition of GnP to foams prepared via WVIPS showed a significant increase of 8 orders of magnitude (from around 10^{-15} to 10^{-7} S/m) for foams containing 2.2 vol% (10 wt%) of GnP. Tunneling model ($\sigma \propto exp(-Ad)$) was considered as the main conduction mechanism, first of all due to the concentration range of GnP and secondly, due to the fact that the percolation model does not consider that the samples are already electrically conductive for GnP concentrations below the critical value. As recently shown, tunnel conduction is a better match for experiments with wide range of filler concentrations before the formation of a continuous conductive particle network in carbon-reinforced nanocomposites, as direct contact between conductive particles would lead to much higher final electrical conductivities.

Further investigation on these foams showed that by the application of high power ultrasound the dispersion level of GnP throughout the cellular structure was improved noticeably. Additionally, the results showed that incrementing the porosity provokes an additional increase in electrical conductivity due to the further reduction of GnP inter-particle distance as a consequence of a decrease in the characteristic dimension of the solid phase in the foams through a more favorable reorientation of GnP particles. These two factors led to remarkable increase of six orders of magnitude (from around 10^{-7} to 10^{-1} S/m) when compared to previous set of foams prepared by WVIPS method containing 10 wt% of GnP.

With respect to electrical conductivity of WVIPS foams containing CNT, much higher values were achieved (6.4×10^{-3} S/m) for only 2 wt% of CNT when compared to that of foams containing similar amounts of GnP (2.8×10^{-8} S/m). Additionally, using a hybrid nanofiller composition (GnP and CNT), the electrical conductivity was improved even further by more than 1 order of magnitude. The foams containing 1/1 ratio of CNT and GnP resulted in electrical conductivity value of 8.8×10^{-3} S/m, positioning itself as one of the highest values recorded for foams prepared using phase separation method only containing 2 wt% of nanofillers.

Although the XRD results indicated an incomplete exfoliation on nanofillers in both CNT and Hybrid series, but the results from electrical conductivity measurements showed that an effective formation

of conductive network was achieved through efficient dispersion. Additionally, the combination of GnP and CNT demonstrated a synergic effect due to their high individual aspect ratio levels and their impact on the cellular structure (formation of more homogeneous closed-cell structure).

Interestingly, the electrical conductivity of foams prepared by one-step $scCO_2$ dissolution was clearly higher than that of those containing same amounts of GnP and prepared by WVIPS method with similar porosity values. The one-step $scCO_2$ foams containing only 1.5 wt% (0.35 vol%) of GnP reached 3.5×10^{-10} S/m of electrical conductivity while the WVIPS foams with similar porosities and GnP content (2 wt% or 0.29 vol%) achieved values as high as 3.9×10^{-12} S/m. It is fair to mention that WVIPS foams with higher porosity values were able to increase the electrical conductivity by 4 orders of magnitude containing same amounts of GnP (2 wt%) due to explained effect of porosity on the inter-particle distance and effective formation of conductive network by the nanofillers.

8.1.2 The effects of polymer blending

Regarding the **cellular structure** of the foams, the PEI/PAI blends prepared via WVIPS, showed that the amount of PAI in the blend was a driving factor in determining their final microstructure. At concentrations as low as 25 wt% of PAI the foams showed a very fine homogeneous cellular structure, indicating a good level of miscibility between PEI and PAI. On the contrary, the foams containing 50 wt% of PAI displayed a dual cellular structure, where a relatively bigger population of cells were formed in the initial PAI-rich phase and a second population of smaller cells were formed by the remaining PEI-rich phase. Since PAI has higher affinity for water than PEI [4], the early stage of water absorption and subsequent solvent release would initially be promoted by PAI molecules. At this moment, a PAI-rich phase solidifies around the solvent droplets, owing to a clear excess of PAI over the maximum miscible composition [5].

With respect to the **thermal stability** of PEI/PAI blend foams, differences were mainly found in the first-step, with the onset temperature and decomposition rate of foams containing 25 and 50 wt% of PAI being between those of pure PEI and PAI. Comparatively, foams containing only 25 wt% of PAI were more thermally stable than that of 50 wt% PAI.

The analysis of the **mechanical properties** of these **polymer blends** showed that particularly, the elastic behaviour of PEI/PAI blend foams prepared by WVIPS, the results showed that owing to the higher stiffness of PAI compared to PEI, blend foams demonstrated an increase in storage modulus with incrementing the PAI fraction. Initially, the specific storage modulus was reduced with foaming for both pure polymers, though to a greater extent in the case of PEI (43% reduction) than in PAI (30%), probably related to a lower density in the case of the first. Considering the blend foams, the particularly fine microcellular structure of foams containing 25 wt% PAI was responsible for the highest specific modulus among the blend foams, similar to that of pure PAI foam, in spite of the relatively low content of PAI. On the contrary, albeit having a higher amount of PAI, 50/50 blend foam (containing 50 wt% of PAI) displayed

a comparatively lower specific storage modulus due to its dual cellular structure, particularly the presence of considerably bigger cells.

Regarding the viscous part of results, peaks corresponding to glass transition temperature of both polymers appeared in loss modulus and *tan δ* curves for blend foams containing 50 wt% of PAI while only one peak was observed in the results corresponding to foams with 25 wt% of PAI which can be taken as a clear evidence of good polymer miscibility in these foams

8.1.3 The effects of foaming process

As mentioned before, two main foaming processes were used to prepare PEI-based nanocomposites in this study. Firstly, by utilizing **WVIPS** method where the polymer is dissolved in a solvent and then poured into a recipient in order to initiate the separation of phases due to solvent/non-solvent exchange. Secondly, through dissolution of **$scCO_2$** in a nanocomposite precursor followed by sudden release of pressure leading to formation of cellular materials.

Firstly, the effects of these **foaming methods** on the **cellular structure and morphology** of these foams should be discussed.

Regarding the density of the foams in WVIPS method, samples with densities from 0.28 g/cm^3 to 0.58 g/cm^3 (relative densities between 0.22 and 0.45) were prepared by controlling the amount of polymer dissolved in the solution (15-30 wt%). As expected, the foams containing higher initial amounts of polymer presented higher values of density. These foams showed a homogenous structure which was also affected by the composition (presence of PAI, CNT and GnP). Another factor affecting this process was the thickness of casted solution. By reducing the thickness logically, the higher surface area of thin samples allowed faster induction of water leading to formation of smaller cells and foams with finer cellular structure thus to foams with higher density values.

In term of foams prepared by one-step $scCO_2$ dissolution, they presented densities between 0.52 and 0.63 g/cm^3 (relative densities between 0.40 and 0.49). The foaming parameters in this process such as temperature of saturation and release, pressure and duration of saturation were kept constant but since maintaining the all conditions including the depressurization rate at absolute constant value was not feasible, small deviation in densities were observed.

Considering the effects of both foaming methods on the polymers structure, XRD results showed no sign on crystallinity nor crosslinking. However, the distribution and orientation nanofillers were affected by the foaming process. Firstly, the ultrasonication showed significant influence on improving the nanofillers dispersion in both foaming methods. Secondly, the change in porosity of the foams prepared by WVIPS (as a consequence of changes in density) represented an effective way to decrease the inter-particle distance between the particles by pushing them towards one another by increasing the volume of gaseous phase of the foams. This also resulted in changes of properties such as electrical conductivity. The melt-

mixing process also showed effective in increasing the dispersion of graphene nanoplatelets through shear forces.

Regarding the **thermal stability** of the foams prepared by WVIPS containing only GnP did not show any significant relation between the foam's structure and their thermal stability, however, they represented a slight acceleration in their thermal decomposition when compared to that of foams prepared via $scCO_2$ dissolution.

Variations in decomposition behaviour were spotted in foams prepared by WVIPS containing CNT. Since the addition of CNT resulted in changes in morphology of the foams (foams with open-cell structure), the velocity of decomposition experienced a notable increase when compared with foams containing GnP.

With respect to **dynamic-mechanical-thermal properties** of the foams, as mentioned before, their elastic behaviour was heavily affected by their density and cellular structure. As expected, foams with higher densities presented higher values of storage modulus following the Gibson and Ashby model [6] representing the relation of elastic modulus with density for closed-cell foams assuming cells as a cubic array of individual units (see Equation 2.6 in Chapter 2).

Additionally, the changes in specific storage modulus of the foams were observed in foams with structural differences. Particularly, the foams containing CNT observed a reduction in specific storage modulus due to morphological modification induced by the presence of CNT (closer to open-cell structure).

Regarding the **electrical conductivity** of the foams, the morphology and structure of the samples could influence their electrical conductivity by changing the dispersion level of conductive nanofillers and their positioning. Firstly, the dispersion level of nanofillers was greatly improved by application of high power ultrasound resulting in higher values of electrical conductivity when compared to foams containing same amount of fillers (Chapter 5).

Secondly, the electrical conductivity of the foams showed and increasing trend with increasing the expansion ratio (reduced density or increased porosity) therefore, presenting the possibility to increase the electrical conductivity while decreasing the GnP's volume fraction. These result trends were found contradictive to common responses reported for similar composites in other researches, where the electrical conductivity was reduced with increasing the expansion ratio. One of the important factors is the improved dispersion of nanoparticles with foaming, as proven in XRD analysis illustrated by the reduction of peak intensity corresponding to the (002) crystal plane of GnP, which, combined with a reduction of the available volume, leads to a notable decrease of the distance between nanoparticles and to improved electrical conductivities by mechanisms such as tunneling and percolation [7,8].

In the previous chapter, it was observed that using one-step $scCO_2$ foaming the electrical conductivity was improved by few orders of magnitude for low GnP amounts (< 2 wt%), explained by the improved dispersion. The enhanced dispersion of GnP is believed to be a consequence of the combination of ultrasonication, melt-mixing and sudden depressurization applied during one-step $scCO_2$ foaming,

confirmed by X-ray diffraction results. The foaming process itself could also have promoted an increase in electrical conductivity based on the basis of already explained hypothesis of decreasing the effective distance between conductive nanoparticles for electrical conduction, as the growth of cells pushed GnP nanoparticles closer to each other within the continuous PEI matrix.

8.2 Conclusions

Considering the primary objectives and strategies set at the initiation of this research, following principal conclusions could be extracted:

1. PEI-based foams containing both ultrasonicated and non-sonicated GnP prepared by WVIPS represent a homogenous closed-cell structure with minimal influence from the GnP content on the morphology of the foams.

2. Thickness and polymer concentration in the casted solution played a key role on determining the eventual density and average cell size of the foams in WVIPS method. Foams prepared with lower thickness of casted solution presented higher values of density and average cell size due to faster solvent/non-solvent exchange.

3. Carbon nanotubes had a clear effect on the cellular morphology of the foams prepared by WVIPS. Addition of CNT resulted in foams with more inter-connected cells and eventually, entirely consisting of only open-cells at higher CNT amounts.

4. The thermal stability of the foams was slightly improved by the addition of nanofillers due to their contradictive influence on degradation behaviour of the foams. The opposed effects were due to their barrier property hindering the escape of volatile gases and increased heat transfer throughout the solid phase due to their high thermal conductivity.

5. The mechanical properties of the foams prepared by WVIPS were highly dependent on the density and structure of the foams with addition improvements obtained by incorporation of both GnP and CNT.

6. The PEI/PAI blend foams prepared by WVIPS showed that their cellular structure could be modified by the amount of PAI content. Due to differences in foaming behaviour of the two polymers through WVIPS process, a dual cellular structure was formed in foams containing 50 wt% of PAI.

7. The mechanical properties of the PEI/PAI blend foams were improved and optimized for the foams containing 25 wt% of PAI as a result of morphological aspect of these foams and higher stiffness of PAI compared to PEI.

8. The application of ultrasonication showed promising results in terms of enhancing the dispersion levels of nanofillers in both methods of foaming (WVIPS and one-step $scCO_2$ dissolution). Consequently, the electrical conductivity of foams prepared with the application of high power ultrasonication was significantly improved.

9. All foams containing only GnP showed significant enhancement of their electrical conductivity by increasing the GnP content up to 10 wt% following a tunneling model for conduction. The foams with increased porosity showed further improvement of their electrical conductivity due to reduction of inter-particle distance between the conductive particles.

10. The addition of CNT to PEI-based foams resulted in higher values of electrical conductivity when compared to that of foams containing same amounts of GnP. Nevertheless, the foams containing CNT/GnP hybrid reinforcement, showed even higher values of electrical conductivity for foams containing same amounts of filler content (2 wt%) due to the synergic effect of hybrid nanofillers.

11. Foams prepared by one-step $scCO_2$ dissolution presented a homogeneous closed-cell structure with relative density of around 0.45.

12. The combination of ultrasonication, melt mixing and foaming process provided foams with improved dispersion of GnP in one-step $scCO_2$ dissolution foams which resulted in foams with higher values of electrical conductivity when compared to that of foams prepared via WVIPS method with similar relative densities and GnP content.

8.3 Future studies

During the conduction of this thesis, numerous foams were prepared and analyzed with different foaming methods and compositions which provided a glimpse of possible existing strategies to produce multifunctional foams based on high-performance polymers and carbon-based nanofillers. Nevertheless, due to the novelty and diversity of both high-performance polymers and carbon-based nanofillers, significant numbers of possibilities remain untouched. Particularly, the following lines of research could be investigated in future in order to give a deep insight on multifunctional foams and their applications:

- Further experiments are essential in order to determine the impact of foaming parameters on cellular structure of the foams prepared by dissolution of $scCO_2$ in order to prepare lighter foams with improved functionalities. Future experiments on PEI-based nanocomposite foams should also consider the preparation of foams using other foaming methods such two-step foaming.

- The optimization of ultrasonication process, melt-mixing and one-step $scCO_2$ dissolution foaming parameters could provide the possibility of obtaining foams with fully exfoliated graphene nanoplatelets which could lead to extremely higher values of electrical conductivity with low concentrations of GnP.

- The study of foams prepared by $scCO_2$ dissolution could be extended by varying the composition of the precursors, including the addition of CNT and CNT/GnP hybrid systems since they showed promising results in foams prepared by WVIPS.

- Further analysis of prepared foams through measurements such as thermal conductivity, AC electrical conductivity with varying frequency, EMI shielding efficiency measurements, etc. could help provide a better understanding of these materials and therefore, expanding the possibilities of their applications.

- The polymer blending and foaming of polyetherimide with other polymers such as polysulfones (PSU and PPSU) could be studied since they show promising miscibility.

- The use of adequate surfactants in preparation of nanocomposite foams with GnP and CNT should be considered in order to fully benefit from the intrinsic properties of these fillers since a better interaction between the matrix and filler would result in improvement of various aspects of the foams such as their mechanical properties.

8.4 References

1. Realinho, V.; Haurie, L.; Antunes, M.; Velasco, J.I. Thermal stability and fire behaviour of flame retardant high density rigid foams based on hydromagnesite-filled polypropylene composites. *Compos. Part B Eng.* 2014, *58*, 553–558.

2. Gedler, G.; Antunes, M.; Realinho, V.; Velasco, J.I. Thermal stability of polycarbonate-graphene nanocomposite foams. *Polym. Degrad. Stab.* 2012, *97*, 1297–1304.

3. Wang, X.; Yang, H.; Song, L.; Hu, Y.; Xing, W.; Lu, H. Morphology, mechanical and thermal properties of graphene-reinforced poly(butylene succinate) nanocomposites. *Compos. Sci. Technol.* 2011, *72*, 1–6.

4. Wang, Y.; Jiang, L.; Matsuura, T.; Chung, T.S.; Goh, S.H. Investigation of the fundamental differences between polyamide-imide (PAI) and polyetherimide (PEI) membranes for isopropanol dehydration via pervaporation. *J. Memb. Sci.* 2008, *318*, 217–226.

5. Palsule, S.; Cowie, J.M.G. Miscibility in molecular composites of polyamide-imide/polyetherimide. *Polym. Bull.* 1994, *33*, 241–247.

6. Gibson, L.J.; Ashby, M.F. *Cellular solids: structure and properties*; Cambridge university press, 1999.

7. Ryvkina, N.; Tchmutin, I.; Vilčáková, J.; Pelíšková, M.; Sáha, P. The deformation behavior of conductivity in composites where charge carrier transport is by tunneling: theoretical modeling and experimental results. *Synth. Met.* 2005, *148*, 141–146.

8. Stauffer, D.; Aharony, A. *Introduction to percolation theory*; CRC press, 1994.